Causes and Mitigation of Sedimentation along the Northern Side of Johns Pass Channel

Final Report

Submitted By

Ping Wang and Jun Cheng
Coastal Research Laboratory
School of Geosciences
University of South Florida
Tampa, FL 33620

Submitted to

Pinellas County
22211 US Hwy. 19 N.
Clearwater, FL 33765

October 26, 2021

Table of Contents

Table of Figures

EXECUTIVE SUMMARY

Purpose of Study: Stakeholders along the northern side of Johns Pass channel, including the City of Madeira Beach and property owners, have expressed concerns about sedimentation just northeast (and landward) of the cross-channel bridge. The stakeholders partnered to fund a study by University of South Florida (USF) Coastal Research Lab to address this issue. Building upon the recently completed inlet management study at Johns Pass and Blind Pass, this study aims to:

1) understand the causes of the sedimentation along the northern side of the channel;

2) examine the rate of sedimentation on the interior of the inlet;

3) collaborate with stakeholders and decision makers to develop and evaluate various mitigation strategies; and

4) recommend an optimal mitigation measure.

Methodology: The above goals are achieved by using a verified numerical model simulating the current and wave fields and an extensive literature review on the natural and engineering history of Johns Pass. Historical variations of the interior sedimentation along the north bank of Johns Pass and shoreline changes along the adjacent beaches were depicted in time-series aerial photos from 1926 to 2020. Human impacts to the project area were summarized based on the engineering records and previous studies. A numerical model was constructed and verified with field measurements. The model was used to simulate the current and wave fields at the project site and to evaluate various mitigation measures.

Findings: The interior sedimentation at Johns Pass is driven by a natural process that occurs at many tidal inlets. Specific to the project site, the sand moving southward along Madeira Beach can be brought into the inlet by the flood current. Sand accumulation occurs at locations within the channel where the ebb tidal current is not adequate to flush all the sand out of the inlet. This natural process can be modified by various engineering activities. At Johns Pass, engineering activities have been quite intensive over the past 90 years. The north jetty, constructed in 1961, blocks some of the sand from entering the inlet. However, the jetty filled to the tip almost immediately after construction suggesting that the jetty has not been blocking all the sand. A question was posed whether beach nourishment, particularly along the updrift beach to the north,

may constitute a major sand source for the interior sedimentation in the recent years. However, abundant sand supplies existed along Madeira Beach and over Johns Pass ebb shoal before beach nourishment projects occurred. The nourishment projects along Sand Key since 1988, which are more than 3 miles from the inlet, have not fundamentally changed the sand supplies to Johns Pass interior sedimentation. The construction of the existing bridge coincides with a large amount of visible sand at the project area as seen on the 2010 aerial photo. However, numerical modeling results suggest that the present bridge-piling configuration increases ebb flow along the north jetty, which would prevent sand from entering the inlet. The bridge pilings also block waves from the open Gulf from reaching the marina area. The marina facilities do not seem to have significant influence on flow patterns and therefore sedimentation processes. Lastly, the intensive dredging in the 1960s associated with the Federal channel authorization, along with the construction of the north jetty and seawalls, is likely responsible for the removal of the substantial interior sedimentation observed in the 1950s. The north side of the channel appears to be clear of emergent sand till the late 1990s, at least not visible on the aerial photos. The above understanding of the causes of sedimentation along the Johns Pass interior serves as the basis for the development of mitigation alternatives.

Mitigation Alternatives and Recommendations: It is proposed by this study that local removal of the sand accumulation should be the main mitigation approach. A crucial consideration in evaluating the alternatives is that local sand removal should be least likely to induce negative impacts at other parts of Johns Pass and along adjacent beaches. Three categories of mitigation measures are examined. Category 1 (C1) involves removal of excess sand from the seaward tip of the north jetty to the marina, i.e., along the entire north side of the channel; five sand removal alternatives (C1-A1 to C1-A5) are examined. Category 2 (C2) involves removal of excess sand from the seaward tip of the north jetty to the marina, while excluding the area within 100 ft from the Johns Pass bridge; five sand removal alternatives (C2-A1 to C2-A5) are examined. Category 3 (C3) examines the option of blocking the sand from reaching the marinas by constructing a barrier between the north seawall and the north most bridge piling; no sand removal would be conducted.

Based on the modeling results, the ten alternatives of C1 and C2 have negligible influence on the overall flow and wave fields within the Johns Pass channel, while alternative C3 would not

directly solve the existing sedimentation problem. All 11 alternatives have minimal influence on the processes along the adjacent beaches. The evaluation of the 11 mitigation alternatives and recommendations are summarized in the following table with the recommended alternatives in gray.

ALTERNATIVE	CY REMOVED	RECOMMENDATION
C1-A1	3,200	NOT recommended, volume too small
C1-A2	11,100	NOT recommended, volume too small
C1-A3	**14,000**	**Recommended as lower limit for sand removal**
C1-A4	**18,700**	**Recommended**
C1-A5	**23,700**	**Recommended as upper limit for sand removal**
C2-A1	2,900	NOT recommended, volume too small
C2-A2	7,000	NOT recommended, volume too small
C2-A3	9,700	NOT recommended, volume too small
C2-A4	**13,100**	**Recommended ONLY if no activity can be conducted near the bridge**
C2-A5	**16,600**	**Recommended ONLY if no activity can be conducted near the bridge**
C3	0	NOT recommended, not solving the existing sedimentation problem.

Conclusions: The sedimentation within the Johns Pass channel is mainly caused by natural processes. The various engineering activities over the past 90 years, including jetty construction, channel dredging, bridge construction, marina facilities and operations, and beach nourishments modified the natural processes. However, none of these engineering activities have fundamentally changed the sand supply to the channel interior and the natural process that brings the sand into the channel. Based on the above understanding and results of numerical modeling, local sand removal, which imposes negligible impacts on the overall flow and wave fields through the inlet and along the adjacent beaches, is recommended to mitigate the present sedimentation problem. The local sand removal approach is also supported by the past conditions as observed from time-series aerial photos since 1926. Based on the sedimentation rate estimated from existing bathymetry data, the three recommended alternatives, C1-A3, C1-A4, and C1-A5 should have a life span of 8, 11, and 14 years, respectively.

Limitations: Estimating future rate of sedimentation constitutes a major limitation of this study. It is assumed that the sedimentation rate obtained during a short period of time, 2018 through 2020 for this case, can be applied to approximate future sedimentation at the project site. This assumption can be significantly influenced by the unpredictable nature of storms and engineering activities.

1.0 Introduction

1.1 Purpose of the Study

Stakeholders along the northern side of Johns Pass channel, including the City of Madeira Beach and property owners, have expressed concerns about sedimentation just northeast (and landward) of the cross-channel bridge. The stakeholders partnered to fund a study by USF Coastal Research Lab to address this issue. Building upon the recently completed inlet management study at Johns Pass and Blind Pass, this study aims to

1) understand the causes of the sedimentation along the northern side of the channel;

2) examine the rate of sedimentation on the interior of the inlet;

3) collaborate with stakeholders and decision makers to develop and evaluate various mitigation strategies; and

4) recommend an optimal mitigation measure.

The above goals are achieved by using an extensive literature review on the natural and engineering history of Johns Pass in addition to a verified numerical model simulating the current and wave fields.

1.2 General Background Knowledge

Sand deposition along the banks of an inlet channel is a common phenomenon and is observed at many inlets. This section introduces the general knowledge on sediment sources and processes that drive the sedimentation within an inlet channel using the north bank of Johns Pass as an example. The north side of the Johns Pass channel is heavily engineered including, from landward to seaward, numerous boat docks and basins bounded landward by a seawall and an elevated boardwalk (referred to as marina facilities in this report), a seawall and riprap, a cross-channel bridge with a large piling about 20 m (60 ft) from the seawall, continued seawall and riprap, and the Johns Pass north jetty (Figure 1).

Sedimentation within an inlet channel is controlled by two main factors. The first factor is sediment supply. Generally, the sand that is deposited within the channel can come from the updrift beach driven by longshore transport which is sand that moves along the shoreline. For the case of Johns Pass (Figure 2), this longshore moving sand would go around the seaward tip of the north jetty (black arrows) and enter the inlet channel. The sand can also come from the ebb shoal, mainly the shallow channel margin linear bar (red arrow). The channel margin linear bar refers to the shallow linear feature over which the red arrows were drawn. In both cases, the intense turbulence associated with breaking waves play a major role in suspending sediment into the water column, which can be subsequently transported into the inlet by flood tidal current and landward propagating breaking waves.

The beaches along the 14-mile-long Sand Key to the north of Johns Pass have been nourished several times since 1988. The artificial infusion of sand along the updrift beach may contribute to the sand source from longshore transport, i.e., the black arrows in Figure 2. However, the south end of the nourishment project terminates about 3 miles north of the inlet. Therefore, local beach conditions particularly in the vicinity of the north jetty would play a more direct role in the channel sedimentation with the nourishment possibly serving as a background sand input. To counterbalance the potential sand input from beach nourishment projects, the Johns Pass channel and ebb shoal have served as the sand borrow areas for the federal nourishment projects seven times since 1980.Those sand borrow areas function as efficient traps for longshore moving sand.

In addition to being transported along the beach and entering the inlet channel around the north jetty, some of the nourishment sand could also be transported onto the Johns Pass ebb shoal, and therefore contribute to the sand source as indicated by the red arrow in Figure 2. Overall, both the distal sand supply through beach nourishments and the proximal beach conditions at the north

jetty and the channel margin linear bar should be considered in analyzing the sand sources for the channel sedimentation.

The second factor controlling channel sedimentation is related to the specific hydrodynamic conditions at the project site that favor sedimentation. Typically, sand is brought into the inlet channel by the flood tidal current and flushed out of the channel by the ebb current. The flood tidal current refers to the landward-directed flow into the bay driven by rising tide. The ebb tidal current refers to the seaward-directed flow exiting the back bay driven by falling tide. Therefore, the spatial distribution of tidal currents within the channel plays a significant role in determining where scour and sedimentation occur within the channel. For example, if the ebb (outgoing) flow along the northern side of the channel is weaker than the flood (incoming) flow, then flood currents would dominate and there would be a net landward transport resulting in sand deposition at locations where the flood velocity decreases. When the water depth becomes shallow enough to induce wave breaking, the offshore approaching waves would begin shoaling and breaking and induce sand transport pushing the shallow "sand shoal" landward.

1.3 Applicable Tools and Data from Recently Completed Studies

This Johns Pass channel sedimentation study is built upon the Johns Pass and Blind Pass Inlet Management Study, funded by the Florida Department of Environmental Protection (FDEP) and completed in 2016 (Wang et al., 2016). The results of the inlet management study were used by FDEP to update the inlet management plans for Johns Pass and Blind Pass. The products from the inlet management study that are directly relevant to this study include 1) a sediment budget for the Johns Pass and Blind Pass inlet system, and 2) a calibrated and verified numerical model. The sediment budget was developed based on a series of beach profiles and ebb shoal bathymetry data collected from 2010 to 2014, concurrent with one beach-nourishment cycle on Sand Key and Treasure Island. The sediment budget can be directly used to analyze the sand source for the sedimentation along the north side of the channel.

A numerical model for the Johns Pass and Blind Pass system was developed by USF as a major product of the Inlet Management Study (Wang et al., 2016). The Coastal Modeling System (CMS) developed by the US Army Corps of Engineers (Buttolph et al., 2006; Wang et al., 2011; Lin et al., 2011; Sanchez and Wu, 2011; Sanchez et al., 2014) specifically for inlet studies was

used to simulate the flow field, wave field, sediment transport, and morphology change at the dual inlet system. Since Johns Pass and Blind Pass are connected to the same bay, the circulation model incorporated both inlets. Extensive field measurements of tidal water-level fluctuations, flow field, and nearshore waves were conducted during the inlet management study. The field data were used to calibrate and verify the numerical model. The Johns Pass-Blind Pass model can be used for this study with minor modifications described in Section 3.4.

During this study, field data collection was conducted to ensure bathymetry was as accurate as possible at the project site. The USF Coastal Research Lab has an on-going project, funded by Pinellas County, to monitor the beach changes along Sand Key (including Madeira Beach), Treasure Island, and Long Key. Beach profiles at 1000 ft intervals are being surveyed quarterly. The ebb-shoal bathymetries of Johns Pass, Blind Pass, Pass-a-Grille, and Bunces Pass have also been surveyed annually since 2018. The ebb shoal surveys also include the inlet entrances and channels. The 2020 bathymetry survey was completed in June 2020. Special attention was paid to the project area to ensure that accurate bathymetry with adequate spatial resolution was obtained. This new bathymetry data was used directly to update the improved modeling grids.

1.4 Study Scope of Work and Specific Tasks

This study aims at developing an optimal strategy to mitigate the sedimentation along the northern side of Johns Pass east of the bridge. The strategy is based on sound understanding of the sand sources and transport mechanism causing the sedimentation as derived from field measurements and numerical modeling. This study was built upon a recently completed Johns Pass and Blind Pass inlet management study and an on-going beach and ebb-shoal monitoring study conducted by the USF Coastal research lab. The following specific tasks were completed:

Task 1: Time-series aerial photos and existing bathymetry data were analyzed to document the history of shoaling within the Johns Pass channel, and if there is an increased rate of sedimentation in the last three decades. Recent operational difficulties at the marina seem to indicate an increased sedimentation rate. Engineering activities at Johns Pass over the past 90 years, including jetty constructions and extensions, ebb shoal and channel dredging, bridge constructions, marina construction and modifications, and beach nourishments, etc. were summarized. Potential influences of these activities on channel sedimentation were analyzed.

Task 2: A large amount of field data were collected during the recently completed Johns Pass-Blind Pass inlet management study (Wang et al., 2016). Data that are directly relevant to the northern side of the channel were compiled and analyzed with the specific goal of examining the sedimentation at the project area. Earlier analyses for the inlet management study were focused on the entire system of Johns Pass and Blind Pass.

Task 3: The numerical model that was constructed during the inlet management study were modified and verified to ensure that the tidal flow pattern at the project site were accurately simulated. It was hypothesized here that the flood tidal flow along the northern side is stronger than the ebb flow which was examined as part of this investigation.

Task 4: Modest field measurements were conducted. The field measurements were focused on the project area to ensure that the modified numerical model accurately represents the land-ocean boundary, project area bathymetry, significant marina structures, and any other features that may influence local flow patterns. An additional survey was conducted to quantify the sedimentation pattern at the project site. In addition, short-term current measurements were conducted at specific locations of concern.

Task 5: A numerical wave model was established. The wave model constructed during the inlet management study was modified with updated bathymetry and improved resolution at the project site. The wave modeling was designed to examine how the wave pattern contributes to the suspension of sand on the ebb delta.

Task 6: A series of tidal flow models were conducted based on existing and various other bathymetry conditions at the project site. The modeling scenarios were designed to examine what flow conditions may be favorable for sedimentation at the project site and what flow conditions tend to prevent sedimentation.

Task 7: A series of tidal flow models were conducted to investigate the interaction of the bridge pilings, particularly the northmost one, as well as the marina pilings and structures with the tidal flow pattern under existing conditions and under proposed modifications. Scenarios consisted of cases with and without the bridge pilings. The results were analyzed to examine the potential influence of the bridge-current interaction on sedimentation or scour at the project site. The flow fields under various degrees of sedimentation were also simulated.

Task 8: A series of wave modeling was conducted based on statistical wave conditions for the greater study area. The modeling scenarios were designed to investigate what wave conditions are more favorable for bringing sediment into the inlet and what wave conditions do not tend to mobilize a large amount of sediment. Wave propagation patterns at various water levels, e.g., low tide, mean sea level, high tide, and with storm surge, etc., were also simulated and analyzed.

Task 9: The findings from Tasks 1 through 8 provided a solid understanding of sediment and hydrodynamic conditions that are responsible for transporting sand into the northern side of the inlet channel. These findings were presented to the stakeholders and decision makers (i.e., the TAC: Technical Advisory Committee), along with initial thoughts on various mitigation methods. The input from the stakeholders and decision makers was incorporated to the refinement of the mitigation measures.

Task 10: Various mitigation alternatives were developed in collaboration with the stakeholders and decision makers (i.e., TAC). Numerical modeling of the various mitigation alternatives was conducted. The mitigation alternatives were evaluated based on numerical modeling. Optimal mitigation alternatives are recommended.

Task 11: This final report including results from all the above tasks was compiled to be presented to the stakeholders and decision makers.

2.0 Local Conditions

2.1 Study Area

The greater study area of Johns Pass and Blind Pass is described systematically in the inlet management study and other studies (Wang et al., 2016; Beck and Wang, 2019; Beck et al., 2020). Here, a summary of the Wang et al. (2016) report is provided with an emphasis on Johns Pass, particularly the channel between the two barrier islands. Regionally, the Johns Pass-Blind Pass system is part of the west-central Florida barrier-island chain that extends north from the mouth of Tampa Bay (Beck and Wang, 2019). The entire area, from the beaches to the inlets to the back-bay, is densely populated and heavily developed since the 1930s. Several causeways and bridges and numerous dredge and fill finger channels dissect the back-barrier bay (Figure 3).

Figure 3. Johns Pass and Blind Pass inlet system.

2.2 General Wave and Tide Conditions

The study area is located along a generally low-energy coast facing the Gulf of Mexico (Davis, 1994; Davis, 1997; Wang and Beck 2012). Figure 4 illustrates the statistical wave climate obtained from computed wave conditions by the numerical wave model WAVEWATCHIII (http://polar.ncep.noaa.gov/waves/index2.shtml) from 2000 to 2014. The numerical wave station is located approximately 7 km from the shoreline. Based on the comparison with measured wave height by Wang et al., (2016), WAVEWATCHIII under-predicted the measured wave height by approximately 9%. Therefore, in Figure 4 the WAVEWATCHIII wave heights were multiplied by 1.09 to correct for the discrepancy. As illustrated in Figure 4, a large portion of the nearshore wave approached from the west. Most of the waves were lower than 0.5 m. Higher waves tend to approach from the west-northwest generated by the passages of winter cold fronts and the associated wind patterns. These statistical wave conditions were used to design the input wave

conditions for the numerical wave modeling. The coast along the Johns Pass area faces the southwest. which would generate southerly sediment transport when waves interact with the coast as shown in Figure 4. These wave conditions are consistent with the morphological characteristics of the inlet system.

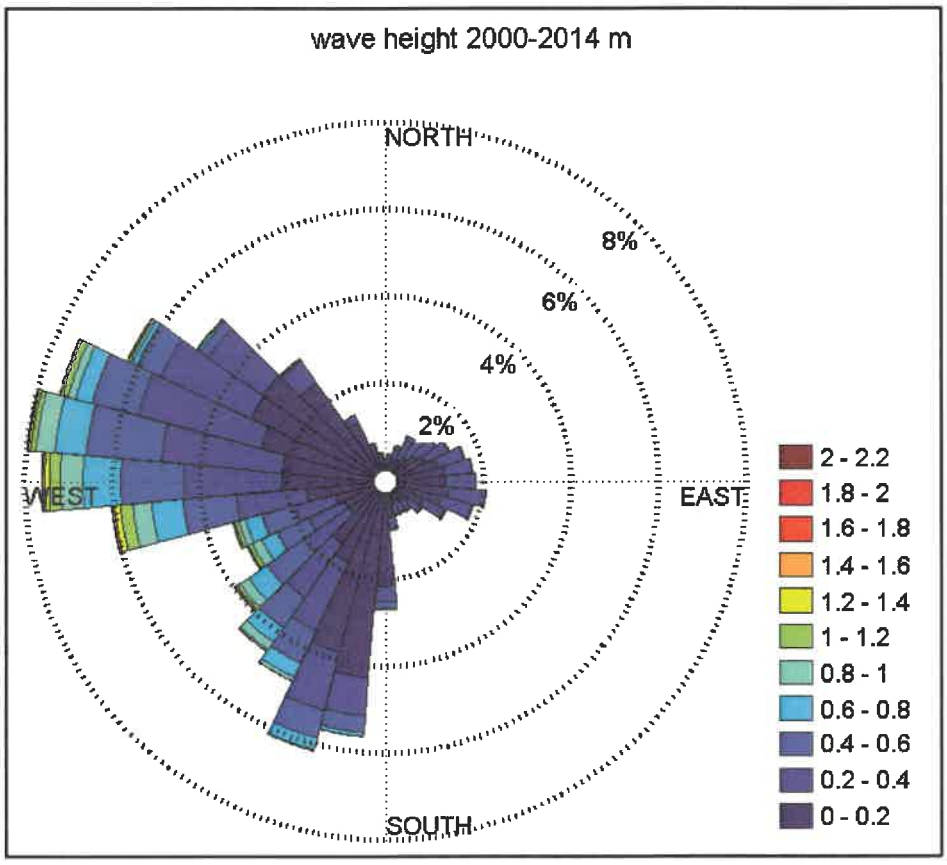

Figure 4. Wave rose composed from computed wave conditions.

The study area is characteristic of a mixed tidal regime. The spring tide is typically diurnal with a range of roughly 0.8 to 1.2 m, whereas the neap tide is semi-diurnal with a range of 0.4 to 0.5 m (Figure 5). Although the spring tide tends to be diurnal, a short pause or slight water-level fall typically occurs during the prolonged rising phase, whereas the shorter ebbing phase is typically not interrupted. The magnitude of the slight water-level fall during the spring flooding phase increases as the tidal cycle changes to a neap cycle, and eventually becomes a semi-diurnal tide during the neap phase (Figure 5). Detailed tide conditions were measured at seven locations including offshore, in the inlet, and in the back-barrier bay during the inlet management study

(Wang et al., 2016) Tide-driven flow was also measured at various locations within the Johns Pass and Blind Pass system for the calibration and verification of the numerical model.

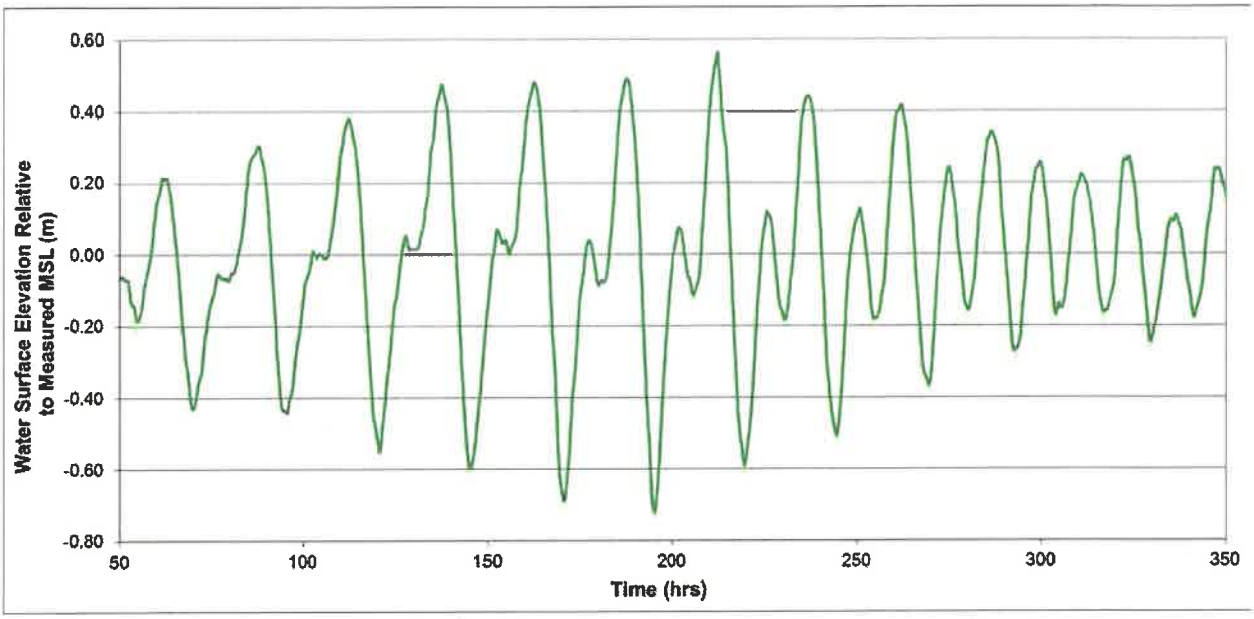

Figure 5. Measured tides from July 23, 2008 to August 5, 2008 approximately 3 km offshore of Johns Pass.

2.3 Past Engineering and Shore-Protection Measures at Johns Pass

In 1926, bridges across Johns Pass and Blind Pass (landward of the bend) and a road on Treasure Island were constructed, marking the first major anthropogenic activity which paved the way for decades of intense engineering modifications to Johns Pass and Blind Pass inlets, adjacent Gulf facing beaches, and northern Boca Ciega Bay. Since then, the hydrodynamics, sediment processes, and morphodynamics of the two inlets and their adjacent beaches have been significantly influenced by anthropogenic activities.

Once public road access between Sand Key, Treasure Island, and Long Key was established, extensive development of the barrier islands, as well as the back-bay began, as evident from the time-series photos (Figure 6). Some of the developments were accomplished without adequate consideration of their long-term effects on beach and inlet morphodynamics, often reflecting historically lower environmental standards and more lenient regulations. Limited knowledge of the cause-and-effect relationships between the back-bay, inlets, and adjacent beaches at the time was also a factor. Following the bridge and road construction, one of the earliest

engineering efforts included the 1934 construction of two 150-ft groins at the Veterans Administration Beach (Mehta et al, 1976) designed to mitigate the aggressive erosion and shoreline retreat occurring along the southern end of Sand Key (i.e., Madeira Beach) at that time. Appendix I compiles a tabulation of engineering activities that have taken place at Johns Pass and the adjacent beaches including southern Sand Key and northern Treasure Island over the past 90 years. This shortened list is selected from the engineering activities compiled by Wang et al. (2016) for the entire Johns Pass and Blind Pass system.

Figure 6. Time-series aerial photos of Johns Pass from 1926 to 2010.

Engineering modifications to Johns Pass inlet, adjacent beaches, and nearby Boca Ciega Bay have been extensive. In addition to the 2016 inlet management study conducted by Wang et al. (2016), two earlier inlet management studies (CPE, 1992; CTC, 1993) provided a detailed summary of the engineering activities at Johns Pass and Blind Pass. In general, the engineering history illustrates a pattern of action/reaction events which are generally related to maintaining safe navigation through the inlets or to mitigating erosion along adjacent beaches. Since the 1980s both issues seem to have been satisfied, at least for a certain duration of time (with a relatively regular dredging cycle), in that materials dredged from the inlets to improve navigation safety were commonly placed on adjacent stretches of eroding beach.

In general, the engineering activities at Johns Pass can be grouped based on the time periods reflecting our preferred methods and goals of inlet management and shore protection at that time. The following four phases of engineering activities and corresponding morphology response are detailed below. The starting and ending times of each phase may overlap.

1) Before 1926: natural state, with continued inlet development after its opening by a hurricane in 1848,
2) 1926 – late 1960s: substantial engineering activities, mostly construction of hard engineering structures, including:
    a. Constructions of causeways and bridges, resulting in increased dissection of the back-barrier bay,
    b. Finger channel dredge and fill resulting in a reduction of tidal prism,
    c. Construction and extension of inlet jetties and groin field on the adjacent beaches.
3) Early 1960s - 1970s:
    a. Shortly before and after the authorization of Johns Pass as a Federal channel, frequent channel dredging to improve navigability,
    b. Nearshore sand placement and formation and evolution of the O'Brian's Lagoon.
4) Late 1960s to present: mostly soft engineering (beach nourishment and dredging), with minor hard engineering structure (jetties) extensions, including:
    a. Frequent channel and ebb shoal dredging,
    b. Frequent beach nourishment on Treasure Island and north Long Key, with some of the beach nourishment projects using the sand dredged from Johns Pass channel and ebb shoal.

Somewhat unique to the Johns Pass and Blind Pass inlet system, in addition to the stabilization of the inlets using seawall and jetties, the finger-channel dredge and fill construction in the back-barrier bay is much more significant than that along most of the Florida Gulf coast. Tidal prism is the product of back-bay area and tidal range and represents the amount of water flowing through the inlet during a rising or falling tide. Over a temporal scale of decades, tidal range should remain constant. However, the area of Boca Ciega Bay has declined as a direct consequence of anthropogenic modifications including dredge and fill projects and construction

of causeways (Figure 7). The practice of infilling the back-bay to create land became popular in the 1940's through the 1950's and was not confined to Boca Ciega Bay (Davis and Barnard, 2000).

Based on Wang et al. (2016), for the portion of the bay that serves Johns Pass and Blind Pass, the bay area reduction due to dredge and fill projects is 20% (Figure 1). Since both Johns Pass and Blind Pass are confined by jetties on both sides, the reduced tidal prism may cause additional sedimentation within the channel. This is particularly apparent at Blind Pass as illustrated by the sedimentation in the northern portion of the entrance channel.

Since the first recorded dredging in 1960, a total of 1,445,000 cubic yards of sand were dredged from Johns Pass channel and its ebb shoal. It is worth noting that in Appendix I the 390,000 cubic yards of sand dredged in 2000 were from both Johns Pass and Blind Pass. It is not clear how much was from each inlet, although most of the sand should be from Johns Pass. Therefore, the overall volume from Johns Pass should be slightly smaller than the 1,445,000 cubic yards. Most of the dredged sand was placed along Treasure Island which is downdrift of Johns Pass but some of the Johns Pass sand was placed on the updrift beach. This included the placement of 30,000 cubic yards of sand from the very first dredging project in 1960 directly north and updrift of the constructed north jetty, to mitigate the severe erosion at Madeira Beach. In 1988, during the first Sand Key nourishment project, about 300,000 cubic yards of sand from Johns Pass were placed on the updrift North Redington Beach. This updrift placement has not been conducted since 1988 due to modern inlet management practices.

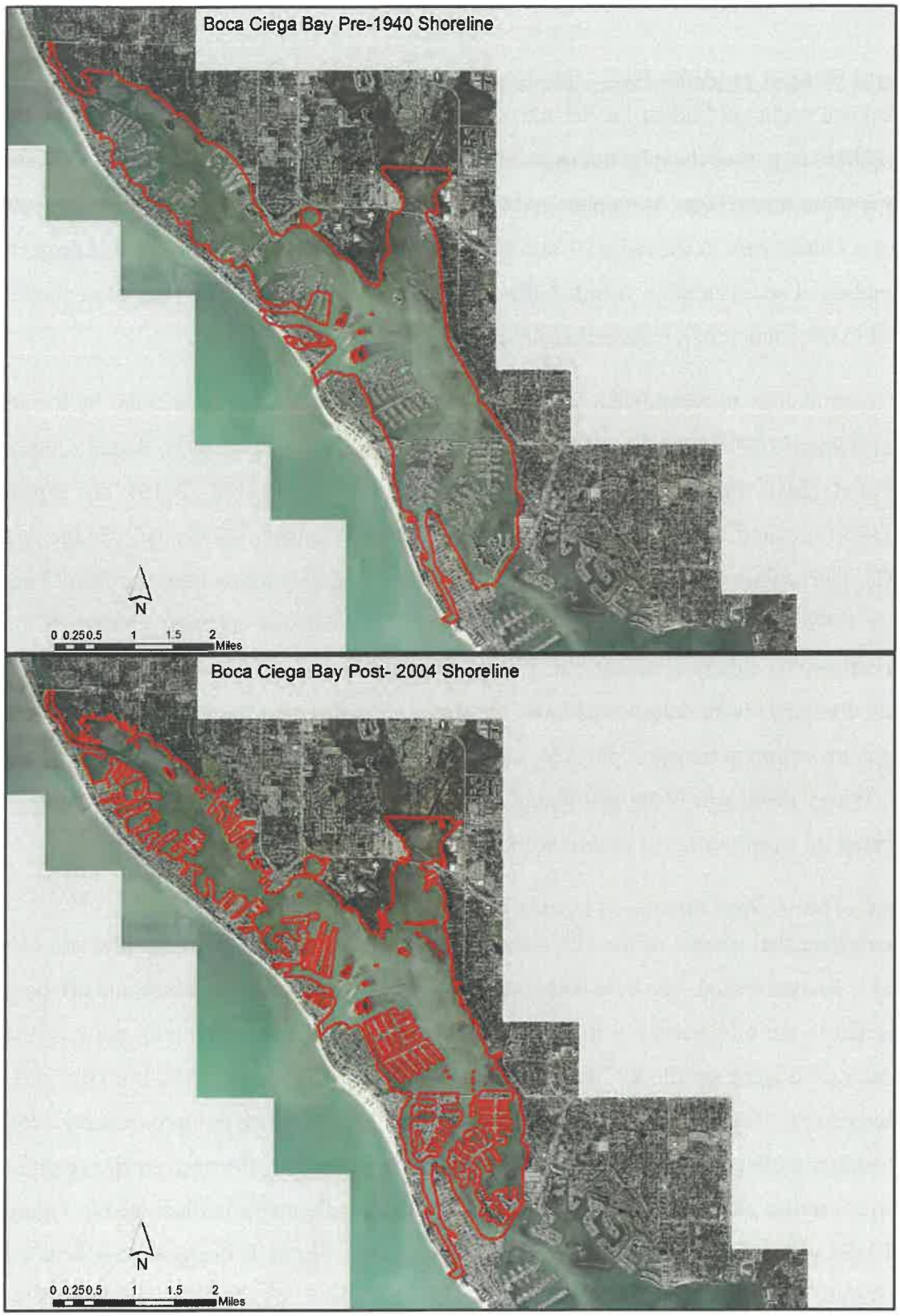

Figure 7. Surface area reduction of the back-barrier bay serving John's Pass and Blind Pass.

2.4 Sediment Budget at Johns Pass Developed by Wang et al. (2016)

A detailed sediment budget for the Johns Pass and Blind Pass system was developed by Wang et al. (2016) as part of the inlet management study. The Johns Pass budget directly relevant to this study is summarized here. As emphasized by Bodge and Rosati (2002), an accurate sediment budget plays a crucial role in the regional sediment management at tidal inlets. For this project, the understanding of sedimentation within Johns Pass, as well as the mitigation measures, should be developed in the context of a balanced sediment budget of the entire system.

The methodology to formulate a tidal inlet sediment budget, discussed in detail by Rosati and Kraus (1999 and 1999b), Kraus and Rosati (1998), Rosati and Kraus (2003), Rosati (2005), and Walton et al., 2012 was used in the inlet management study (Wang et al., 2016). The Rosati and Kraus (1999) method is also recommended in the Coastal Engineering Manual (Bodge and Rosati, 2002). The sediment budget (Wang et al., 2016) developed for Johns Pass and Blind Pass was based on the Rosati (2005) method. The volume of ebb shoal was calculated based on the multi-beam bathymetry survey conducted in 2014. Volumetric changes of the ebb shoal since 2010 (after the last dredging) were determined based on time series surveys conducted by USF-CRL. Rate of longshore sediment transport plays a central role in sediment budget (CERC, 1984; Wang et al., 1998; Wang, 1998; and Wang and Kraus, 1999). The rate of longshore sand transport was calculated based on a time-series of beach profile surveys.

2.5.1 Volume of Johns Pass Ebb Shoal from Wang et al. (2016)

To calculate the volume of the ebb shoals, a base bathymetry without the inlet and ebb shoal needed to be established. The base bathymetry was constructed using the beach and offshore profiles adjacent to the inlet surveyed in June 2014. At Johns Pass, the bathymetry north of the inlet was constructed using profile R120 which is approximately 1500 m (5000 ft) from the inlet. The bathymetry south of the inlet was constructed using profile R134 which is approximately 2700 m (9000 ft) from the inlet. Due to the southward skew of the ebb shoal, the base profile south of the inlet is much farther than the profile to the north. The base bathymetry is illustrated in Figure 8. The tidal inlet was also removed from this base bathymetry. Figure 9 illustrates the detailed 2014 multi-beam surveyed bathymetry of the John's Pass ebb shoal overlaying the base bathymetry. The ebb shoal feature is apparent. The area of the ebb shoal is 2,043,000 m^2

(21,991,000 ft^2). The volume of the ebb shoal as calculated from the base bathymetry is 3,286,000 m^3 (4,298,000 yd^3). It is worth noting that the landward limit of both ebb-shoal area and volume calculation is at the shoreline, defined by NAVD88 zero. The 1,445,000 cubic yards of sand that was dredged from the Johns Pass channel and ebb shoal since the 1960s, as summarized in Appendix I, constitute a substantial portion (34%) of the entire ebb shoal.

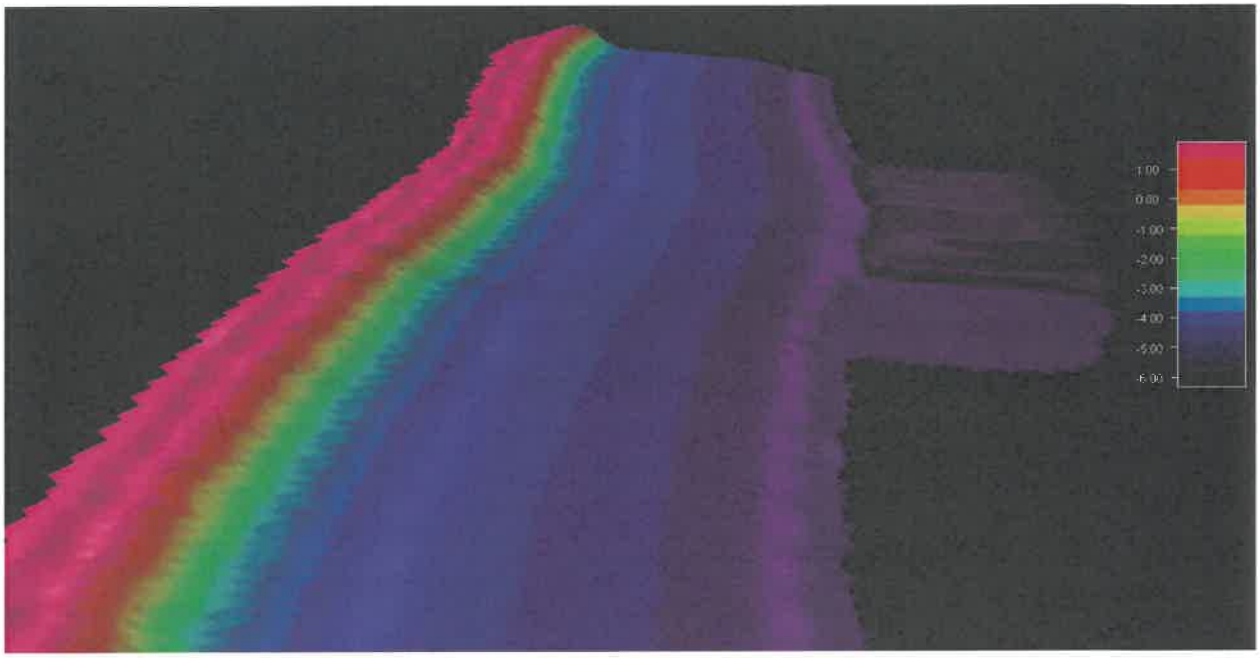

Figure 8. Base bathymetry in the area of Johns Pass constructed using beach and offshore profiles from the adjacent beaches, with 20X vertical exaggeration.

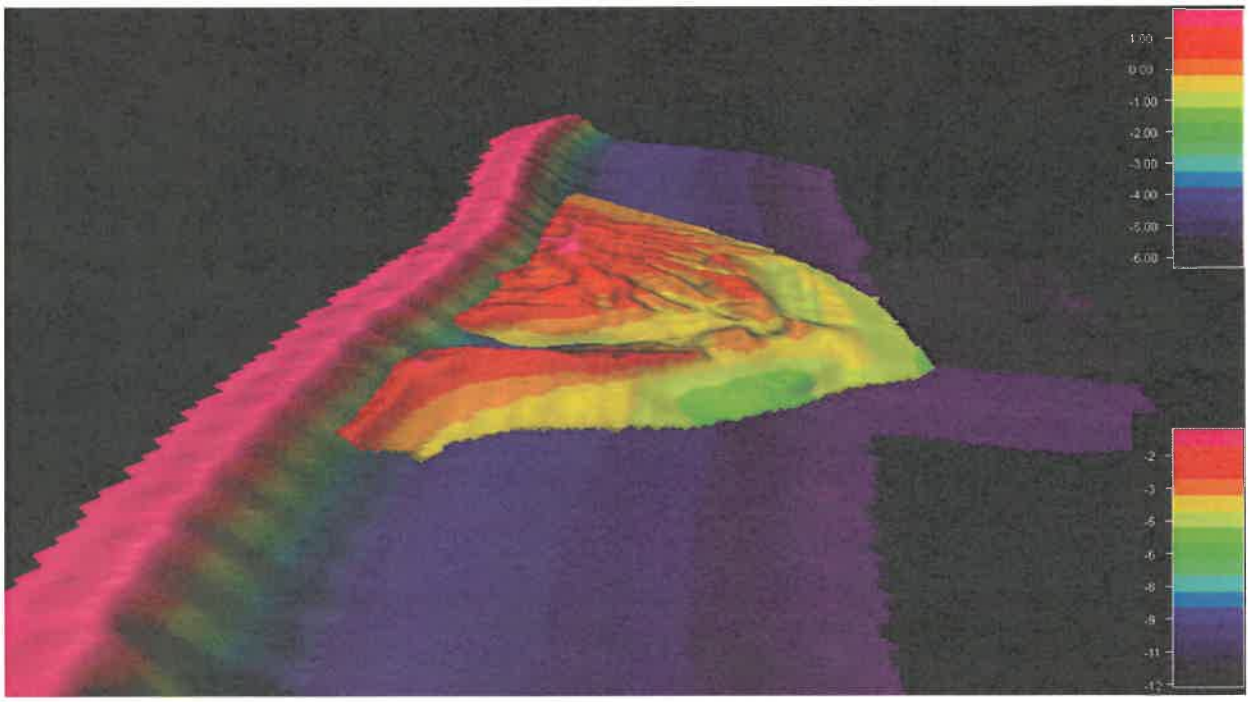

Figure 9. Johns Pass ebb shoal

2.4.2 Regional Sediment Budget at Johns Pass

The Wang et al. (2016) sediment budget for Johns Pass and Blind Pass are constructed based on data collected from October 2010 to June 2014. The surveys were performed after the dredging of Johns Pass and Blind Pass in 2010 (and associated beach nourishment on Treasure Island and Long Key) and before the following beach nourishments on Treasure Island and Long Key in 2014. In addition, Sand Key beach to the north, and updrift, of the Johns Pass and Blind Pass system was nourished in 2012. Therefore, the sediment budget is influenced by the artificial sand supply from the 2010 Treasure Island and Long Key beach nourishments and 2012 Sand Key nourishment. Since the beaches in the study area are nourished regularly and the budget period incorporates a large portion of a beach nourishment cycle, the Wang et al. (2016) sediment budget should represent a period when artificial sand supplies from beach nourishments are incorporated. The total budget period was 44 months, or 3.7 years, started immediately after the channel dredging and beach nourishment in 2010 and ended right before the 2014 nourishment. The budget duration was determined mainly based on the availability of field data (Wang et al., 2016).

The Johns Pass regional sediment budget formulation was bounded to the north at Profile R60 on Sand Key. Based on Sand Key beach-profile monitoring since 2006 (Roberts and Wang,

2012), profile R60 had the peak profile-volume loss along North Sand Key. This volume change pattern was interpreted as being caused by the diverging zone, north of which the net longshore transport was to the north toward Clearwater Pass while south of which the net longshore transport was to the south toward Johns Pass. Therefore, profile R60 was determined to be the north boundary for the formulation of John's Pass and Blind Pass regional sediment budget.

The Wang et al. (2016) regional balanced sediment budget for the entire Johns Pass and Blind Pass system is illustrated in Figure 10 and Figure 11. Figure 10 illustrates the entire sand budget over the 44-month (or 3.7-year) period. Figure 11 illustrates the annualized budget. Over the 44-month period, a total of 453,000 m^3 (593,000 yd^3) (or 122,000 m^3/yr (160,000 yd^3/yr)) of sand from Sand Key entered Johns Pass inlet system, including the ebb shoal, channel and immediate adjacent beaches. The 2012 Sand Key beach nourishment contributed significantly to the sand input. The Johns Pass inlet system gained 251,000 m^3 (328,000 yd^3) of sand over the 44-month period, or at 68,000 m^3/yr (89,000 yd^3/yr). A total of 202,000 m^3 (264,000 yd^3) of sand bypassed Johns Pass onto Treasure Island beach over the 44-month period, at 54,000 m^3/yr (71,000 yd^3/yr) annual rate. The entire Treasure Island beach lost 50,000 m^3 (65,000 yd^3) of sand over the 44 months, or at 14,000 m^3/yr(18,000 yd^3/yr). Most of the sand loss can be attributed to Sunset Beach.

Figure 10. Regional sediment budget of Johns Pass and Blind Pass system, in m^3.

Figure 11. Regional annualized sediment budget of Johns Pass and Blind Pass, in m^3/yr.

Figure 12 and Figure 13 illustrate detailed sediment budget within the Johns Pass inlet system. Here the Johns Pass inlet system is composed of the main channel and all the branches, the ebb shoal, the flood shoal, and the immediate adjacent beaches which include the south end of Sand Key (R121-R124) (i.e., Madeira Beach) and Sunshine Beach (R127-R129) at the north end of Treasure Island. The adjacent beaches were determined based on the extent of the ebb shoal. The south end of Sand Key gained a total of 37,000 m^3 (48,000 yd^3) of sand over the 44-month period (Figure 12), at an annualized rate of 10,000 m^3/yr (13,000 yd^3/yr) (Figure 13). This sand gain can be attributed to the 2012 beach nourishment on Sand Key and the net annual southward longshore transport.

The Johns Pass system receives 453,000 m^3 (593,000 yd^3) of sand from the Sand Key beach, or at an annualized rate of 122,000 m^3/yr (160,000 yd^3/yr). Within this amount, 37,000 m^3 (48,000 yd^3) was deposited at the south end of Sand Key; 270,000 m^3 (353,000 yd^3) was deposited on the Johns Pass ebb shoal; and 4,000 m^3 (5,000 yd^3) (or at roughly 1,300 yd^3/yr) was deposited within the main channel between the barrier islands. Combined with the sand volume loss of 60,000 m^3 (78,000 yd^3) from Sunshine Beach, a total of 202,000 m^3 (264,000 yd^3) of sand bypassed the Johns Pass system and contributed to the sediment budget on Treasure Island and further south (Figure 12). The annualized volume change rate is illustrated in Figure 13.

It is worth emphasizing here that the sand volume of roughly 1,000 m^3/yr (1,300 yd^3/yr) obtained by Wang et al. (2016) for the Johns Pass entrance channel might carry large uncertainties. The Wang et al. (2016) budget encompassed the entire Johns Pass and Blind Pass system with the goal of developing a budget for the overall system. The spatial resolution of the inlet management study at the Johns Pass interior channel was not adequate. However, the relatively small volume gain did not indicate massive sand input into the Johns Pass channel.

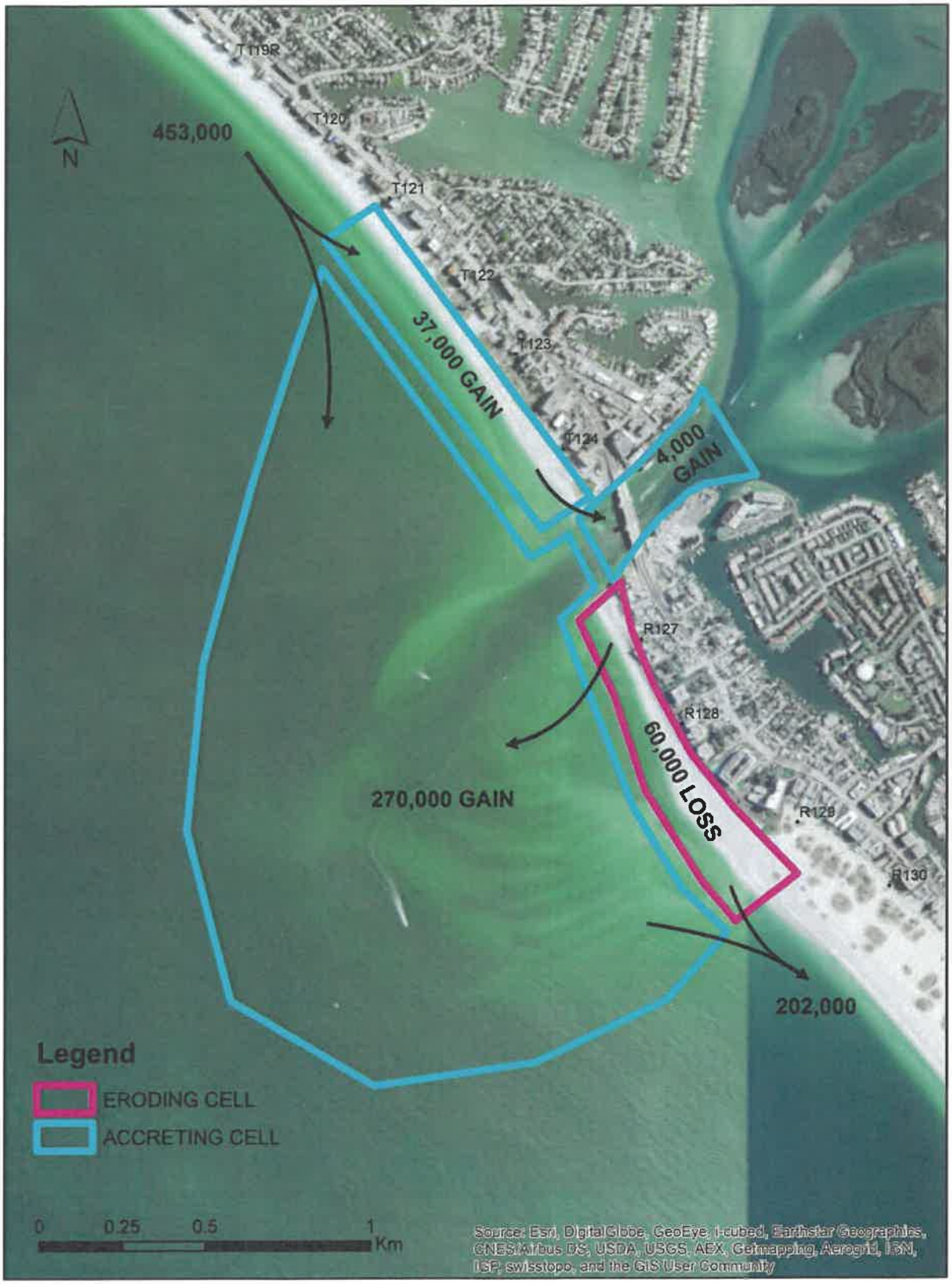

Figure 12. Sediment budget at Johns Pass, in m^3.

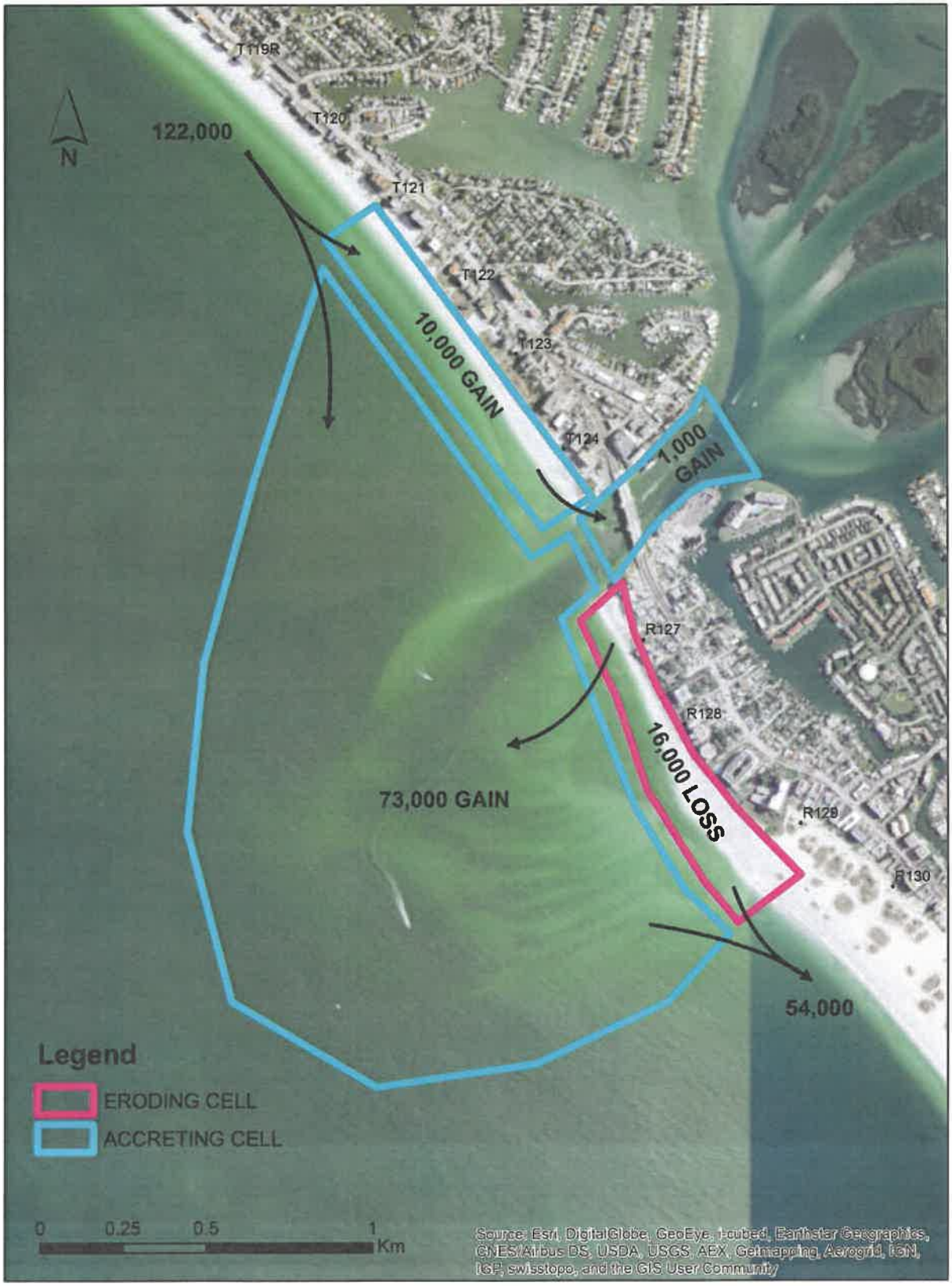

Figure 13. Annualized sediment budget at Johns Pass, in m3/yr.

3.0 Methodology

3.1 Analysis of Time Series Aerial Photos

This study compiled multiple aerial photos at Johns Pass dating back to 1926. These aerial photos provide valuable information on the changes at the inlet caused by natural processes as well as engineering activities.

3.2 Time Series Bathymetry

Bathymetry surveys of Johns Pass ebb shoal and entrance channel have been conducted by USF CRL since 2010. This large data set was used by Wang et al. (2016) to develop the sediment budget (Figure 10 through Figure 13) during the inlet management study. In this study, a focused analysis in the project area was conducted with the goal of obtaining a more accurate sedimentation rate than the estimate provided by Wang et al. (2016), which included the entire Johns Pass and Blind Pass system.

Figure 14 illustrates the survey coverage in June 2020. In anticipation of this study, an attempt was made to have dense coverage within the channel. However, due to the numerous boat docks and typically busy boat traffic, most of the project area could not be surveyed by the vessel. In addition, the RTK GPS could not obtain accurate position under the bridge, the positions of survey point shown in Figure 14 were interpolated, and therefore may carry considerable uncertainty. An Additional survey, shown in Figure 14 as scatter points in the project area, was conducted using a level-and-transit method. The survey coverage shown in Figure 14 was used to construct the numerical model.

The survey with the most areal coverage was conducted in 2014 using a multi-beam echo sounder during the inlet management study (Figure 15). Like the 2020 and other surveys (Figure 16), the 2014 survey coverage was limited by the boat docks and the bridge. In addition, the survey vessel could not get close to the north jetty. The poor coverage in the 2018 survey (Figure 16) was caused by the dredging operation during that time.

Due to the rather sparse survey coverage in the project area, in addition to the rather rapid and complicated depth changes, interpreted bathymetry between the shoreline (obtained from aerial photos and surveyed during this study) may carry large uncertainty. Therefore, reliable bathymetry changes in the project area, which would yield the sedimentation rate could not be

obtained based on the Johns Pass ebb shoal and channel surveys conducted by USF CRL, which was focused on the ebb shoal. Several land-based surveys were conducted during the study to monitor the accumulation and movement of the sand body. However, the surveys conducted during this study were limited by the short study duration and cannot provide longer term sedimentation rates.

Figure 14. Coverage of the bathymetry survey conducted in June 2020.

Figure 15. Coverage of the multi-beam bathymetry survey conducted in 2014.

Figure 16. Coverage of the multi-beam bathymetry surveys conducted in 2018 and 2019.

3.3 Field Data Collection

The field measurements collected during the study were designed to aid in understanding the sedimentation processes and to ensure that the numerical model have adequate spatial resolution and precise representation of the project site. The Johns Pass and Blind Pass numerical model constructed by Wang et al. (2016) during the inlet management study was for the entire dual inlet system. Due to surveying difficulties, some crucial details were not adequately resolved. In addition, the time-series bathymetry data collected by USF CRL during the inlet management study do not have adequate spatial resolution at the project site limited by the survey vessel accessibility. Four land-based surveys were conducted during the study at the project site to quantify short-term morphology changes at the project site.

Given the small study area relative to the entire Johns Pass and Blind Pass system, it was essential that the Wang et al. (2016) model be refined to accurately represent the important features at the project site. A precise land boundary was surveyed using a RTK GPS(Real-Time Kinematic

Global Positioning System), including the land boundary beneath the boardwalk (Figure 17 left panels) and the boundary defined by the jetty (Figure 17 top right panel). The section of seawall under the bridge and the inlet jetty were lined by a rock riprap, the slope and seaward edge of the riprap were also surveyed. Accurately capturing the configuration of the riprap was also important for designing the mitigation measures. The nearshore water depths directly seaward of the seawall or riprap were also surveyed. This provides at least one nearshore survey point to interpolate with the vessel-based channel survey (Figure 14). This allows for accurate representation of the nearshore bathymetry.

Figure 17. Survey of land boundary and the bridge piling positions using RTK GPS.

As apparent from the top right panel of Figure 17, the bridge pilings represent significant features within the inlet channel and may have significant influence on the flow field pattern in the project site. The footprints of the bridge pilings were surveyed during this study (Figure 17 lower right panel) to ensure that the dimensions of the pilings were accurately captured by the numerical

model. The Wang et al. (2016) model was calibrated and verified with current measurements in the main channels of Johns Pass and Blind Pass.

To ensure that the model yields accurate current velocities at the project site, short-term current measurements were conducted between the shoreline and the north most bridge piling. A considerable amount of rocks is distributed between the shoreline and the bridge piling, which may change the bottom friction. The measured tidal current velocities were also used to define the friction coefficient in this area (Figure 18) to ensure the numerical model captured this local condition.

Figure 18. Short-term tidal current measurement at the project site.

Four surveys were completed during this study, on December 22, 2020, February 24, 2021, March 29, 2021 and May 12, 2021, to quantify the morphology changes at the project site. The December 2020 survey did not extend seaward of the bridge, while the other three surveys

extended further seaward. The measured spatial patterns of sand accumulation and erosion are shown in Figure 36 through Figure 38.

3.4 Numerical Model for Johns Pass

The numerical model used in this study was modified based on the model constructed by Wang et al. (2016) during the inlet management study. The initial model construction was discussed in the detail by Wang et al. (2016). Figure 19 illustrates the overall grid. To maximize the computation efficiency, the domain is composed of grids of different sizes. In the offshore area, the grid size is 320 x 320 m (1050 x 1050 ft). This very large grid size was reduced to 20 x 20 m (66 x 66 ft) in the nearshore and ebb shoal area, as well as in most of the back-bay area. The grid size was further reduced to 10 X 10 m (33 ft) at the inlet channel and the Intracoastal Waterway. To better resolve the shoreline and the sand body at the project site, the grid size was reduced to 2.5 X 2.5 m (8.2 ft) (Figure 20). This very small grid is capable of accurately resolving the shoreline position, the north most bridge piling, the riprap along the jetty and seawall, and the emerged and intertidal portion of the sand body. However, the 2.5 m grid is still too large to resolve smaller features such as dock support pilings and pilings for boat tie downs.

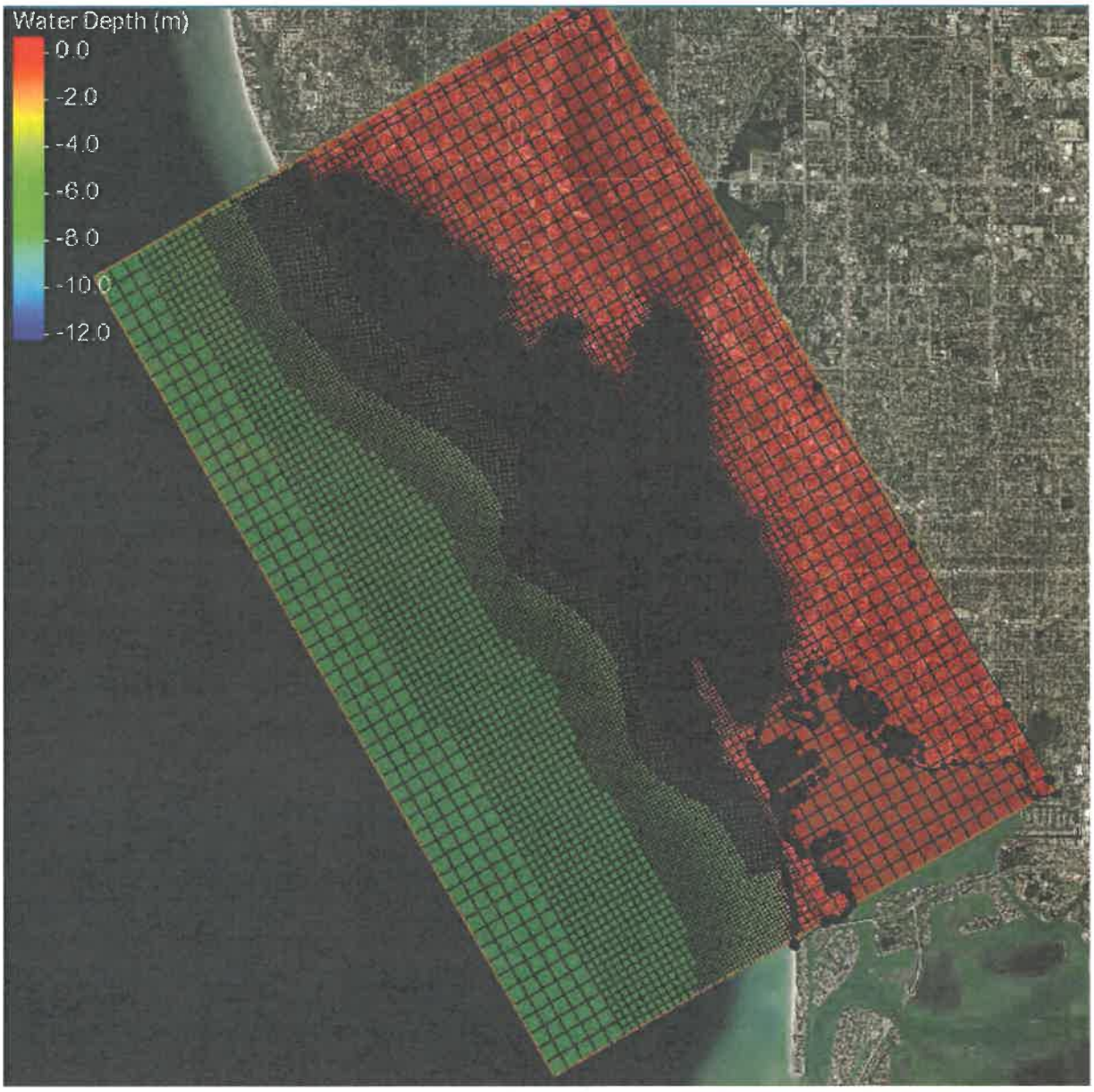

Figure 19. Overall coverage of the Johns Pass and Blind Pass model.

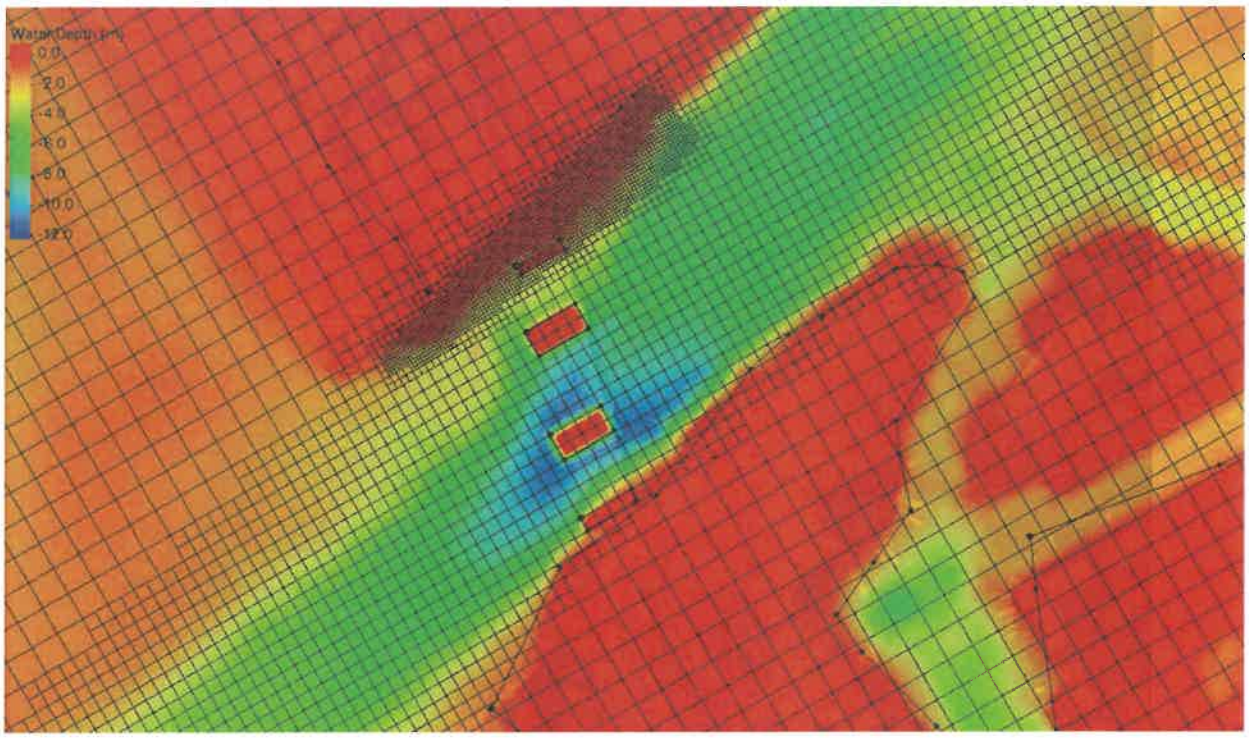

Figure 20. Small modeling grid of 2.5 X 2.5 m (8.2 ft) at the project site.

The telescoping grid described above accurately represented bathymetry of the entire study area (Figure 21), as well as at the project site. The Intracoastal Waterway, which has significant influence on the tidal circulation pattern within the bay (Wang et al., 2016), is well captured. The shallow channel margin linear bar, which has substantial influence on wave propagation, is also well represented. This modeling grid is used in all the circulation simulations. The 1-month tide record measured during the inlet management study (Wang et al., 2016) was used in this study to compute the tidal current velocities at the project site. The measured tidal fluctuations were used in the modeling, instead of computed tides, to provide more realistic simulations.

Figure 21. Detailed bathymetry resolved by the modeling grid.

The numerical model constructed by Wang et al. (2016) during the inlet management study was well calibrated and verified using the Willmott (1981) model skill. The local modifications conducted by this study had minimal influence on the computed flow velocity over the entire system, as expected. The same calibrated friction coefficient of 0.025 (Manning's n) was used over most of the domain, except over the very small area between the north most bridge piling and the shoreline (discussed in the following). The computed flow velocity in the Johns Pass main channel matched the measured velocity very well (Figure 22), similar to the results from the inlet management study (Wang et al., 2016). In addition to resolving the detailed features at the project area, the numerical model used in this study also included updated bathymetry of Johns Pass and

Blind Pass channels and ebb shoals as surveyed in 2020. It is worth noting that the current velocities shown in Figure 22 were computed using the 2014 bathymetry to be consistent with the measured data for model verification. The minor modification of the channel and ebb shoal bathymetry should not have any significant influence on the flow computation.

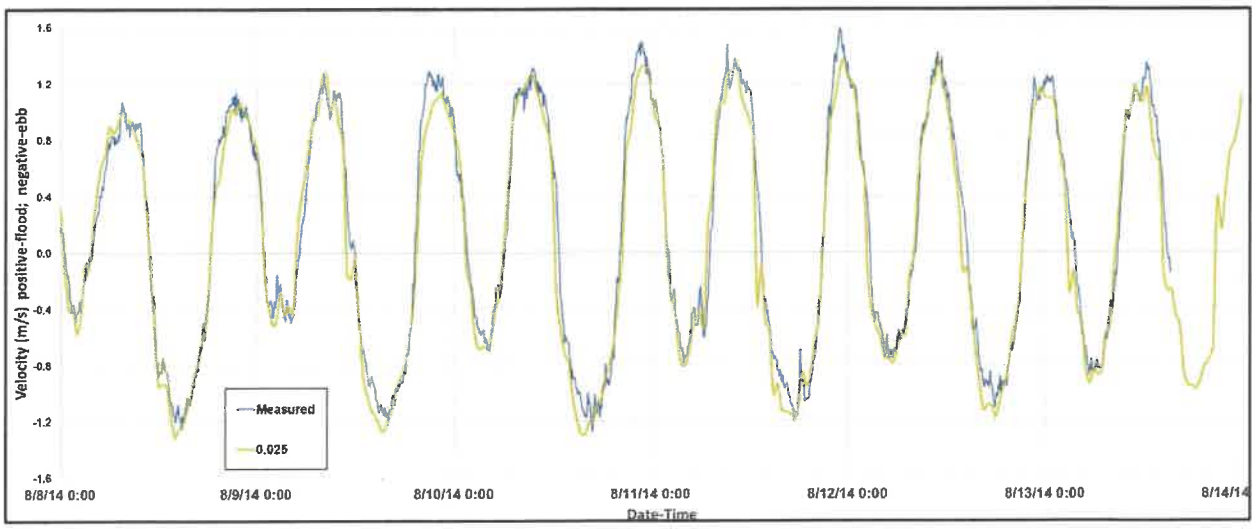

Figure 22. Measured and computed flow velocity at Johns Pass main channel.

Additional verification runs were conducted at the project site to ensure that the John Pass Blind Pass model yields accurate velocities. These additional verification runs were based on current measurements collected during the study (Figure 23 red dots). Because the area between the bridge piling and the shoreline, yellow highlights in Figure 23, is covered with scattered rock debris, the drag force over the tidal flow may be greater than the typical sandy bottom. Therefore, greater friction coefficients, as compared to the 0.025 Manning's n used in the rest of the domain, were applied for this local area. Overall, the computed velocities matched with the measured velocities well at both locations. As expected, greater friction coefficient resulted in slower computed velocity. The friction coefficient of 0.055 yielded the closest match with the measured velocities at both locations based on the Willmott (1981) model skill (Figure 24 and Figure 25). This value was used in the yellow highlighted area in Figure 23 in the existing-condition model runs in this study.

Figure 23. Additional verification of the modified model focusing on the project site.

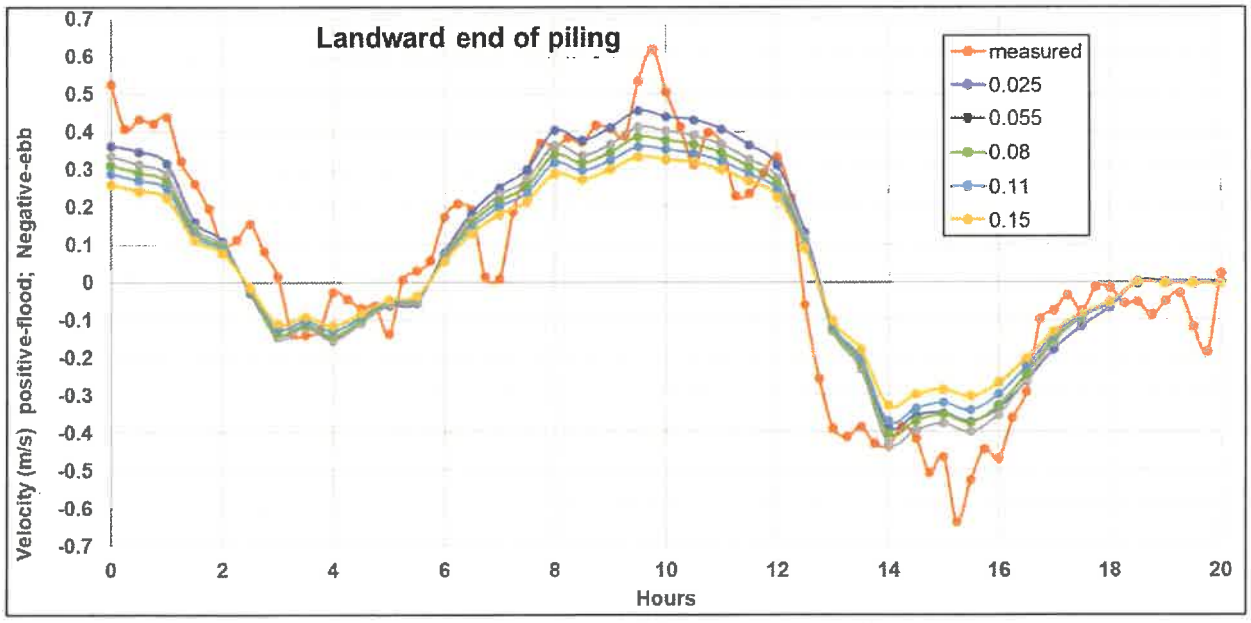

Figure 24. Measured versus computed velocity with different friction coefficients near the bridge piling.

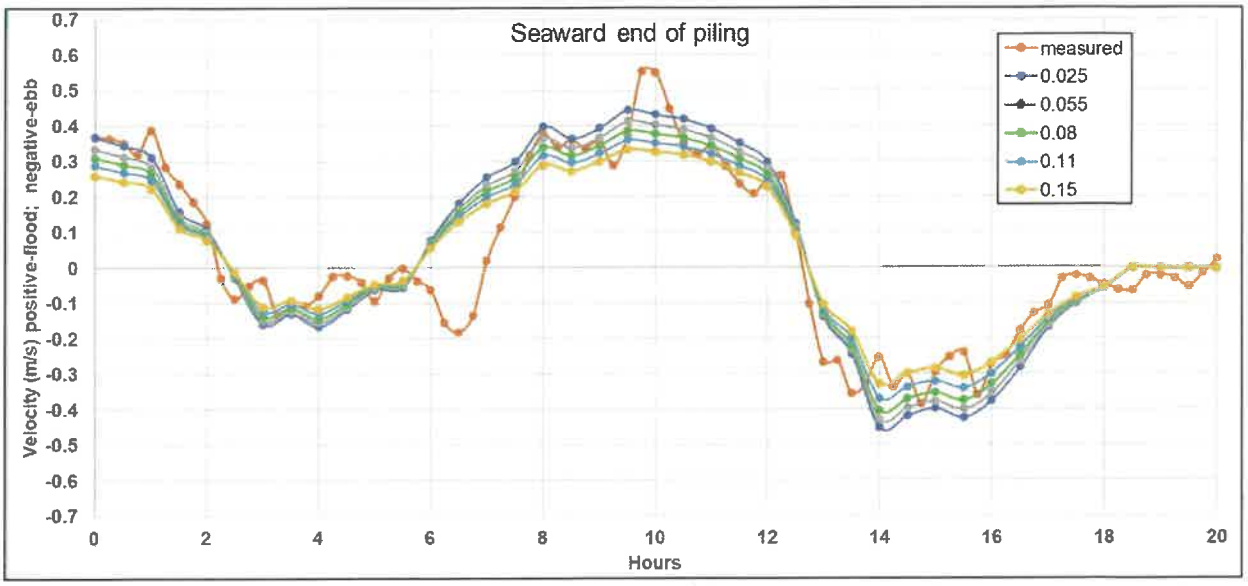

Figure 25. Comparing measured and computed velocity with different friction coefficients near the bridge piling.

4.0 Findings

4.1 Analysis of Time Series Aerial Photos

In this section, the time-series photos are described with the goals of depicting the sedimentation within the entrance channel and potential cause of the sand infilling. Time-series bathymetry surveys of Johns Pass ebb shoal were conducted by USF CRL since 2010. The bathymetry data was compared to identify changes at the Johns Pass channel.

4.1.1 Pre-Engineering Condition

The earliest aerial photo of the greater study area was taken in 1926 (Figure 26). The entire area is mostly pristine with practically no engineering alterations. In this, and all the later aerial photos, a red eclipse is used to mark the general project area, located along the north bank of the inlet. Under natural conditions, it appears that a sandy beach distributed along the interior shoreline. Sedimentation along the updrift bank of an inlet channel is common for natural inlets, as was the case at Johns Pass.

Although not visible on the 1926 aerial photo, the first Johns Pass Bridge and the road on Sand Key and Treasure Island were completed shortly after. By 1942 (Figure 27), portions of the two islands adjacent to Johns Pass have become quite densely developed. The marina had not been constructed at that time. A sand body at the end of Madeira Beach protruded into the Johns Pass entrance. This morphology reflects the active interaction between southward sand transport and the tidal flow through the inlet channel and illustrates a common morphodynamic balance at tidal inlets, i.e. inlet stability (Bruun et al., 1978).

In general, longshore transport tends to bring sand into the inlet, while tidal flow through the inlet tends to flush the sand in and out of the main channel between the two barrier islands forming flood shoals and ebb shoals. If longshore sand transport overwhelms tidal flushing, the inlet channel would become filled in or be pushed to migrate in the downdrift direction, as is the case of Blind Pass. If tidal flushing is strong enough to flush the sand out of the inlet, a large ebb shoal would form, and the inlet would remain stable. However, localized sedimentation may still occur depending on the specific channel configuration which is the case at Johns Pass.

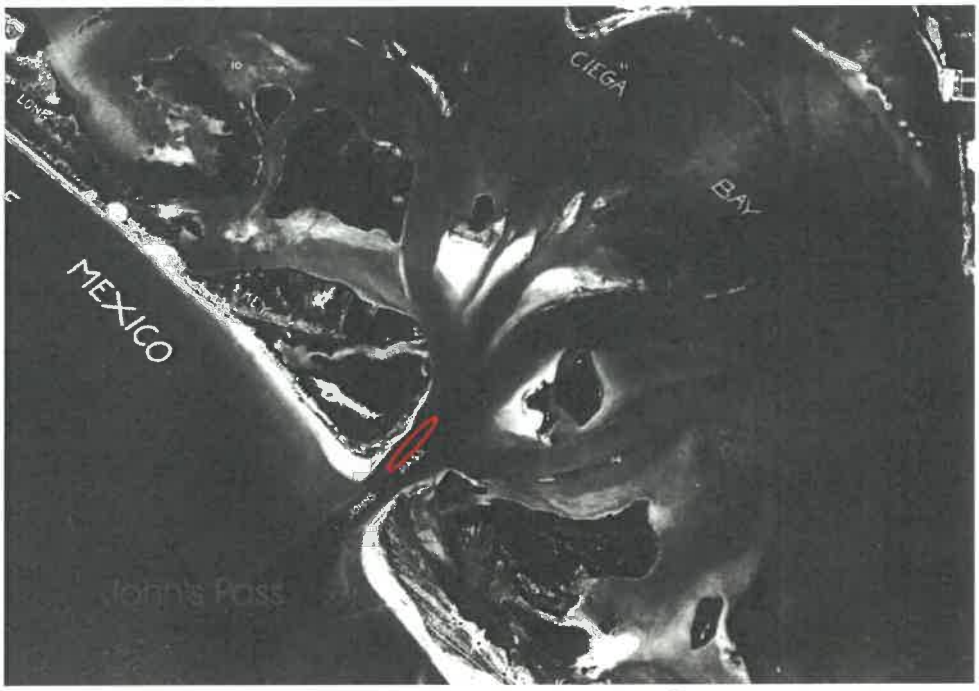

Figure 26. 2016 aerial photo of Johns Pass.

Figure 27. 1942 aerial photo of Johns Pass.

4.1.2 Engineering Activities

Engineering activities can influence inlet stability in various ways by modifying the natural processes as briefly introduced above (Mehta, 1993; Bruun et al., 1978). Here, a brief summary is presented to provide some context for the following discussion on Johns Pass channel sedimentation. Engineering activities at tidal inlets can be categorized into two general groups: hard structures and soft structures. Hard engineering structures used at tidal inlets typically include jetties, seawalls, groin fields along adjacent beaches, and breakwaters. Except breakwaters, all the above structures had been installed at Johns Pass. Hard engineering structures were commonly used in the 1940s through the early1980s. Due to their permanent nature, recent applications of hard structures have been very carefully evaluated to ensure that no prolonged negative impact would occur to adjacent or downdrift beaches. A large amount of hard engineering structures has been constructed at Johns Pass (Appendix I), as evident from aerial photos.

Soft engineering activities typically involve dredging and beach fill. Generally, dredging occurs to accomplish two goals: to improve the navigability of a channel or to extract sand for beach nourishment. As is the case for Johns Pass (Appendix I), earlier dredging projects tend to be designed to improve navigation safety, while more recent dredging projects were designed to provide sand for beach nourishment and to balance the sediment budget. Over the past four decades, beach fill has become the dominant method for beach erosion mitigation.

As apparent from the 1945 aerial photo (Figure 28), Madeira Beach was experiencing aggressive beach erosion. Two groins, marking the first shore protection structure, were installed to mitigate the erosion (Appendix I). The groins are not visible on the 1945 photo. The large sand body at the mouth of Johns Pass and along the interior of the channel as seen on the 1941 photo remained, illustrating the morphologic consequence of the natural process, i.e., longshore sand transport and flood currents, that brings sand into the interior of the channel.

Rapid human development in the vicinity of Johns Pass can be seen on the 1951 aerial photo (Figure 29). It appears that marina installation had occurred by that time. Different from the 1945 view of Madeira Beach, the depleted shoreline was replaced by a healthy-looking sandy beach. A rather extensive emerged sand body was present in the interior of the Johns Pass channel directly seaward of the developing marinas. The finger island dredge and fill operations had also started in the back bay.

Figure 28. 1945 aerial photo of Johns Pass.

Figure 29. 1951 aerial photo of Johns Pass.

The 1957 aerial photo (Figure 30) shows considerable changes at Johns Pass, as compared to the conditions in 1951. Aggressive erosion at Madeira Beach seems to have resumed, leading to the installation of the 37 low-profile groins, which still exists today. The sand accumulation directly seaward of the marina remained. A dredge-pit looking feature occurs directly channel-ward of the sand pile. However, no dredging record can be found in the literature (Appendix I). Given the active dredge and fill development during that period, sand removal from the shallow inlet entrance would not be unreasonable. As a matter of fact, the most striking change illustrated by the 1957 aerial photo is the aggressive dredge-and-fill development in the back-bay, converting a large portion of the mangrove environment into finger-channel islands. As discussed in the inlet management study (Wang et al., 2016), this finger-channel development resulted in a roughly 20% reduction of the back-bay area, and subsequently a 20% reduction in tidal prism.

It can be argued that 1960 and the following few years marks a new era of Johns Pass in that a series of significant engineering work was conducted with the main goal of improving the navigability of inlet. The 1964 authorization of Johns Pass as a federal channel was likely a main driver. The north jetty is visible on the 1960 photo (Figure 31), although the engineering record show that it was completed in 1961 (Appendix I). The first significant dredging project also occurred in 1960, with 94,000 cubic yards of sand removed from Johns Pass channel. The dredged sand was placed on the southern flank of the ebb shoal. This implies that the navigation channel had much higher priority at that time than adjacent beach. Otherwise, the sand would have been placed on eroding beaches, as is typical practice today. The exact dredging footprint is not clear. However, based on the navigation goal and the 1960 aerial photo, the Johns Pass channel between the two barrier islands and through the ebb shoal should be the focus. Comparing the 1960 aerial photo with all the previous ones, it is apparent that the channel between the two barrier islands was "cleared", which makes sense for navigation improvement. The emerged sand directly seaward of the marinas, as can be seen from all the previous photos, was removed. Although no direct record of dredging in that area can be found, it is more likely that the sand was removed through dredging than through flushing associated with the newly constructed north jetty. The dredge-pit looking feature directly channel-ward of the jetty support the dredging interpretation. Another 30,000 cubic yards of sand was dredged, likely from the Johns Pass channel, and was placed along the severely eroding Madeira Beach at that time Appendix I). Despite the erosion at Madeira Beach, the sand filled to the tip of the new jetty (Figure 32).

Figure 30. 1957 aerial photo of Johns Pass.

Figure 31. 1960 aerial photo of Johns Pass.

The 1962 aerial photo shows a "clean" Johns Pass channel with no emerged sand in the vicinity of the marinas (Figure 32). Perhaps the most significant feature relating to this channel sedimentation project that can be seen from the 1962 aerial photo is that the north jetty was filled to the tip just one year after its completion. This occurred despite the fact that Madeira Beach was experiencing severe erosion during that period of time. The completely filled north jetty would not have been effective in blocking sand from moving around the tip and entering the Johns Pass channel. The filled north jetty is observed on all the following aerial photos. Different from all the previous photos, the section of Madeira Beach directly north of the jetty appears to have been stabilized since 1962.

The next three decades since the mid-1960s is characteristic of a stable Madeira Beach and "clean" Johns Pass channel in the vicinity of the marina, accompanied by a rapid and substantial changes along the south side of the inlet. Severe erosion along the south bank of the inlet and the adjacent Sunshine Beach occurred, as apparent from the 1969 aerial photo (Figure 33). A series of seawall and revetments was constructed between the mid- and late-1960s, in addition to numerous beach and berm nourishment projects (Appendix I). A new bridge was constructed at a more seaward position than the old bridge. The 1969 photo (Figure 33) still shows the old bridge. The new bridge is shown in the 1971 aerial photo. As discussed in the inlet management study (Wang et al., 2016), the substantial morphology changes in the downdrift part of the channel and ebb shoal were likely the response to the Johns Pass channel work, e.g., realignment and straightening, in the 1960s which may have significantly altered the sediment bypassing mechanism and pathway.

From 1971 to 1993, the project area as depicted from the aerial photos appears rather similar over the 23-year period, with no visible sand emergence in the vicinity of the marinas. These photos are listed in the Appendix II (Figures A1 through A8). The north jetty remained filled to the tip during this time and Madeira Beach appeared to be quite stable. The large changes at the downdrift side of the inlet are not directly related to this project and were discussed in the inlet management study (Wang et al., 2016). All the aerial photos during this period are still provided here to illustrate the rather extended stable condition.

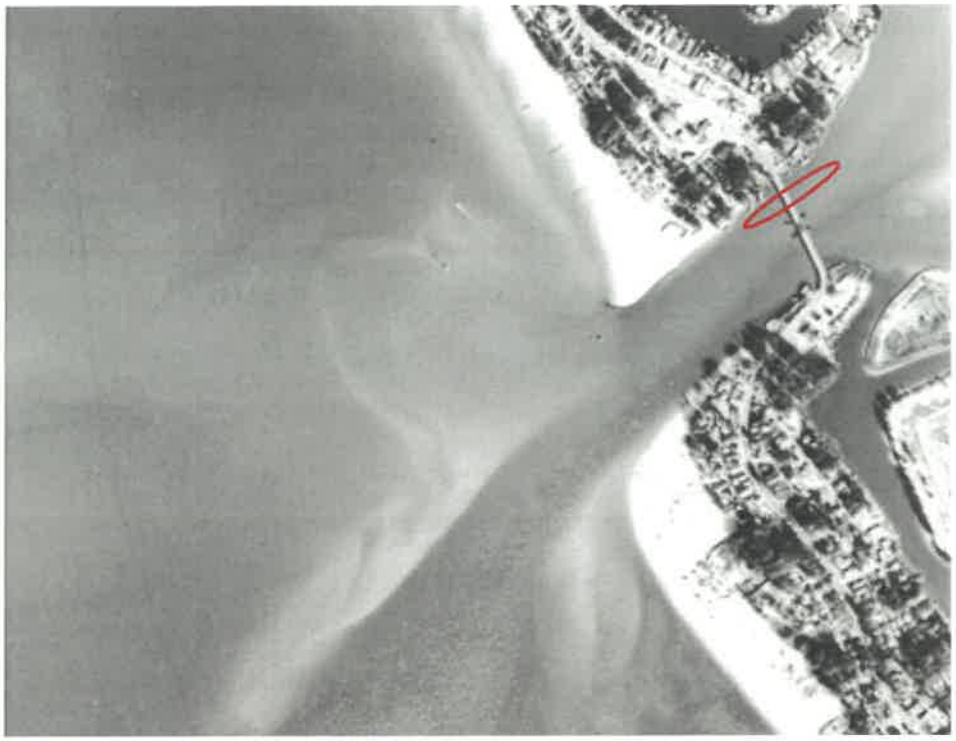

Figure 32. 1962 aerial photo of Johns Pass.

Figure 33. 1969 aerial photo of Johns Pass.

An emergent sand body was first seen on the 1998 aerial photo from Google Earth (Figure 34). Although the extent of the sand body visible from aerial photos can be influenced by the tide stage when the aerial photo was taken, a trend of accretion can be observed since then (Appendix I Figures A9 through A14). To mitigate aggressive erosion at Sunshine Beach and to increase the intervals of beach renourishment, the south jetty at John Pass was extended in 2000 following the substantial repair of the north jetty in 1987 (Appendix I). The rather intensive construction of hard engineering structures had largely stopped by the end of the 1960s after the installation of the seawall and revetments along the southern side of the channel (Appendix I). The extended south jetty in 2000 served as a terminal structure for the rather frequent Sunshine Beach nourishment, instead of a traditional inlet jetty with the purpose of stabilizing an inlet. It achieved its goals of improving the nourishment performance and extending the renourishment interval at Sunshine Beach, while not inducing negative responses from the inlet channel and the adjacent beach to the south, particularly in the vicinity of the attachment point (Wang et al., 2016).

Over the past 20 years, the most significant event occurring at Johns Pass inlet was the construction of the 3rd and present bridge. Likely influenced by the severe scour at the bridge pilings for the previous two bridges, the new bridge has much larger pilings. Near the completion of the new bridge in 2010 (Figure 35), an extensive emerged sand body both landward and seaward of the bridge is visible on the aerial photo. Subsequent photos show a reduction of the sand body, as compared to the 2010 situation. The influence of the bridge pilings on the inlet processes and sedimentation along the north bank is examined using numerical modeling and discussed in sub-section 4.2 Sedimentation Along Johns Pass.

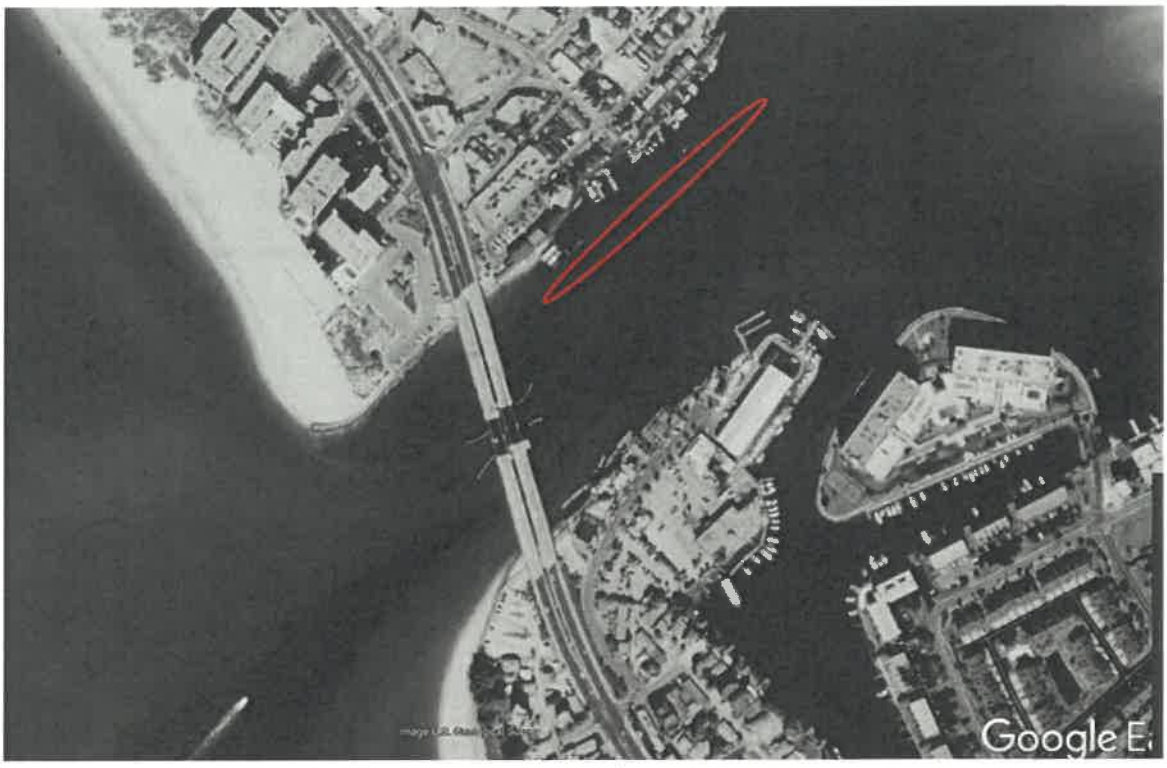

Figure 34. 1998 aerial photo of Johns Pass.

Figure 35. 2010 aerial photo of Johns Pass.

Another significant engineering activity over the past 30 years is the large-scale beach nourishment along the updrift Sand Key (Appendix I). As illustrated in the sediment budget developed by Wang et al. (2016), a considerable volume of the placed sand was transported southward and deposited on the Johns Pass ebb shoal. As discussed earlier, most of the sand was bypassed to the downdrift Treasure Island via natural processes or artificially through periodic channel and ebb shoal dredging and beach fill (Appendix I). The contribution of the additional sand supply from Sand Key beach fill to the sedimentation within the channel is not apparent from the analysis of the time-series aerial photos. As illustrated in Figure 2, channel interior sedimentation is caused by sand that is moved around the tip of the inlet jetty or landward from the shallow channel margin linear bar. As evident from the time-series aerial photos (Figure 26 through Figure 35, and Appendix II Figures A1 through A14), the shallow channel margin linear bar existed before the large-scale Sand Key beach nourishment. No apparent trend of a growing and shallower channel margin linear bar can be identified from the aerial photos since the 1990s suggesting that the nourishment did not cause significant change to the direct sand source for the channel interior sedimentation.

Approximately one year after the completion of the north jetty, the beach extended to the tip of structure, which would allow the sand to be transported around the jetty and enter the inlet. The north jetty remained to be filled to the full capacity since 1962 and is about the most consistent feature easily identifiable from all the subsequent aerial photos (Figures 23 through 26, and Appendix II Figures A1 through A14). Therefore, the influence of the beach fill to this sand pathway around the north jetty cannot be evaluated based on the time-series aerial photos. In other words, the north jetty was filled to the seaward tip before the large-scale beach nourishment began and the recent Sand Key nourishment did not result in any significant change of the beach condition at the jetty. Although it is reasonable to assume that the Sand Key beach nourishment projects could contribute more sand to the Johns Pass interior sedimentation, no apparent evidence can be identified from the time-series aerial photos.

4.2 Sedimentation Along Johns Pass

Comparing the bathymetry surveys conducted by USF CRL in 2019 and 2020 (Figure 16 and Figure 14), a sedimentation of roughly 1,200 cubic yards occurred seaward of the bridge. This rate is comparable with the rate (1300 cubic yards per year) obtained by Wang et al (2016) for the

regional sediment budget. Combined with the negligible net change landward of the bridge, the 1,200 cubic yards per year is used here as the infilling rate along the northside of the Johns Pass channel. The measured spatial patterns of sand accumulation and erosion are shown in Figure 36 through Figure 38.Overall, no persistent trend of sand accumulation was measured during the five-month period. Instead, patterns of erosion and deposition were measured. From December 2020 to February 2021, a distinctive pattern of deposition and erosion was measured (Figure 36). Considerable sedimentation was measured near the landward end of the Johns Pass bridge north piling, encroaching toward the boat basins. This landward movement of sand was caused by landward directed waves associated with wave breaking over the shallow shoal. Sand accumulation under the bridge was also measured.

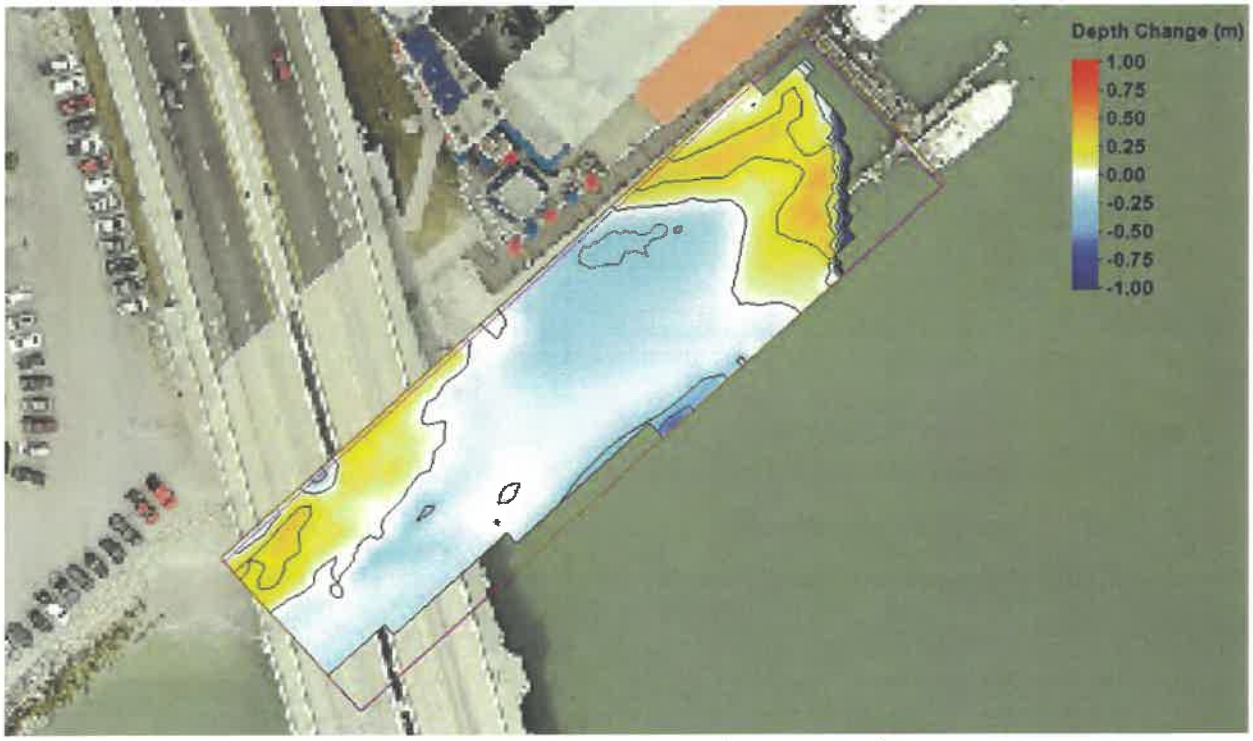

Figure 36. Sedimentation and erosion pattern measured between 12/22/2020 and 02/24/2021.

The sedimentation and erosion pattern measured between 02/2021 and 03/2021 (Figure 37) is more complicated than that during the previous period (Figure 36). However, the landward encroaching of sedimentation continued. Field observation during the survey showed that the sand had extended landward of the first boat dock and into the boat basin and was apparently influencing the boating operation. Also like the previous period, the encroaching sand came from the erosion of the shallow shoal from the seaward end.

Figure 37. Sedimentation and erosion pattern measured between 02/24/2021 and 03/29/2021.

The sedimentation and erosion pattern measured between 03/2021and 05/2021 (Figure 38) is quite different from those measured during the previous two periods (Figure 36 and Figure 37). The erosion in the immediate vicinity of the boat basin and the adjacent sedimentation might be caused by the boat operations.

The net sand-volume changes during the three periods are all negative indicating an overall loss of sediment, ranging from 100 cubic yards to 180 cubic yards. The net volume losses are quite small and likely within the range of survey uncertainties. Figure 38 shows the survey coverage. Although dense points were surveyed, the small net volume changes are likely within the range of interpolation uncertainties. Over the nearly 6-month monitoring period, no trend of sedimentation was measured landward of the bridge although considerable sediment redistribution occurred. This suggests that if sand removal is proposed as a mitigation measure, the entire shoal should be removed to prevent the rather rapid sand redistribution.

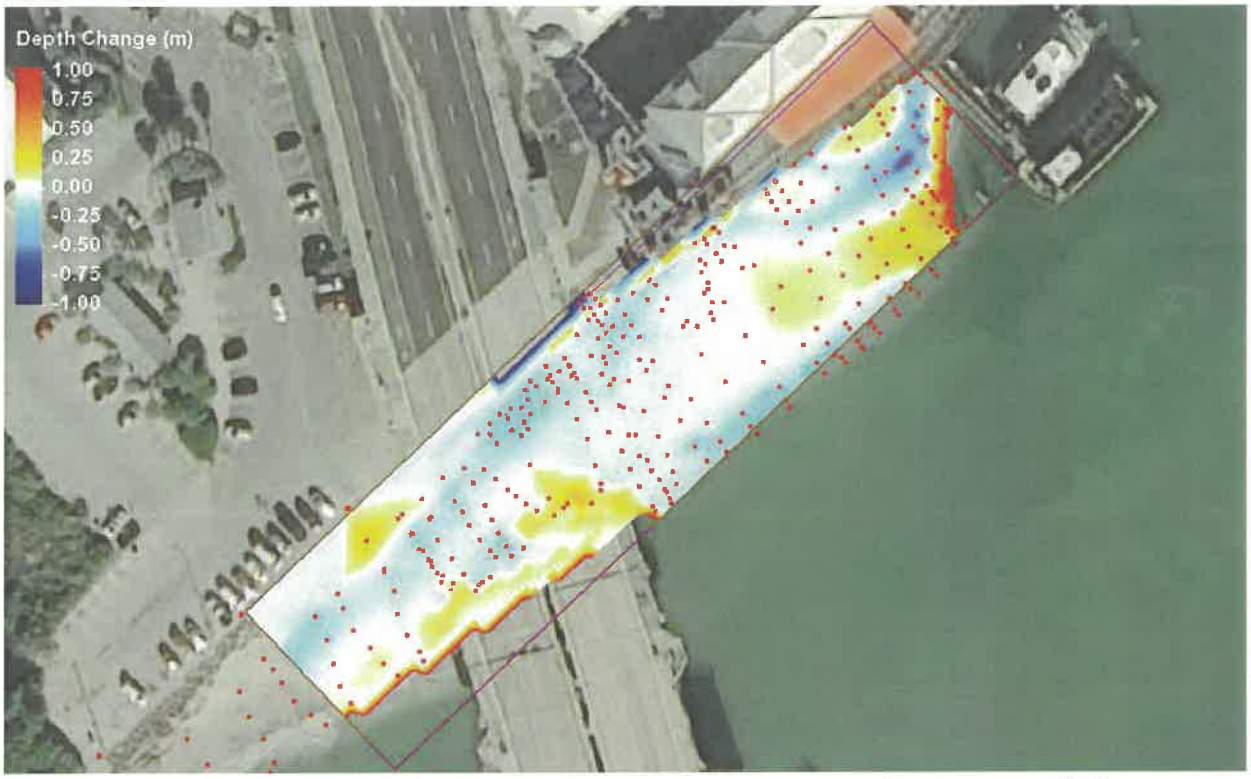

Figure 38. Sedimentation and erosion pattern measured between 03/29/2021 and 05/12/2021.

4.3 Modeled Flow Patterns

4.3.1 Modeled Flow Patterns under Existing Conditions

Tidal flow, especially flood tidal flow, plays a major role in transporting and depositing sand in the project site. Figure 39 and Figure 40 illustrate the modeled flow field under a peak ebb flow condition and a peak flood flow condition, respectively. The upper panels show the entire Johns Pass channel and the lower panel show a zoomed-in view of the project site. Overall, the ebbing flow follows a rather different pattern than the flooding flow (Figure 39 and Figure 40 upper panels). The ebb current, which is also often referred to as the "ebb jet," extends much farther into the sea as compared to the spatial pattern of the flood current. The flood flow tends to converge into the inlet with a faster velocity along the beach. This alongshore flowing flood current, in addition to wave generated longshore sand transport, provides the main mechanism to bring sand into the inlet channel. The sand that is brought into the channel is subsequently flushed out by the ebb current and may deposit on the large ebb shoal. The sand can also be brought further into the bay and deposit on the flood shoal. The spatial flow pattern within the inlet channel controls where the sand may be transported to and deposited at. The lower panels of Figure 39 and

Figure 40 illustrate zoomed-in view of the peak ebb and flood flows in the main channel. The tidal flow, both ebb and flood, in the vicinity of the project site, i.e., along the northern side of the channel, is considerably weaker than flow in other areas of the channel. This generally weak tidal flow explains the sedimentation in that area. The weak flow might also be the reason that the marinas were installed in that area in the first place. The tidal flow at the entrance and in the vicinity of the marina is further analyzed in the following.

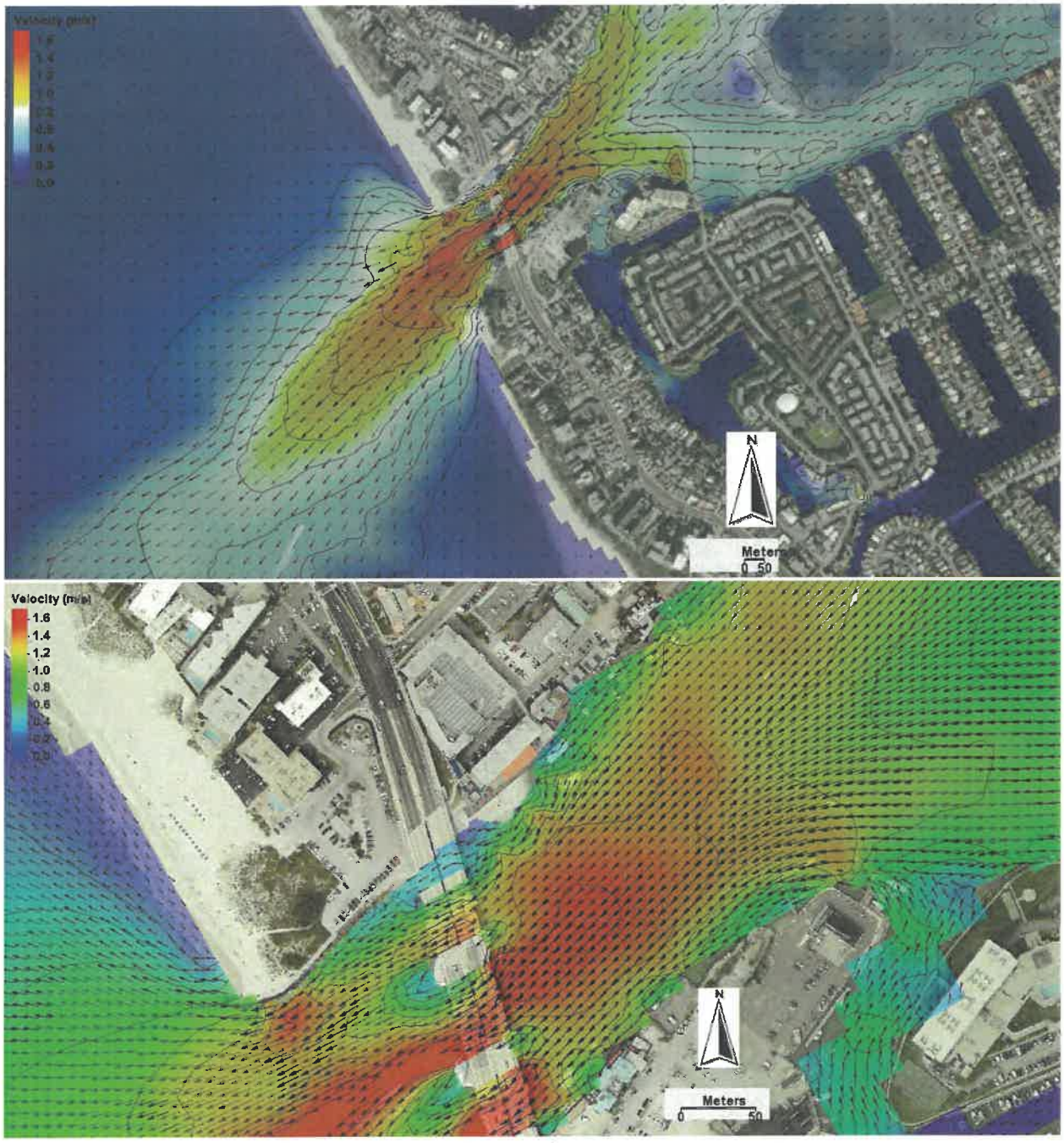

Figure 39. Computed flow field under a peak ebbing tide.

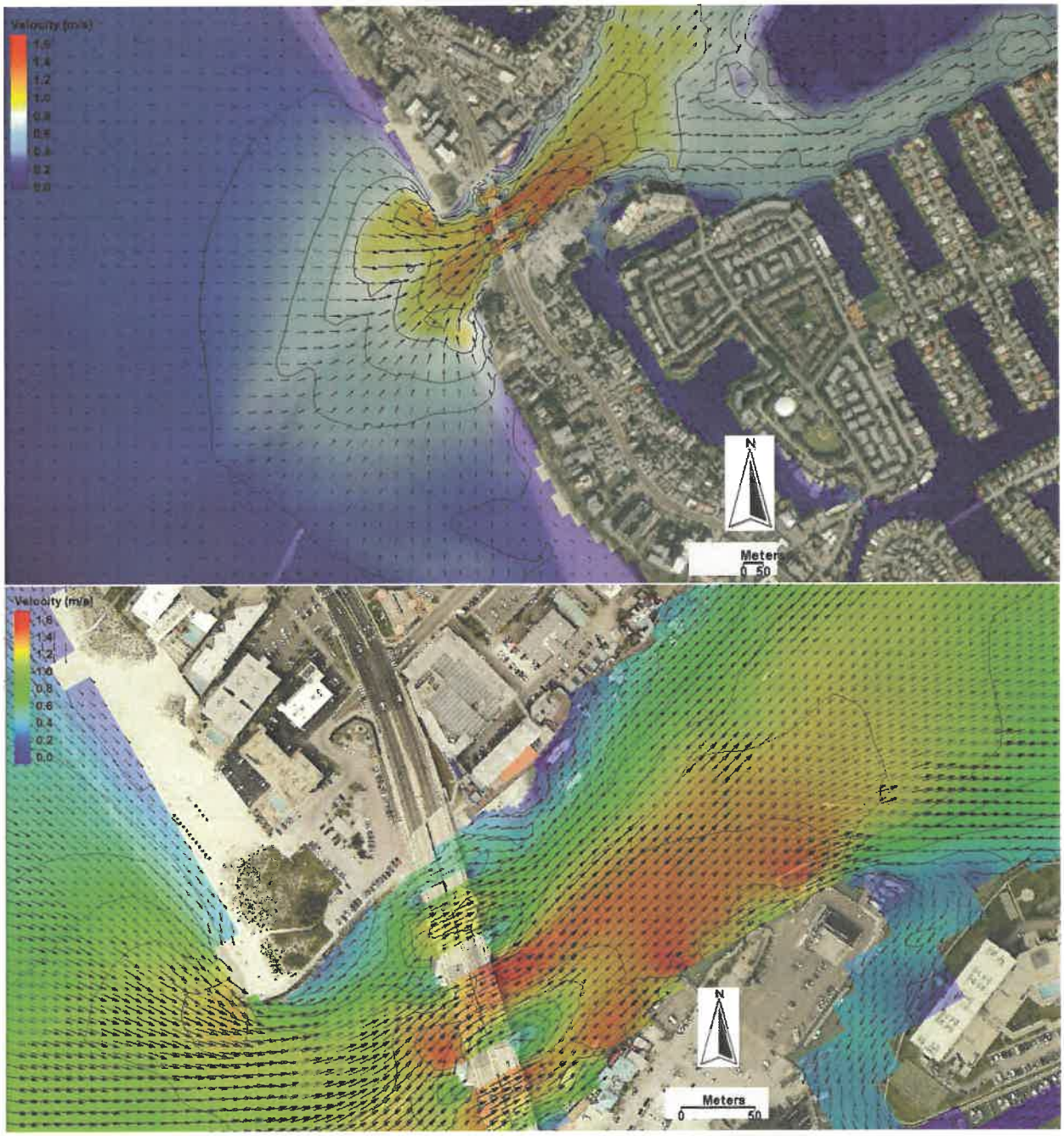

Figure 40. Computed flow field under a peak flooding tide.

Figure 39 and Figure 40 illustrate a snapshot of the flow field under peak ebb and flood conditions respectively. Here, temporal variations of tidal flow at six strategically selected locations are discussed. The six locations, referred to as "current stations", along the northern side of the entrance and in the area of sedimentation are shown in Figure 41. Station 1 is located at the entrance to Johns Pass. Stations 2 and 3 are further insider the channel. Stations 4 and 5 are in the area of active sedimentation. Station 6 is located immediately landward of the sedimentation area. The flow conditions at these six locations should provide insights on the trend of landward or seaward sand transport by tidal currents.

Figure 41. Six locations where time-series of tidal flow are extracted from numerical model

The computed tidal flow fluctuations over a ten-day period at the six stations are shown in Figure 42 through Figure 47, where positive velocity represents flood current and negative represents ebb current. Strong tidal flow was computed at Station 1, reaching over 1 m/s during

both flooding and ebbing tides (Figure 42). At this location, the average flooding current over the 10-day period is 0.66 m/s, which is faster than the average ebbing current of 0.57 m/s. This is consistent with the flooding and ebbing flow pattern as shown in Figure 39 and Figure 40. The converging flood current (Figure 40 upper panel) at the entrance results in an overall faster velocity than the jetting ebb current (Figure 39 upper panel). This stronger flood flow tends to transport sand into the inlet channel and therefore constitutes a major mechanism for interior sedimentation.

At station 2 (Figure 41 and Figure 43), the ebb current reaches over 1 m/s, which is much stronger than the flood current that is generally slower than 0.5 m/s. The average ebb flow over the 10-day period is 0.56 m/s, more than 2.3 time the average flood flow of 0.24 m/s. The much stronger ebb flow should lead to effective flushing of sand entering the inlet. In other words, imbalanced ebb and flood currents at this entrance location may serve to effectively prevent sand from being transported further into the inlet. The much stronger ebb flow is related to the bridge pilings.

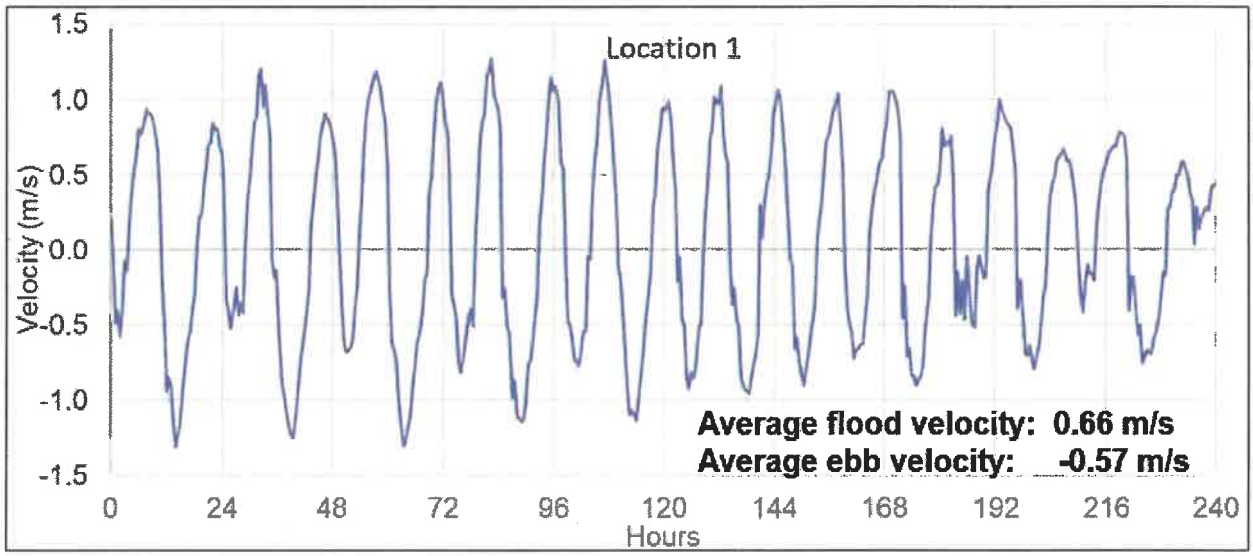

Figure 42. Computed tidal flow velocity at Station 1 (see Figure 41 for the location).

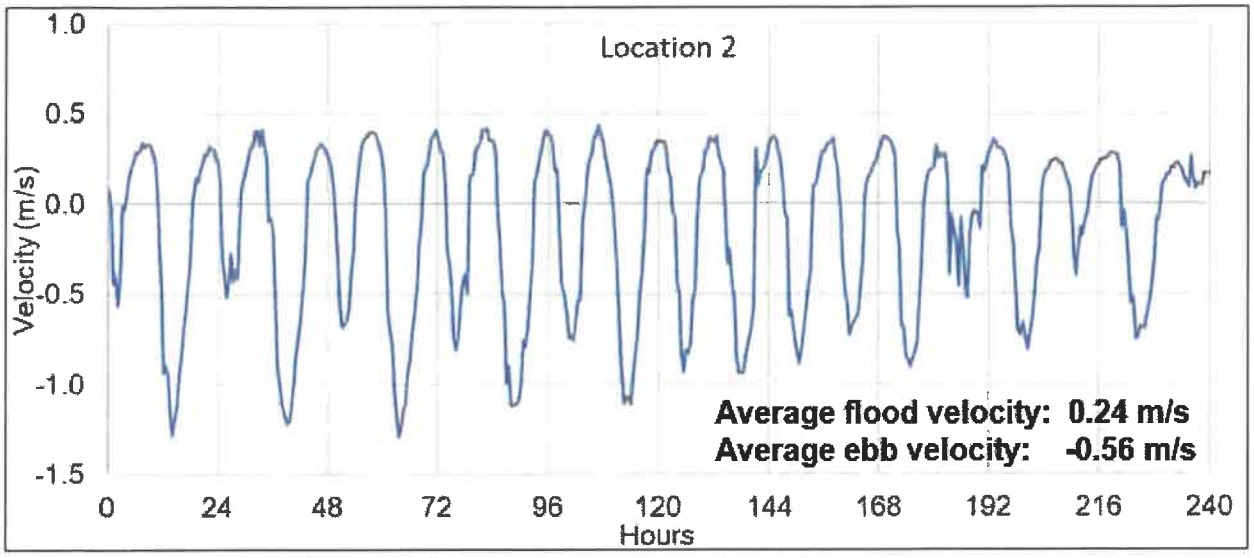

Figure 43. Computed tidal flow velocity at Station 2 (see Figure 41 for the location).

As compared to the two seaward stations discussed above, the tidal flow at Station 3 is considerably weaker (Figure 41 and Figure 44), with flood and ebb velocity mostly slower than 0.4 m/s and 0.6 m/s, respectively. The average ebb current is 0.28 m/s, or about 27% faster than the average flood current of 0.22 m/s. Therefore, similar to Station 2, there is still a tendency of ebb flushing at this location.

Station 4 is located directly seaward of the bridge (Figure 41). The computed tidal current at this location is significantly different from that at Station 3. The flood current reaches nearly 0.7 m/s, which is much stronger than the ebb current which is mostly slower than 0.4 m/s (Figure 45). The average flood flow is 0.31 m/s, which is more than twice the average ebb flow over the 10-day period. These measurements show the ebb flushing tendency at the two further seaward locations is replaced by a strong tendency of landward transport, which would directly contribute to the sedimentation at the project site. The flood-current skew also occurs at Station 5, directly landward of the bridge (Figure 46). The tendency for landward sand transport by a dominant flood current therefore continues across the bridge, and likely to the seaward edge of the marina. Stations 4 and 5 are located in the present sedimentation area with rather shallow water. Both stations, particularly Station 5, would become emerged near low tide, which results in no velocity (referred to as "drying" in the numerical modeling). This is the reason for the gaps in the velocity curves.

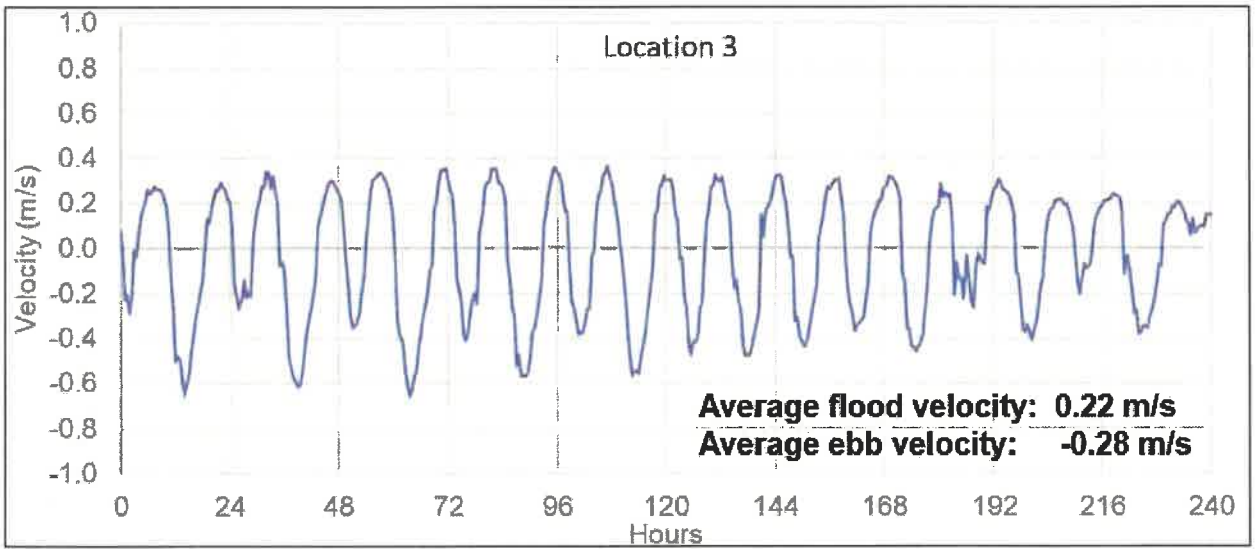

Figure 44. Computed tidal flow velocity at Station 3 (see Figure 41 for the location).

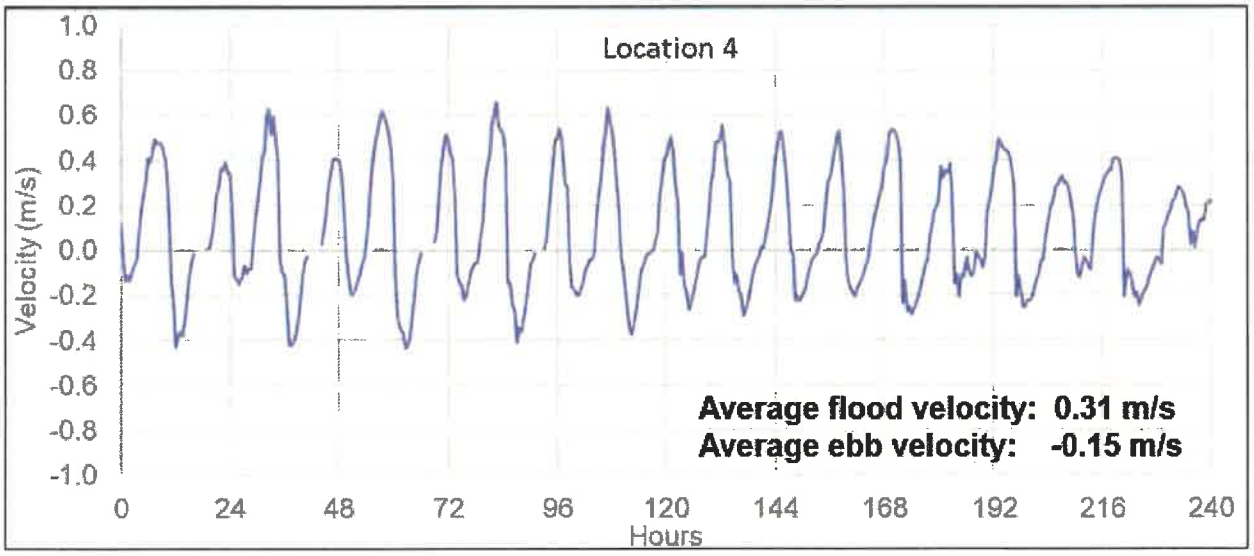

Figure 45. Computed tidal flow velocity at Station 4 (see Figure 41 for the location).

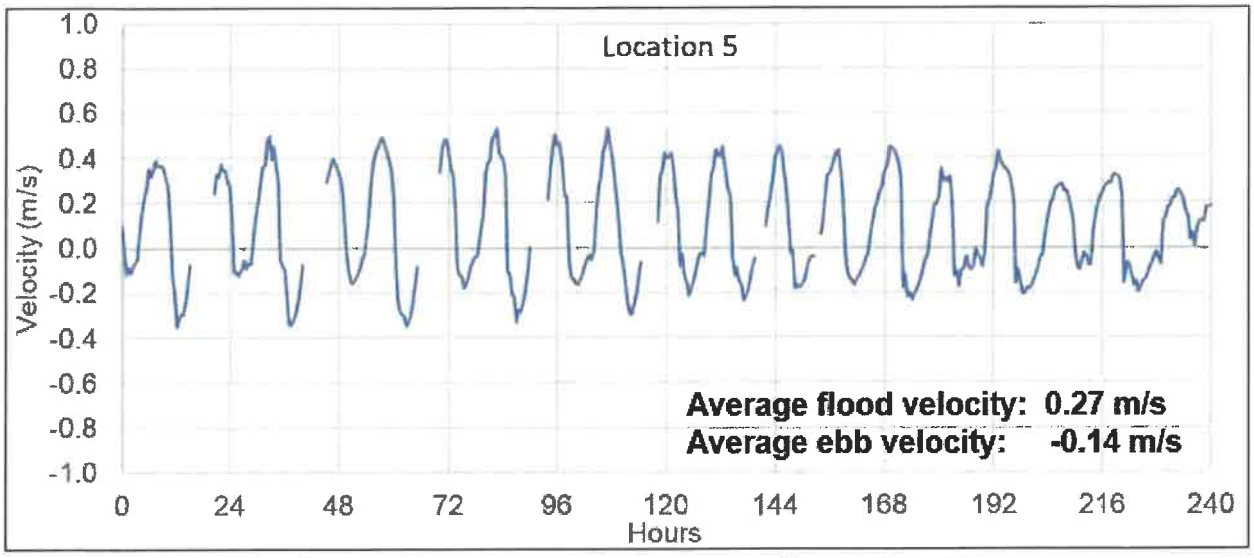

Figure 46. Computed tidal flow velocity at Station 5 (see Figure 41 for the location).

The landward transport preference ends at Station 6 (Figure 41 and Figure 47), where the ebb flow becomes much faster than the flood flow. The ebb flow reaches near 1 m/s versus the flood flow which was predominately 0.3 m/s. The average ebb current at Station 6 is 0.41 m/s, nearly 3 times faster than the average flood flow of 0.14 m/s. This ebb dominance may serve to prevent sand from being carried into the inlet farther.

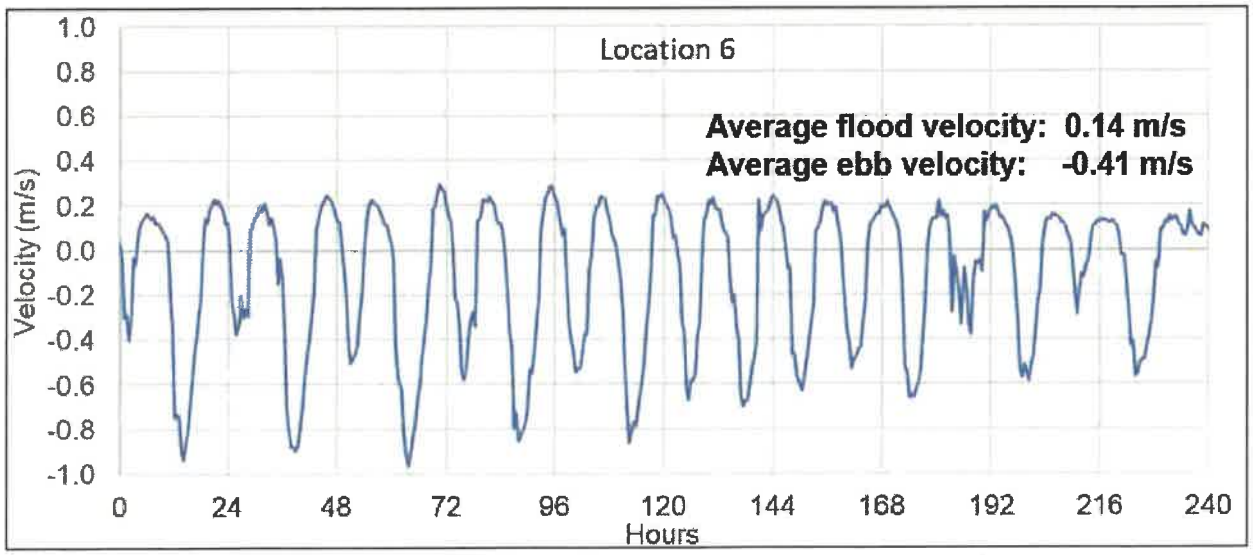

Figure 47. Computed tidal flow velocity at Station 6 (see Figure 41 for the location).

The imbalance of flood and ebb currents at the six locations along the north jetty as discussed above is summarized in a conceptual model shown in Figure 48. At the tip of the north

jetty (Location 1), the different spatial patterns of tidal current entering and exiting the inlet results in a stronger flood current at the entrance. This flood dominance, combined with wave-generated longshore currents and sand transport, tends to move sand into the inlet. This tendency of landward transport is met with an ebb dominance at locations 2 and 3. This strong ebb flushing may prevent, or delay, the sand from entering the inlet further. At locations 4 and 5 further inside the inlet and near the present sand pile, flood dominance resumes. This suggests that the sand presently there would not be flushed out of the inlet naturally by tidal flows. On the contrary, there may be a tendency to transport the existing sand further landward, as observed during the study period (Figure 36 and Figure 37). The strong ebb dominance at Station 6 serves to prevent the existing sand to be transported further into the boat basins landward to the east.

This conceptual model is used in this study to develop and evaluate various mitigation measures. It is worth emphasizing here that the conceptual model illustrated in Figure 48 does not consider wave forcing. Contributions of wave-induced currents are discussed in section 4.4.2.

Figure 48. A concept model for the tidal flow pattern directly related to the sedimentation at the project site.

4.3.2 Influence of the Bridge on Tidal Flow Patterns

Although the bridge does not have significant influence on Johns Pass hydraulics in terms of the tidal prism and overall flow pattern (Figure 39 and Figure 40, upper panels) based on the inlet management study (Wang et al., 2016), the pilings do have substantial influence on flow patterns directly adjacent to them. The pilings may also have considerable influence on wave propagation. Since the north most piling is at the location with interior sedimentation, its influence on the flow pattern and subsequently sediment transport and deposition potential were examined with the numerical model.

The influences of the bridge pilings on local flow pattern were examined by removing the pilings from the numerical model. The simulated flow patterns were then compared with the patterns including the bridge pilings. The difference can then be attributed to the bridge pilings. It is worth noting that the overall channel bathymetry for the model runs with and without bridge used the same bathymetry. It can be argued that the local channel bathymetry might change if the pilings were removed. However, it is beyond the scope of this study to estimate potential channel bathymetry adjustment associated with bridge piling removal. Most of the influence should be related to the obstruction of the bridge pilings to the tidal flow. Influence due to bathymetry adjustment should not be significant, particularly in terms of depth-averaged flow.

The modeled flow field under a peak ebbing condition without the bridge is shown in Figure 49 upper panel, with the lower panel illustrating the difference in velocity magnitude. Negative values indicate increased velocity with the bridge, positive values indicate decreased velocity. Compared to the existing condition (Figure 39 lower panel), the flow is more uniform across the entire channel without the bridge piling (Figure 49 upper panel), as expected. The flow between the pilings is significantly weakened due to the removal of the bridge since the inlet has no obstructions that can concentrate and block water flow. (Figure 49 lower panel).

Directly relevant to this sedimentation study is the substantially increased ebb flow velocity seaward of the bridge under the existing conditions with the pilings, where the stations 1, 2 and 3 are located (Figure 41). This faster ebb velocity would increase the flushing power in this crucial area that supplies the sand for the interior sedimentation. The presence of the bridge increased tidal flushing near the inlet entrance along the north jetty, as compared with the no bridge scenario. This ebb flow increase is caused by the specific orientation of the bridge relative to the channel. The

bridge extends at an oblique angle compared to the orientation of the inlet main channel. Therefore, the bridge pilings which are nearly 40 m long extend at an angle to the inlet bank, as apparent in Figure 49 lower panel. This angle funnels the ebb flow toward the north, resulting in increased velocity along the north jetty. In this aspect, the bridge improves the tidal flushing at a crucial location and should serve to slow the input of the sediment into the channel. This piling orientation results in a slightly decreased ebb velocity landward of the bridge.

The bridge also leads to an increase in flood current velocity at the northern portion of the entrance (Figure 50 lower panel). However, the flood velocity increase near the north jetty under flooding tide is considerably less than the increase under ebb phase. This results in a net increase of ebb flushing along the north jetty, as shown in Figure 43 and Figure 44.

In summary, the presence of the bridge does not directly contribute to increased tendency of sedimentation in the project area. On the contrary, the bridge increased the ebb tidal flushing along the north jetty, which should delay the sediment input to the project area. However, slightly reduced ebb flushing landward of the bridge would not contribute to the flushing of the existing sand pile there. It is worth noting here that a relatively large body of sediment already existed at the time the bridge construction was completed.

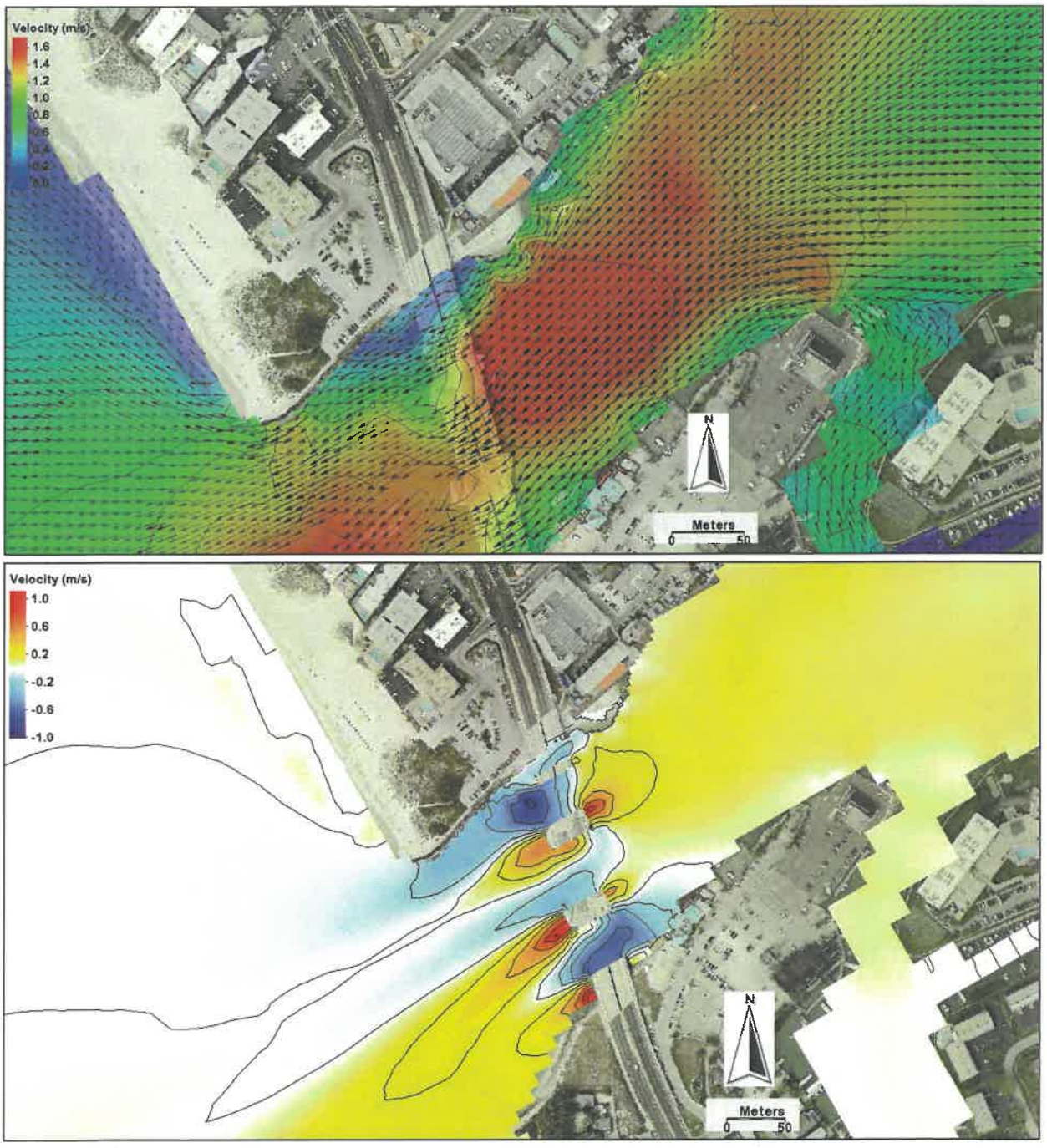

Figure 49. Upper panel: peak ebb flow without the bridge. Lower panel: difference between the flow field with and without the bridge.

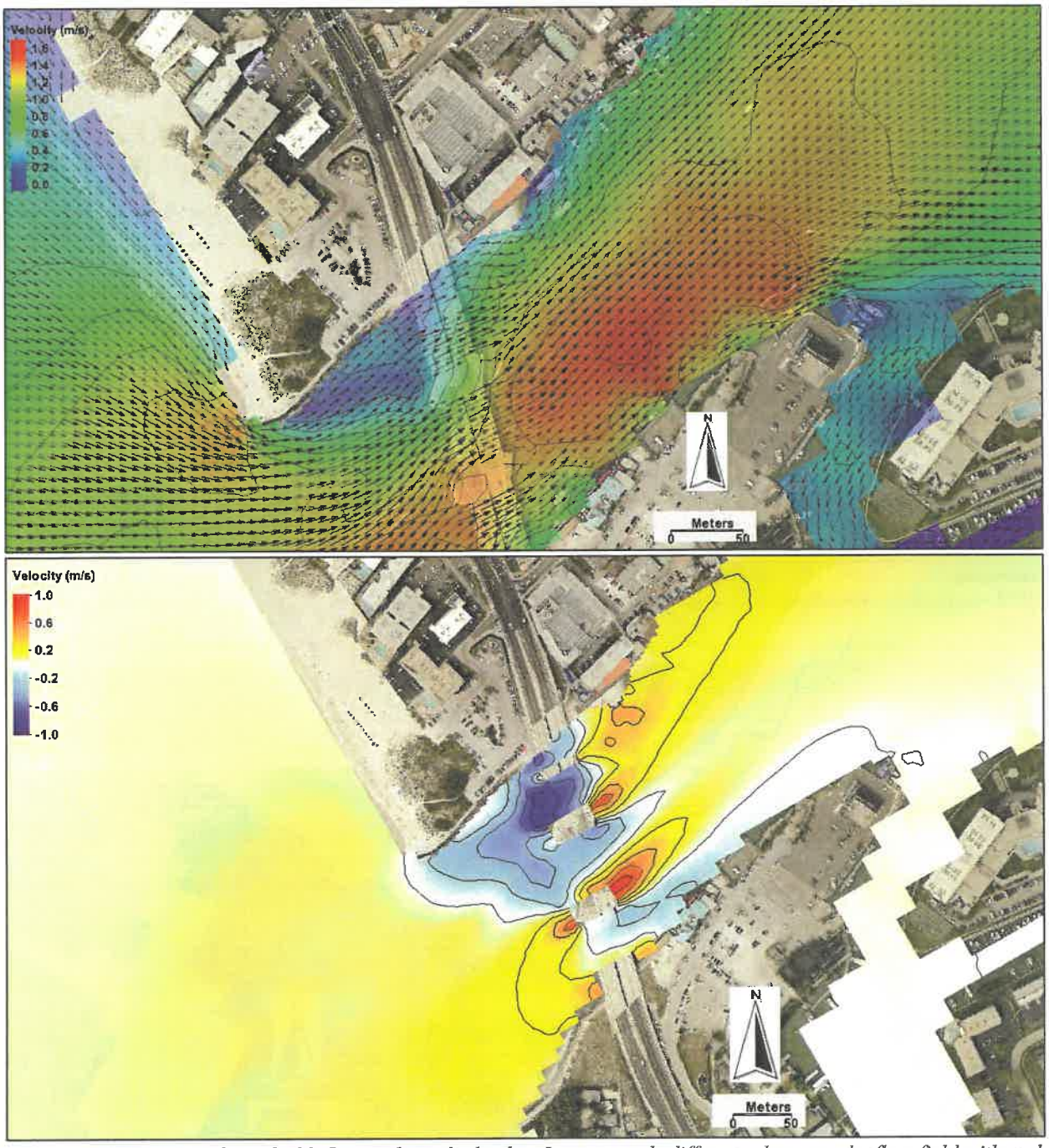

Figure 50. Upper panel: peak ebb flow without the bridge. Lower panel: difference between the flow field with and without the bridge.

4.4 Modeled Wave Field and Wave-current Interaction

4.4.1 Modeled Wave Field near the Inlet Entrance and within the Channel

Incident waves, particularly breaking waves, play a major role in initiating sediment motion. The sediment that is entrained by breaking waves is then transported by flood current into the inlet. In addition, wave-induced longshore current also contributes significantly to the sediment transport and deposition in the vicinity of tidal inlets. The numerical model constructed by this study also simulates wave propagation and longshore current.

The wave conditions in the greater study area were introduced earlier (Figure 4). The 15-year WAVEWATCHIII data from 2005 to 2020 were reanalyzed by this study to obtain input wave conditions for the numerical modeling. The waves were partitioned into sixteen 22.5-degree brackets based on incident wave angle. Eight of the brackets represent onshore-directed waves and are modeled here. The rest of the offshore-directed waves are not relevant for this sedimentation study. Here, the storm wave conditions, as represented by the average of the highest 5% waves in each angle bracket and corresponding wave period, referred to as the "95% percentile wave height", were used in the wave modeling. The 95% wave is often used to represent storm conditions (Lemke and Miller, 2020; Cheng et al., 2021). The input storm wave conditions for the numerical modeling are summarized in Table 1. Wave propagation in the vicinity of a tidal inlet is strongly influenced by tidal water level. High tide and therefore deeper water would allow more wave energy to propagate over the shallow terminal lobe and channel margin linear bar. Therefore, wave propagation at various tide levels were simulated. In the following, representative examples of wave propagation at low tide, mean tide, and high tide are discussed.

Table 1. Input storm wave conditions for numerical modeling.

Wave angle	151.25	173.75	196.25	218.75	241.25	263.75	286.25	308.75
95% height (m) H_{sig}	0.91	0.85	1.51	2.22	2.28	2.39	2.14	2.01
95% period (s) T_p	3.80	5.04	6.69	10.68	10.13	9.37	7.29	6.23
% occurrence	2.3%	15.2%	11.0%	6.9%	4.3%	9.7%	12.3%	10.0%

The Johns Pass channel has an orientation of roughly 225 degrees. The left three columns in Table 1 represent southerly approaching waves. The 218.75-degree wave approaches roughly perpendicular to the shoreline. The right four columns in Table 1 list northerly approaching waves which would drive southward longshore sand transport providing favorable conditions for interior

sedimentation. It is worth noting that significant refraction occurs as the wave propagates onshore. The offshore incident wave angle as listed in Table 1does not represent nearshore wave angles. Although all the waves listed in Table 1 were simulated, only three cases as highlighted in Table 1 are discussed here: the southerly incident 173.75-degree wave, the roughly perpendicular 218.75-degree wave, and the northerly 286.25-degree wave. The rest of the cases can be implied from the patterns of the three examples. In addition, wave propagation patterns at three water levels, 0.45 m below mean sea level representing low tide, mean sea level, and 0.45 m above mean sea level representing high tide are discussed.

The southerly incident waves tend to be lower than the northerly waves (Table 1). The 173.75-degree wave represent the most frequent incident wave occurring at 15.2% of the time. The modeled wave field is illustrated in Figure 51. Overall, this wave has little influence on the project area with wave height mostly lower than 0.2 m under all three tidal water levels. It is worth noting that the simulated wave represents the average of the highest 5% waves. The waves should be much lower than that illustrated in Figure 51 most of the time. Given that this wave tends to generate northward longshore sand transport and does not contribute directly to the sedimentation at the project site, this relative low southerly approaching wave, although occurring frequently, should not play a major role.

The shore-perpendicular 218.75-degree wave is much higher than the previous 173.75 wave, with a storm wave height of 2.22 m versus 0.85 m; although they occur less frequently, 6.9% versus 15.2% of time. The incident wave energy is significantly dissipated by the broad ebb shoal, which is controlled by water depth. The wave-energy dissipation is much greater under low tide (Figure 52 upper panel) than under high tide (Figure 52 lower panel), resulting in considerably higher waves at the mouth of the inlet and inside the channel at high tide. The higher waves along the north jetty at mean tide (Figure 52 middle and lower panel) can contribute significantly toward moving sand near the inlet mouth into the interior. This wave should be carefully considered in the design of the mitigation measures.

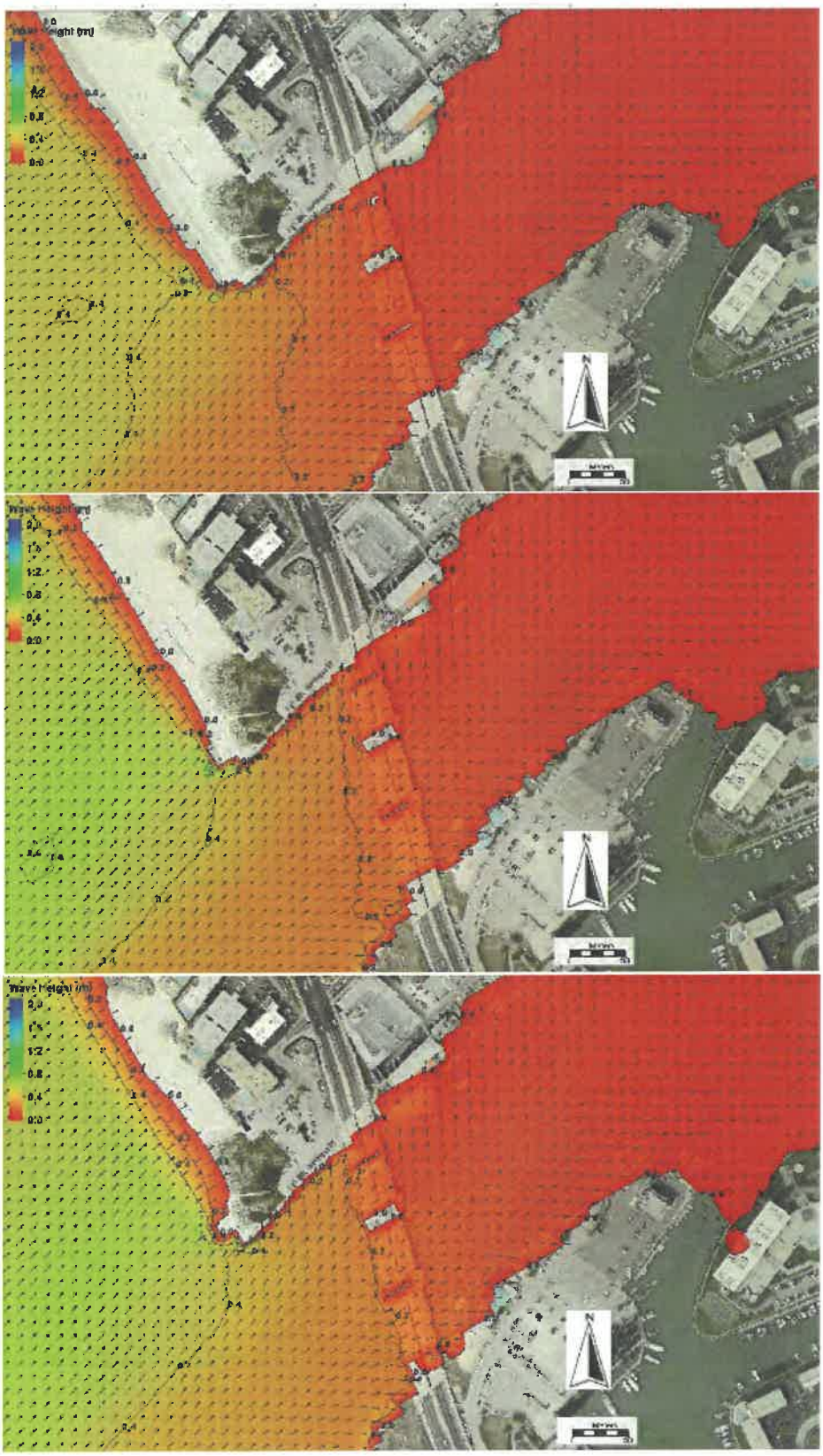

Figure 51. Modeled wave field for the 173.75-degree incident wave, Hsig = 0.71 m, Tp = 5.04 s. Upper panel: low tide; middle panel: mean tide; lower panel: high tide.

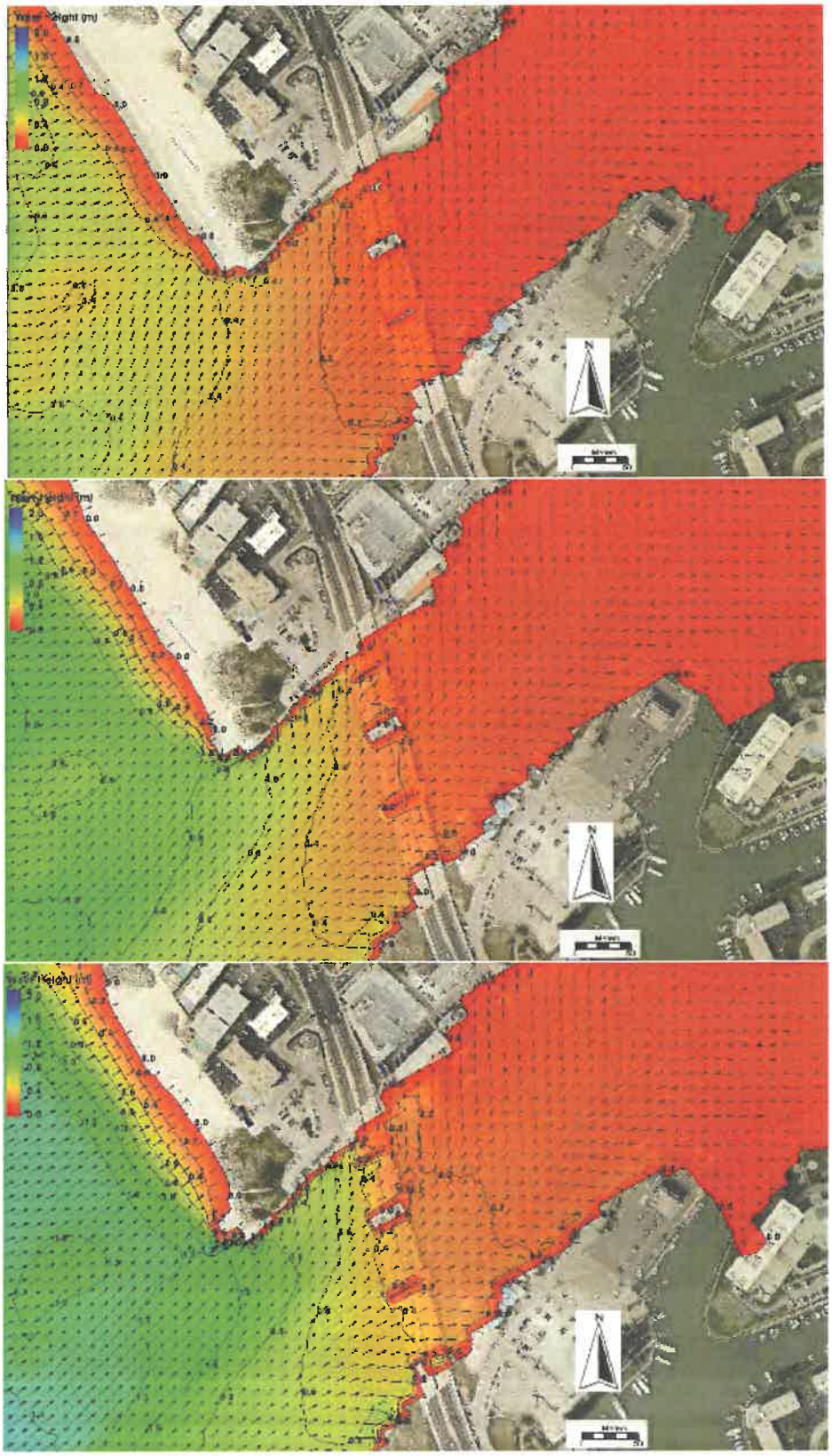

Figure 52. Modeled wave field for the 218.75-degree incident wave, Hsig = 2.22 m, Tp = 10.68 s. Upper panel: low tide; middle panel: mean tide; lower panel: high tide.

The northerly 286.25-degree wave can be quite high and with a frequent occurrence of 12.3%. The modeled wave height near the entrance of the inlet and in the interior can reach 1 m during this storm condition under high tide (Figure 53). In addition, this northerly approach wave would induce southward longshore sand transport, which can bring sand around the tip of the north jetty into the inlet. The high wave along the north jetty may induce active sediment suspension for the flood current to carry the sand further into the inlet. The wave patterns for the other three northerly approaching waves are similar to this case.

It is worth emphasizing that the active sediment suspension by larger waves does not necessarily relate to landward (toward the back bay) sand transport. Landward (eastward) sand transport is carried by flooding current during rising tides. By the same token, the active sediment suspension by high waves can also provide sand for ebb flushing. The situation can become more complicated when active wave breaking occurs. This is the case for the shallow shoal presently existing between the boat dock and the bridge. This area is mostly shallow subtidal to intertidal, to low supratidal. Active wave breaking occurs under almost all tidal stages. Field observation also indicate considerable contributions from boat wakes due to the heavy vessel traffic.

The landward (eastward) propagating waves associated with wave breaking over the mostly intertidal sand body between the marinas and the seaward edge of the bridge would actively transport sand landward toward the marinas. This is likely responsible for the landward redistribution of sand measured by this study and discussed above (Figure 36 and Figure 37). This wave breaking-induced sand transport is also a major mechanism for sand encroachment into the boat basin. Wave breaking can be eliminated by increasing the water depth. It is therefore important that the mitigation measure be designed such that the landward (eastward) wave-induced sediment transport be eliminated.

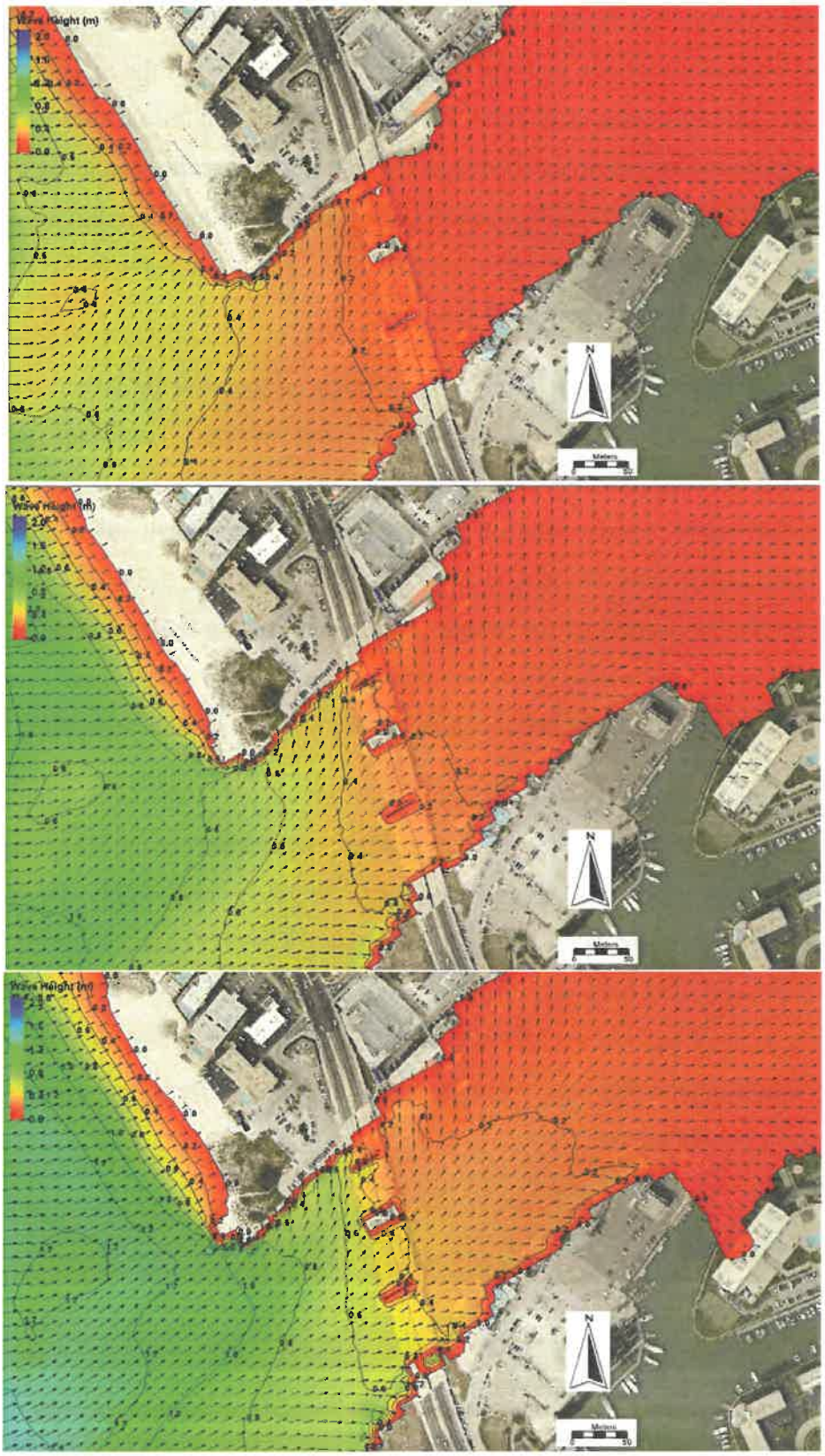

Figure 53. Modeled wave field for the 286.25-degree incident wave, Hsig = 2.14 m, Tp = 7.29 s. Upper panel: low tide; middle panel: mean tide; lower panel: high tide.

The pilings of the bridge effectively block incident waves from reaching landward of the Johns Pass bridge. Figure 54 shows the wave-height difference between existing conditions and the case with the bridge removed. Positive values (warm color) indicate the waves are higher without the bridge. As expected, for the three cases illustrated here the waves are about 0.1 to 0.2 m higher landward without the presence of the bridge. The wave shadow zones are larger for northerly approaching waves (Figure 54 lower panels) than for the southerly approaching waves (Figure 54 upper panels).

4.4.2 Modeled Wave-current Interaction near the Inlet Entrance and within the Channel

The breaking of oblique incident waves can generate a strong longshore current (Komar, 1996; Wang et al., 1998). This longshore current can interact with tidal flow and have significant influence on the morphodynamics of tidal inlets and their ebb shoals (Wang and Beck, 2012). When examining the combined forces of waves and tides instead of looking at them individually, a coupled wave-current model is necessary. Since breaking waves also play a major role in entraining sediment into the water column, the combined wave-tidal currents constitute an important factor in understanding the interior sedimentation. The contributions of three representative storm waves on tidal flow are examined here (Table 1 yellow highlights). These examples represent top 5% energetic conditions at each incident angle. The results from the other wave conditions (Table 1) can be inferred from these examples.

Active sediment suspension induced by the breaking of the above three energetic waves is expected. However, net sediment transport, which directly relates to erosion and deposition, is caused by temporal and spatial patterns of current, including both tide and wave-driven currents. Since the flow conditions at the six locations (Figure 41) are directly related to the trend of interior sedimentation, the following discussion focuses on the modification by wave forcing on the current fluctuations at the six locations. The results of coupled wave-current model runs are compared with the current-only model runs to examine the contribution of wave forcing. It is worth noting that the waves applied here represent energetic conditions that occur substantially less than 5% of the time.

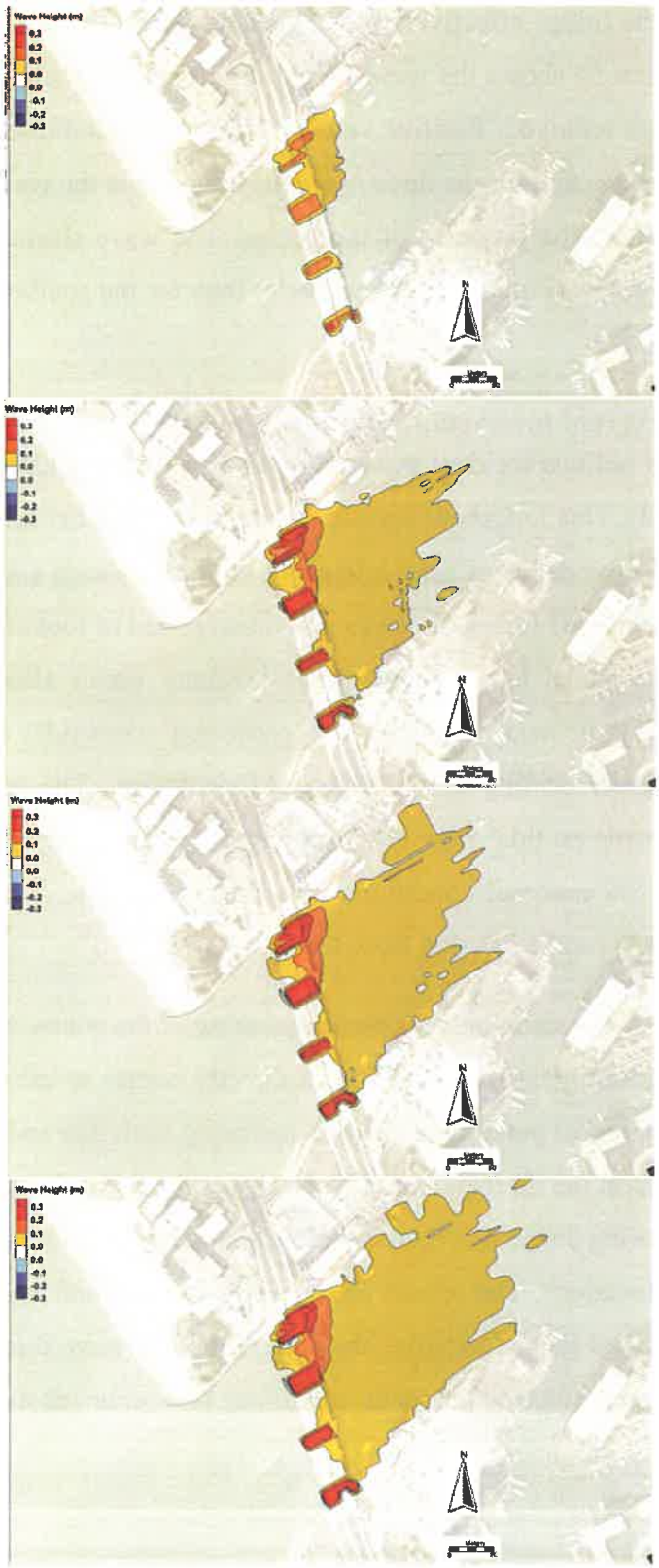

Figure 54. Wave-height difference at high tide between cases with and without the bridge. From top to bottom, incident wave angles are 173.25, 196.25, 218.75, and 286.25 degrees (see Table 1 for detailed wave information).

The wave forcing has significant influence on the computed current velocities at the six locations. Table 2 summarizes the percent changes of time-averaged velocities at the six locations under three incident wave conditions. The percent change was obtained by comparing with the tide-only case. Detailed comparison is shown in Figures A14 through A20 listed in Appendix III. Overall, wave forcing resulted in decreased ebb flow velocity when compared with the tide-only case. On the contrary, an increase in flood current velocity occurred for the southerly incident and channel-parallel wave, while the northerly approaching wave resulted in a decrease in flood velocity except at Station 1 (Table 2).

Table 2. Percent changes of current velocities at the six stations (see Figure 41for locations) under three incident wave conditions. The percent change was obtained by comparing with the tide-only case.

Input Wave conditions		Locations					
		1	2	3	4	5	6
1.5 - 196.3	Flood	13%	65%	30%	4%	2%	45%
	ebb	-24%	-20%	-13%	-21%	-12%	-12%
2.2 - 218	Flood	33%	68%	23%	8%	4%	65%
	ebb	-45%	-34%	-19%	-37%	-19%	-20%
2.1 - 286	Flood	8%	-28%	-19%	-4%	-4%	-3%
	ebb	-35%	-22%	-22%	-33%	-41%	-12%

The three storm wave conditions (Table 1 yellow highlights) superimposed on the tidal fluctuations included the southerly incident wave at 196.25 degrees with a significant wave height of 1.51 m and a peak wave period of 6.69 s (labelled as 1.5-196.3 in Appendix III Figures A15 through A20), the channel-parallel wave at 218.75 degrees with a significant wave height of 2.22 m and a peak wave period of 10.68 s (labelled as 2.2-218.7 in Appendix III Figures A15 through A20), and the northerly approaching wave at 286.25 degrees with a significant wave height of 2.14 m and a peak wave period of 7.29 s (labelled as 2.1-286 in Appendix III Figures A15 through A20). In the illustrations Appendix III (Figures A15 through A20), the computed velocities under tidal-only case are also plotted to serve as comparisons to identify contributions from wave-induced current.

At Station 1 (Figure 41 and Appendix III Figure A15), the ebb velocity decreased up to 45% for the channel-parallel incident wave. For the northerly approaching wave which plays a major role in bringing sediment into the inlet channel, the ebb velocity decreased 35% suggesting a significant reduction of ebb flushing due to the wave forcing. A modest 8% increase in flood velocity would enhance inlet-ward sand transport. It is worth noting that the values listed in Table 2 represent storm wave conditions at spring high tide. Therefore, they should represent approximately maximum values.

At Station 2 (Figure 41 and Appendix III Figure A16), for the southerly and channel-parallel incident waves, the 20-34% decrease in ebb velocity was accompanied by a more than 60% increase in flood current. This would significantly reduce the ebb flushing potential at this crucial location. However, for the more important northerly approaching waves, both flood and ebb velocities were reduced by the wave forcing. A similar trend of change occurred at Stations 3 and 4 Figure 41 ,Appendix III Figure A17 and Figure A18), although with different percentages.

At Station 5 (Figure 41 and Appendix III Figure A19), wave forcing has minimal influence of less than 5% on flood velocity. A rather large decrease of ebb velocity of 41% occurred for the northerly incident wave, which would enhance the landward sediment transport. At the landward most Station 6 (Figure 41 and Appendix III Figure A20), significant increase of flood velocity occurred for the southerly and channel-parallel incident waves, accompanied by a 12-20% decrease in ebb velocity. This, again, would result in reduced ebb flushing.

In summary, although with some minor variations, wave forcing tends to enhance landward sand transport due to increased flood velocity as compared to the tide-only case. This enhanced landward sand transport is accompanied by reduced ebb flushing due to decreased ebb velocity. Therefore, wave forcing plays a significant role in bringing sediment into the channel interior and should be carefully considered in developing the mitigation alternatives.

5.0 Mitigation Alternatives for the Channel Interior Sedimentation

5.1 Summary on the Cause of the Interior Sedimentation

Interior sedimentation along the updrift bank of a tidal inlet is common, with or without human influences. This is demonstrated by interior sedimentation observed at other inlets, e.g., the neighboring Blind Pass (Figure 55). Sediment accumulation occurred near the inlet entrance at the beginning of the winter season, and subsequently migrated landward (eastward). At Johns Pass, interior sedimentation at the project site is visible on aerial photos taken both before and after the intense human engineering activities. Interior sedimentation is the morphologic result of longshore moving sand being carried into the tidal inlet by the flooding current and settles in the part of the channel where current velocity decreases. This natural process constitutes the fundamental cause of the interior inlet sedimentation independent of the engineering changes.

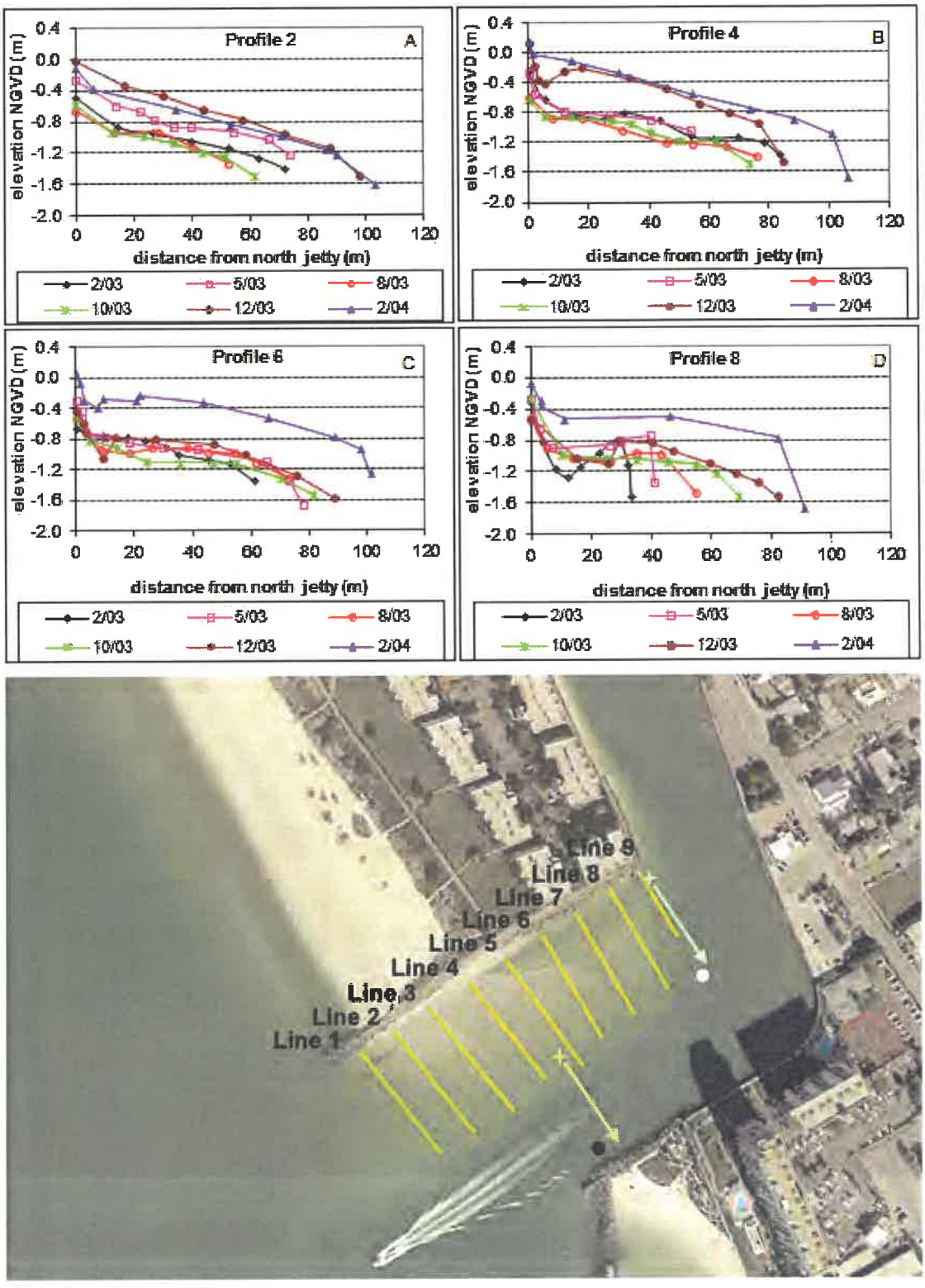

Figure 55. Profiles from the monthly survey at the entrance channel of Blind Pass (Top). Locations of the profiles are shown in the bottom panel.

The natural processes can be altered significantly by various engineering activities. At Johns Pass, the following anthropogenic activities and their influence on the interior sedimentation are discussed:

1) channel dredging and re-alignment;
2) nearby beach fill;
3) cross-channel structures, the bridge in this case;
4) the numerous boat docks and pilings; and
5) inlet jetties.

Shortly before and after the authorization of Johns Pass as a Federal channel, the inlet was dredged frequently in the 1960s (Appendix I), likely with the main goal of improving the channel navigability. The exact dredging footprints of these earlier projects are not accurately documented. It is reasonable to believe that a large amount of the channel interior sedimentation was removed by the dredging events in the 1960s and the construction of the north jetty and the seawalls. A dredge-pit looking feature can be observed on the 1960 aerial photo (Figure 31). Although not directly related to this project on interior sedimentation, it is worth noting that the dredged channel through the terminal lobe (also referred to as outer bar) along the seaward edge of the ebb shoal was quite visible on the 1969 and 1971 aerial photos effectively straightened and re-oriented the Johns Pass exit channel (Figure 33 and Appendix II Figure A1). This channel straightening and re-alignment contributed to the substantial shoreline change along the downdrift Sunshine Beach in the 1970s and 1980s, as discussed in Wang et al. (2016).

Numerous beach nourishment projects were conducted along the Sand Key beaches north of Johns Pass (Appendix I). The nourishment projects to the north and updrift of Johns Pass were considered for impact to interior sedimentation at the project site. Large scale beach nourishment on Sand Key started in the late 1980s, with a total of 9.3 million cubic yards of sand placed. The south end of the nourishment area is about 3 miles north of Johns Pass. The Sand Key beach nourishment did not result in an observably shallower and larger channel margin linear bar (Appendix II Figures A7 through A14), as compared to the case before the nourishment (Figures 26 through 33 and Appendix II Figures A1 through A6). It is acknowledged here that the channel

margin linear bar is not visible in all the aerial photos and its spatial extent is influenced by the tide stage at which the aerial photos were taken. However, if an obvious trend exists, it still should be identified from the 24 aerial photos. As for the state of Madeira Beach directly north of the inlet, it filled to the tip of the Johns Pass north jetty roughly one year after the jetty was completed in 1961 and remained filled ever since. Therefore, no direct evidence can be found indicating that the Sand Key beach nourishment projects have significantly changed the morphology of the direct sand sources to the interior sedimentation. In other words, the Johns Pass interior sedimentation is not a direct consequence of Sand Key beach nourishment since the late 1980s because it occurred before the nourishment projects.

Over the past 90 years, three bridges have been built across Johns Pass at different times. The first bridge was located further landward of the past and present areas of sedimentation (e.g., Figure 29 and Figure 30). This first bridge was removed and replaced by the second bridge in 1970. The second bridge was located at roughly the same location as the present bridge. During its life span from 1970 (Appendix II Figure A1) to roughly 2007 (Appendix II Figure A11), sedimentation at the project area became visible in the very late 1990s. Sand accumulation in the vicinity of the bridge became most distinctive near the completion of the third bridge in 2010 (Figure 34). Given the fact that the present bridge is located in the middle of the sand pile, its interaction with the sedimentation should not be ignored. The numerical modeling results, as discussed above, illustrate that the present bridge-piling configuration actually enhances ebb flushing along the north jetty (Figure 49), which would delay the landward sand transport. Furthermore, the wave modeling results show that the pilings, also serve to reduce wave energy arriving at the project site (Figure 54). Overall, the modeling results indicate that the present configuration of the bridge does not enhance landward (eastward toward the marinas) sand transport nor promote further sedimentation. Based on the 2010 aerial photo, the bridge construction may have led to sand accumulation in its immediate vicinity. However, based on the modeling results, the interaction between the present bridge and the current-wave fields should not promote interior sedimentation.

The influence of the elevated boat docks and their associated pilings are too small scale to be incorporated in the numerical modeling. The smallest grid size of 2.5 m (8.2 ft) is too large for these features. Based on qualitative field observations and given the fact that these features are

located mostly landward of the sand pile, their influence on the interior sedimentation should not be significant.

Jetties were constructed on both sides of Johns Pass. In general, jetties are designed to prevent sand from entering the entrance channel and therefore stabilize the inlet. The Johns Pass north jetty was installed quite early, in 1961, likely with the goal of improving navigation. Sand deposition at the mouth of the inlet was apparent from the aerial photos in the 1950s and before. Based on the time-series aerial photos, the north jetty appears to have achieved the goal of stabilizing the north bank. The likely dredging associated with the north jetty and seawall constructions seem to have kept the channel free of emergent sand body for over 30 years till the early 1990s. However, the north jetty was filled to the tip one year after its completed and remained full for the past 60 years. Therefore, the north jetty has not been blocking all the sand from entering the inlet. The south jetty was extended in 2000 with the main goal of mitigating the aggressive erosion at Sunshine Beach and extending the life of the nourishment projects there. The influence of south jetty on the sedimentation along the north side should not be significant.

5.2 Alternatives for Mitigating the Interior Sedimentation

Based on the above understanding of the cause of interior sedimentation and the historical evolution of the sand body as observed from time-series aerial photos, it is proposed here that local removal of the sand accumulation should be the main approach. Local sand removal also should be the least likely to induce negative impacts at other parts of the Johns Pass system, which is a crucial consideration in evaluating the alternatives. Seventeen cross sections were extracted from the most recent bathymetry data (Figure 56). In the following, these 17 cross-channel profiles were used to design and illustrate the sand removal alternatives. The plan view of the proposed sand removal area is shown in Figure 57. In general, the proposed sand removal will be conducted in three areas: landward (east) of the bridge as marked by a black box in Figure 57, in the direct vicinity of the bridge as marked by red hatch lines, and seaward of the bridge. Detailed design is discussed in the following.

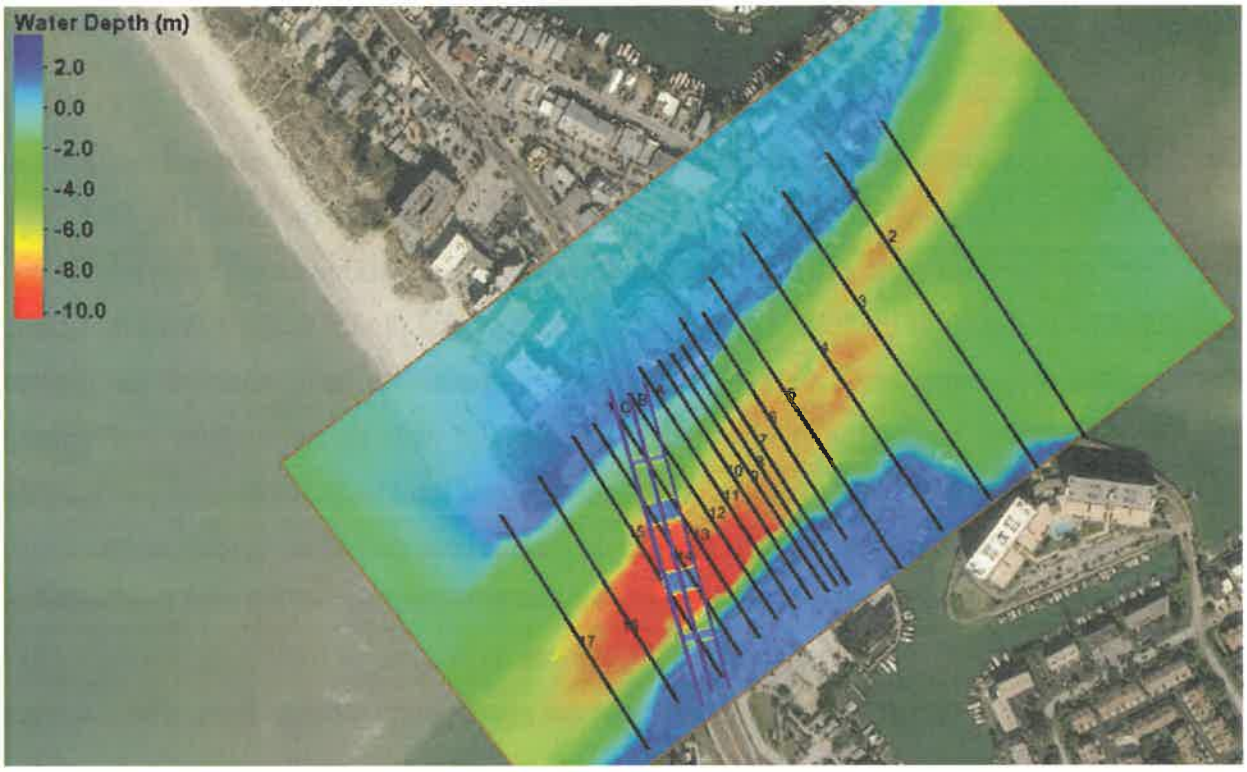

Figure 56. Bathymetry of Johns Pass surveyed in 2020 and the 17 cross sections used in the design of mitigation alternatives. The 17 cross sections are shown in Appendix IV.

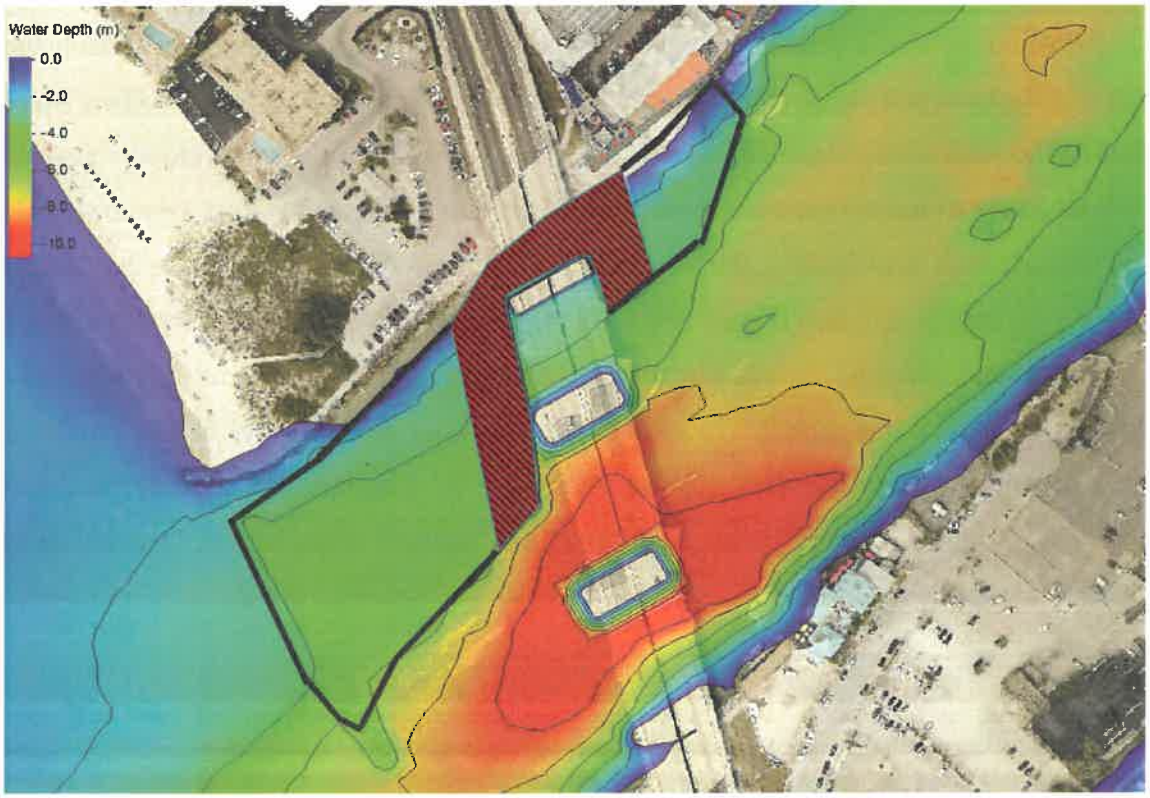

Figure 57. Plan view of the proposed local sand removal.

As apparent from the Johns Pass bathymetry shown in Figure 56, the deepest part of the channel, aka, channel gouge or thalweg, is not located in the middle of the channel. The channel thalweg extends at an oblique angle to the inlet orientation as marked by the two banks. Further inside the bay or at the bayside exit of the channel, the thalweg hugs the north bank, while near the seaward entrance the thalweg hugs the south bank (Figure 56). This particular thalweg orientation coincides in general with the strongest tidal current (Figure 39 and Figure 40) and provides valuable insight on erosion and deposition patterns. For example, the strong flow and corresponding deep channel along the southern side, i.e., the opposite side of the project area, marks the area with an erosional trend. While the relatively weak flow and shallow channel along the project site indicate a trend of sedimentation. In other words, the sedimentation in the project area is related to this particular orientation of the channel thalweg. This channel thalweg orientation has strong control regarding the overall flood and ebb flow patterns, subsequently the morphology of the adjacent beaches and the ebb shoal. It is essential that the mitigation alternatives for the local interior sedimentation should not have significant influences on this channel configuration which would trigger changes at adjacent beaches and the ebb shoal.

Removing the excess sand at the project site is proposed here as the main mitigation alternative. Larger-scale alternatives, e.g., those involving the entire inlet system or parts other than the sedimentation area, would significantly expand the scope of this project. It is the authors' opinion that local sand removal provides the most direct and reliable solution to the existing sedimentation problem. Based on the discussion and input from the TAC (Technical Advisory Committee) and the stakeholders, the following two categories of mitigation alternatives are proposed. Category 1, referred to as C1 in the following, would remove excess sand from the seaward edge of the boat basins to the tip of the north jetty. Category 2, referred to as C2, would not remove sand in the vicinity of the bridge. Five sand removal alternatives are examined within each category. In addition to the two categories, an additional mitigation alternative, C3, involving closing the gap between the bridge piling and the north bank, with the goal of blocking sand from reaching the marinas, is also examined. C3 does not include sand removal with the goal of focusing on the alternative of blocking sand from reaching the marinas. Overall, a total of 11 alternatives

are examined based on the present understanding of the sedimentation mechanisms and numerical modeling results.

Seventeen cross sections (Figure 56) are used to illustrate the detailed sand removal alternatives. The plots of the 17 cross sections are shown in Appendix IV. Cross sections 1 through 6 (Figures A21 and A22) are located landward of the area with sedimentation. No actions are proposed in this part of the channel. Cross sections 7, 8, 9 and 10 (Figure 56, Appendix IV A23 and A24) are located landward of the bridge and presently very shallow to being emergent along the north bank due to the sedimentation. Five sand removal alternatives are proposed at these four cross-sections (Appendix IV Figure A23 and A24) for both C1 and C2 categories. Cross sections 11, 12, 13 and 14 are located within 30 m (100 ft) of the bridge and with significant sand deposition between the shoreline and the north most bridge piling (Figure 56, Appendix IV A24 and A25). For the C1 category, the excess sand would be removed with five proposed alternatives as shown in Appendix IV, Figures A24 and A25. For the C2 category, no sand removal would be conducted at these locations due to their proximities to the bridge. The cross sections would remain the configuration as shown by the "Original Data" (Appendix IV Figures A24 and A25). For the C3 scenario, a barrier would be installed near the landward edge of the north most bridge piling, as proposed by a stakeholder, and no sand removal would be conducted at all the cross sections. Cross sections 15, 16 and 17 are located seaward of the bridge (Figures 58, Appendix IV A25 and A26). Although these cross sections are presently not experiencing excessive sedimentation, five sand removal alternatives are proposed for both C1 and C2 categories, with the goal of creating a sedimentation basin to buffer future incoming sand from the updrift beach and the channel margin linear bar.

The eleven alternatives in terms of actions at each cross section, i.e., sand removal (R) or no action (N A) are summarized in Table 3. In the following discussion, the left column of Table 3 is used to identify each alternative. "A1" corresponds to the least amount of sand removal and "A5" corresponds to the most aggressive sand removal. Detailed design of the dredge pit is shown in Appendix IV, Figures A23 through A26. The total volume of sand that would be removed for each alternative is summarized in Table 4, with C1-A5 removing the most sand at 23,700 cubic yards and C2-A1 removing least amount of sand at 2,900 cubic yards. Each alternative is evaluated based on the wave and current modeling and are discussed in the following section (5.3).

The sand removal alternatives as described above are based on the following considerations:

1) directly removing the excess sand in the vicinity of the marinas (Lines 7, 8, 9 and 10), and therefore, directly solving the present sedimentation issues,
2) applying extra caution at the bridge, by considering no action within 100 ft from the structure (C2 alternatives, Lines 11, 12, 13 and 14), to ensure that no negative impacts occur, and
3) creating a sedimentation basin near the entrance of the inlet (Lines 15, 16 and 17) to serve as a buffer for incoming sediment to prolong the life of the project.

Table 3. Actions at each cross section for the 11 proposed alternatives. "R" represents sand removal, and "NA" represents no action.

Alternatives	CS7	CS8	CS9	CS10	CS11	CS12	CS13	CS14	CS15	CS16	CS17
C1-A1	R	R	R	R	R	R	R	R	R	R	R
C1-A2	R	R	R	R	R	R	R	R	R	R	R
C1-A3	R	R	R	R	R	R	R	R	R	R	R
C1-A4	R	R	R	R	R	R	R	R	R	R	R
C1-A5	R	R	R	R	R	R	R	R	R	R	R
C2-A1	R	R	R	R	NA	NA	NA	NA	R	R	R
C2-A2	R	R	R	R	NA	NA	NA	NA	R	R	R
C2-A3	R	R	R	R	NA	NA	NA	NA	R	R	R
C2-A4	R	R	R	R	NA	NA	NA	NA	R	R	R
C2-A5	R	R	R	R	NA	NA	NA	NA	R	R	R
C3	NA	NA	NA	NA	NA	NA	NA	NA	NA	NA	NA

Table 4. Total volume of sand removed for each Alternative.

Alternatives	Total volume of sand removed	cubic yards	cubic meters
C1-A1		3,200	2,500
C1-A2		11,100	8,500
C1-A3		14,000	10,700
C1-A4		18,700	14,300
C1-A5		23,700	18,100
C2-A1		2,900	2,200
C2-A2		7,000	5,400
C2-A3		9,700	7,400
C2-A4		13,100	10,000
C2-A5		16,600	12,700
C3		0	0

5.3 Evaluation of the Eleven Alternatives

The eleven Alternatives were evaluated using the numerical model developed during this study based on the following criteria:

1) Influence on the tidal flow field locally and inlet wise, specifically:
    a. potential to alter the flow pattern through the entire inlet,
    b. changes in flow at the northern portion of the entrance,
    c. influence on bridge pilings, particularly increased scour potential, and
    d. changes in flow near the marinas.
2) Influence on the wave field locally and inlet wise, specifically:
    a. changes in wave conditions at the northern portion of the entrance,
    b. changes in wave conditions in the vicinity of the marinas, and
    c. potential to alter the wave field in the entire inlet.
3) Influence on the wave-current interaction locally and inlet wise, specifically:
    a. potential influence on flow conditions in the vicinity of the marinas, and
    b. potential influence on flow conditions at the northern portion of the entrance.

4) Potential for sand infilling in the future.

Since the sand removal alternatives are sequential, with option A1 removing the least amount of sand while A5 removes the most amount of sand, the influences on wave and current conditions are also sequential. In the following, results from seven out of the eleven cases are discussed, including C1-A1, C1-A3, C1-A5, C2-A1, C2-A3, C2-A5, and C3. Impacts from in-between cases such as C1-A2 can be estimated based on the adjacent cases such as C1-A1 and C1-A3. The in-between cases are still summarized here. The sand removal alternatives are discussed in comparison with the existing conditions. All the figures for the seven discussed alternatives are listed in Appendix V (Figures A27 through A46). The flow fields under existing conditions are shown and discussed in Figure 39 and Figure 40). The modeled wave fields under existing conditions are shown and discussed in Figure 51 through Figure 54.

5.3.1 Alternative C1-A1

Alternative C1-A1 involves modest sand removal of 3,200 cubic yards (Table 4). The main feature of this alternative is that the excessive intertidal and emerged sand at the project area would be removed (Appendix IV Figures A23 and A24). The slope of the northern side of the channel would be restored to roughly a linear trend at most of the cross sections, e.g., at Lines 8, 9, 10 and 12. At some of the cross sections, e.g., at Lines 7 and 11, the restored slope is gentler than the steep slope into the channel thalweg (deepest area). Appendix V Figure A27 illustrates the modification to the flow fields under a peak ebb and flood conditions by the modest C1-A1 alternative, as compared to the existing conditions (Figure 39 and Figure 40). Except at the project site, the tidal flow velocity in the main channel is not significantly influenced by this alternative, reducing flow mostly less than 0.05 m/s (or less than 3%). In other words, the C1-A1 alternative would have minimal influence on the overall flow pattern through Johns Pass for both ebbing and flooding tides.

The model shows the considerable flow velocity change at the project area, including both increasing and decreasing of up to 0.2 m/s, is caused by the cross-sectional area change due to the sand removal. The flow velocity increase occurred when an existing emerged area (with zero tidal

flow) was converted to a shallow area by the sand removal. While in most of the project area, the flow velocity decreased due to the increased cross-sectional area. These minor changes do not result in significant changes in sediment transport pattern or magnitude.

Due to the rather modest modification to the bathymetry by C1-A1, its influence on wave propagation is negligible at the project site, as well as over the entire inlet (Appendix V Figure A28). The small increase in wave height just seaward of the marinas was caused by the conversion of the emerged area (with zero wave height) to a very shallow water (with small wave height).

The modifications to the flow velocity can be examined in more detail at the six numerical stations (Appendix V Figure A29 and Table 5). In Appendix V Figure A29, the tide-only flow velocities under the existing condition are also included and compared with C1-A1 to examine the influence of the sand removal on the tidal flow (Table 5, top two rows). The contributions of wave-induced current on the flow are obtained through comparison with the C1-A1 tide only case (Table 5, lower six rows).

Since the sand removal occurs landward of Station 1, its influences at that location are small. Due to the relatively small bathymetry modification, the flow at Station 2 is also similar to the existing condition. Considerable changes in terms of percentages occurred at Stations 3 through 6 (Table 5). It is worth noting that the percentage changes are influenced by the magnitude of the flow. Appendix V Figure A29 shows that the overall magnitude changes are not significant.

Similar to the case under existing conditions, wave-generated currents have significant influence on the flow at the six locations. Generally, the wave forcing led to a decreased ebb velocity at all locations for all three wave cases (Table 5). The southerly and inlet-parallel incident waves resulted in an increased flood velocity at all stations while the northerly approaching wave led to decreased flood current at all stations except at station 1. The limited sand removal for alternative C1-A1 does not fundamentally change the sediment processes in the vicinity of the marina. However, the area will remain shallow water and can lead to active sediment re-distribution by breaking waves and the flood current. In addition, the small amount of sand may be replaced rather quickly under a favorable condition, e.g., energetic northerly wave over a flooding tide. For the above two reasons, Alternative C1-A1 is not recommended.

Table 5. Percent changes of current velocities at the six stations (see Figure 41 for locations) under three incident wave conditions for Alternative C1-A1. The percent change was obtained by comparing with the tide-only case.

Input Wave conditions		Locations					
		1	2	3	4	5	6
Tide-only	Flood	-1%	5%	3%	13%	-36%	-7%
	ebb	3%	2%	21%	62%	-13%	18%
1.5 - 196.3	Flood	20%	74%	33%	5%	3%	7%
	ebb	-12%	-13%	-16%	-21%	-27%	-8%
2.2 - 218	Flood	40%	99%	44%	13%	8%	11%
	ebb	-30%	-30%	-31%	-33%	-44%	-16%
2.1 - 286	Flood	4%	-41%	-24%	-2%	-7%	-8%
	ebb	-38%	-28%	-27%	-30%	-38%	-15%

5.3.2 Alternative C1-A2

Alternative C1-A2 involves a modest sand removal of 11,100 cubic yards, or about 21% less than the amount of C1-A3 (Table 4). The project area would be considerably deepened (Appendix IV Figures A23 and A24). At Lines 7, 8, 9, and 10, a 2.7-m (8.9 ft) deep basin would be created, with a landward slope of 1:4. The landward edge of the sand removal is designed to be at 9 m (30 ft) from the seawall. The seaward edge of the dredged basin would intercept the main channel at 2.7 m (8.9 ft) depth. In the vicinity of the bridge, the same design as described above is proposed for Lines 11, 12, 14, and 15. Line 13 extends across the bridge piling. Due to the short distance between the seaward edge of the riprap and the bridge piling, the 1:4 slope would reach the bridge piling at about 2.7 m (8.9 ft) water depth. A 2-m (7 ft) buffer with no dredging is designed at the edge of the riprap. At Lines 16 and 17 (Appendix V Figure A26), a 3.5-m (11.5 ft) deep basin would be created.

The modeling results for C1-A2 are rather similar to that of C1-A3 (discussed in the following), but with a modestly lower magnitude. Also similar to C1-A3, the reduced flow velocity and wave height at the entrance and along the north jetty may lead to sand deposition in the designed sedimentation basin there. Alternative C1-A2 is not recommended because of the concern on the life span of the project, in addition to no apparent benefit for removing less sand than C1-A3.

5.3.3 Alternative C1-A3

Alternative C1-A3 involves a significant sand removal of 14,000 cubic yards, or nearly 4.4 times the amount of C1-A1 (Table 4). The project area would be substantially deepened (Appendix IV Figures A23 and A26). At Lines 7, 8, 9, and 10, a 3-m (10 ft) deep basin would be created, with a landward slope of 1:5. The landward edge of the sand removal is designed to be at 9 m (30 ft) from the seawall. The seaward edge of the dredged basin would intercept the main channel slope at 3 m (10 ft) depth. In the vicinity of the bridge, the same design as described above is proposed for Lines 11, 12, 14 and 15. Line 13 extends across the bridge piling (Appendix IV Figure A25). Due to the short distance between the seaward edge of the riprap and the bridge piling, the 1:5 slope would reach the bridge piling before reaching 3 m (10 ft) water depth. A 2-m (7 ft) buffer with no dredging designed at the edge of the riprap. At Lines 16 and 17 (Appendix IV Figure A26), a 4-m (13 ft) deep basin would be created.

Appendix V Figure A30 illustrates the modification to the flow fields under a peak ebb and flood conditions by the C1-A3 alternative, as compared to the existing conditions. Except at the project site, the model indicated that the tidal flow velocity in the main channel is not significantly influenced by this alternative, reducing flow less than 0.05 m/s (or less than 3%). In other words, the C1-A3 alternative would have minimal influence on the overall flow pattern through Johns Pass for both ebbing and flooding tides. Furthermore, the influences are mostly confined within the inlet channel landward of the tip or the north jetty, with a slight increase in ebb flow just seaward of the dredge pit.

Due to the substantial deepening of the project area, a decrease of the depth-averaged velocity occurred for both flood and ebb flows (Appendix V Figure A30). The localized increases in flow velocity, particularly during the peak ebb flow which occurs at a low tide water level, is caused by the conversion of an existing emerged area (with zero tidal flow) to a shallow area by sand removal similar to alternative C1-A1. These localized minor changes should not result in significant changes in sediment transport pattern or magnitude. The considerable decrease in ebb velocity at the inlet entrance and along the north jetty would result in reduced ebb flushing.

The substantial deepening by C1-A3 resulted in reduced wave height at the entrance (Appendix V Figure A31). The lower wave dissipation at the inlet mouth resulted in modestly higher waves landward of the bridge. The reduced wave height at the entrance, combined with weakened tidal flushing (Appendix V Figure A30) may promote sand deposition. The sedimentation basin at the mouth is designed to buffer the incoming sediment.

The modifications to the flow velocity can be examined in more detail at the six numerical stations (Appendix V Figure A32 and Table 6). Since the sand removal occurs landward of Station 1, its influences at that location are small. Due to the substantial deepening at Stations 2 and 3, a considerable decrease of depth-average flood and ebb velocities occurred (Table 6). Flow velocity at Station 4 increased significantly likely due to the spatial change in the flow field caused by the dredging. Appendix V Figure A32 shows that the overall magnitude changes are not significant, except at Stations 4 and 5. Overall, the wave forcing led to a decreased ebb velocity at all locations for all three wave cases (Table 6). The southerly and inlet-parallel incident waves resulted in an increased flood velocity at all stations, while the northerly approaching waves led to decreased flood currents at all stations except at station 1. As shown in Appendix V Figure A32, except the flood flow at Station 2, the overall influence of wave forcing on the current is modest. Alternative C1-A3 is recommended as an option with the lower limit in terms of sand volume removed.

Table 6. Percent changes of current velocities at the six stations (see Figure 41 for locations) under three incident wave conditions for Alternative C1-A3. The percent change was obtained by comparing with the tide-only case.

Input Wave conditions		Locations					
		1	2	3	4	5	6
Tide-only	Flood	-3%	-52%	-21%	28%	-63%	-12%
	ebb	-2%	-21%	-25%	98%	-32%	18%
1.5 - 196.3	Flood	21%	153%	29%	4%	4%	8%
	ebb	-12%	-13%	-11%	-12%	-11%	-8%
2.2 - 218	Flood	41%	172%	28%	9%	11%	12%
	ebb	-28%	-28%	-21%	-22%	-20%	-16%
2.1 - 286	Flood	4%	-49%	-19%	-3%	-3%	-8%
	ebb	-41%	-30%	-23%	-21%	-20%	-15%

5.3.4 Alternative C1-A4

Alternative C1-A4 involves the second most sand removal of 18,700 cubic yards (Table 4). The project area would be substantially deepened (Appendix IV Figures A23 and A24). At Lines 7, 8, 9, and 10, a 3.5-m (11.5 ft) deep basin would be created, with a landward slope of 1:5. The landward edge of the sand removal is designed to be at 9 m (30 ft) from the seawall. The seaward edge of the dredged basin would intercept the main channel slope at 3.5 m (11.5 ft) depth. In the vicinity of the bridge, same design as described above is proposed for Lines 11, 12, 14 and 15. At Line 13, the sand removal design for C1-A4 is the same as for the other alternatives. At Lines 16 and 17 (Appendix IV Figure A26), a 4.5-m (14.8 ft) deep basin would be created.

The aggressive C1-A4 alternative would remove a substantial amount of sand from the tip of the north jetty to the marinas. The modeling results for C1-A4 fall in between C1-A3 and C1-A5 (discussed in the following). As compared to the existing conditions, this bathymetry change along the north side still does not have significant influence on the flow through the main channel. The considerably reduced flow velocity and wave height at the entrance and along the north jetty would lead to sand deposition in the designed sedimentation basin there. The processes that transport the sand landward, as evaluated at the six stations, are not enhanced by the sediment removal. The substantially deepened water would significantly reduce the sediment mobility. Alternative C1-A4 is recommended as an option between the minimum C1-A3 and maximum C1-A5 in terms of volume of sand to be removed.

5.3.5 Alternative C1-A5

Alternative C1-A5 involves the most sand removal of 23,700 cubic yards (Table 4). The project area would be substantially deepened (Appendix IV Figures A23 and A24). At Lines 7, 8, 9, and 10, a 4-m (13 ft) deep basin would be created, with a landward slope of 1:5. The landward edge of the sand removal is designed to be at 9 m (30 ft) from the seawall. The seaward edge of the dredged basin would intercept the main channel slope at 4 m (13 ft) depth. In the vicinity of the bridge, same design as described above is proposed for Lines 11, 12, 14 and 15. Line 13 design is the same as the previous alternatives. At Lines 16 and 17 (Appendix IV Figure A26), a 5-m (16.4 ft) deep basin would be created.

Appendix V Figure A33 illustrates the modification to the flow fields under a peak ebb and flood conditions by the C1-A5 alternative, as compared to the existing conditions. Model results show that, except at the project site, the tidal flow velocity in the main channel is still not significantly influenced by this alternative, although the flow-modification is more than the other alternatives. A slight increase in peak ebb velocity of about 0.1 m (or about 7%) occurred between the two main bridge pilings, in addition to an increase in the ebb flow just seaward of the dredge pit (Appendix V Figure A33 upper panel). These are caused by the slight modification of the ebb jet due to the substantial dredge pit. The influence on the flood flow is less than that on the ebb flow (Appendix V Figure A33 lower panel). Overall, the influences are mostly confined within the inlet channel landward of the tip or the north jetty.

At the project site, due to the substantial deepening of the project area, a significant decrease of the depth-averaged velocity occurred for both flood and ebb flows (Appendix V Figure A33). Similar to the other cases, the localized increases in flow velocity, particularly during the peak ebb which occurs at a low tide water level, is caused by the conversion of an existing emerged area (with zero tidal flow) to a shallow area by the sand removal. The substantial decrease in ebb velocity at the inlet entrance and along the north jetty would result in considerably reduced ebb flushing.

Due to the substantial deepening by C1-A5 alternative, it resulted in a considerably reduced wave height at the entrance (Appendix V Figure A34). The lower wave dissipation at the inlet mouth resulted in modestly higher wave landward of the bridge. The reduced wave height at the entrance, combined with weakened tidal flushing (Appendix V Figure A33) would promote sand deposition to a greater extent than the other alternatives. The considerably deeper sedimentation basin at the mouth is designed to buffer the potentially increased incoming sediment.

The modifications to the flow velocity can be examined in more detail at the six numerical stations (Appendix V Figure A35 and Table 7). Since the sand removal occurs landward of Station 1, its influences at that location are still limited with a 4% decrease on average ebb velocity and 8% on flood velocity. Due to the substantial deepening at Stations 2 and 3, the depth-averaged flood and ebb velocities decreased substantially (Table 7). Flow velocity at Station 4 increased significantly due to the spatial change in the flow field caused by the dredging. Except at Stations 1 and 6, a velocity decrease occurred at the rest locations. Overall, wave-generated currents have

significant influence on the flow at the six locations. Generally, the wave forcing led to a decreased ebb velocity at all locations for all three wave cases (Table 6). The southerly and inlet-parallel incident waves resulted in an increased flood velocity at all stations, while the northerly approaching wave led to decreased flood current at all stations except at stations 1 and 2. Alternative C1-A5 is recommended as an option with the upper limit in terms of sand volume removed.

Table 7. Percent changes of current velocities at the six stations (see Figure 41 for locations) under three incident wave conditions for Alternative C1-A5. The percent change was obtained by comparing with the tide-only case.

Input Wave conditions		Locations					
		1	2	3	4	5	6
Tide-only	Flood	-8%	-85%	-46%	25%	-64%	-15%
	ebb	-4%	-36%	-56%	101%	-45%	0%
1.5 - 196.3	Flood	23%	464%	36%	4%	3%	9%
	ebb	-13%	-15%	-11%	-12%	-10%	-7%
2.2 - 218	Flood	45%	643%	50%	10%	12%	18%
	ebb	-33%	-34%	-18%	-24%	-20%	-16%
2.1 - 286	Flood	10%	38%	-13%	-2%	-2%	-7%
	ebb	-34%	-25%	-17%	-15%	-13%	-11%

5.3.6 Alternative C2-A1

Alternative C2-A1 involves the least amount of sand removal of 2,900 cubic yards (Table 4). Similar to C1-A1 discussed above, the main feature of this alternative is that the excessive intertidal and emerged sand at the project area would be removed (Appendix IV Figures A23 and A24). The slope of the northern side of the channel would be restored to roughly a linear trend at most of the cross sections, e.g., at Lines 8, 9, and 10. At some of the cross sections, e.g., at Line 7, the restored slope is gentler than the steep slope into the channel thalweg. The main difference between C2-A1 and C1-A1 is that no action would be taken within 100 ft from the bridge, i.e., at Lines 11, 12, 13 and 14.

For the C2-A1 alternative, the modeled wave and current fields are very similar to those of the C1-A1 case (Appendix V Figures A36 and A37). As compared to the existing conditions, this minor bathymetry change does not have significant influence on the flow and wave fields, except locally at where the emerged area is converted to shallow area. Alternative C2-A1 should not have significant influence on the inlet hydraulics and along the adjacent beaches. However, this limited sand removal does not fundamentally change the sediment processes in the vicinity of the marina, i.e., the present situation. The small amount of sand may be replaced rather quickly under a favorable condition. For the above two reasons, Alternative C2-A1 is not recommended.

5.3.7 Alternative C2-A2

Alternative C2-A2 would remove 7,000 cubic yards of the sand (Table 4). The modeling results are quite similar to those of C1-A2 and C2-A3 (discussed in the following) and are not repeated here. Alternative C2-A2 is not recommended by this study for similar reasons that C1-A2 and C2-A3 are not recommended.

5.3.8 Alternative C2-A3

Alternative C2-A3 involves a modest sand removal of 9,700 cubic yards (Table 4). The project area would be substantially deepened (Appendix IV Figures A23 and A24). At Lines 7, 8, 9, and 10, a 3-m (10 ft) deep basin would be created, with a landward slope of 1:5. The landward edge of the sand removal is designed to be at 9 m (30 ft) from the seawall. The seaward edge of the dredged basin would intercept the main channel slope at 3 m (10 ft) depth. In the vicinity of the bridge within 100 ft from the structure, no action would be taken at Lines 11, 12, 13 and 14. Sand removal at Line 15 is similar to that at Lines 7 through 10. At Lines 16 and 17 (Appendix IV Figure A26), a 4-m (13 ft) deep basin would be created.

The modeling results are illustrated in Appendix V Figure A38, A39 and A40, in addition to Table 8. Overall, the modeled flow field (Figure A38), wave field (Figure A39) and wave-current interaction (Figure A40 and Table 8) for alternative C2-A3 are similar to those for C1-A3 (Figures A30, A31 and A32) and are not repeated here. Not removing the sand within 100 ft from the structure would have minor influence on the overall flow field. The small changes in the vicinity of the bridge, particularly the two pilings to the north, would not alter the hydrodynamic and sediment-dynamic processes. No additional bridge piling scour or sedimentation are anticipated whether the sand in that area is removed or not. The excess sand in the vicinity of the

bridge is likely transported landward and deposited in the dredged basin, and therefore may reduce the lift span of the project. For this reason, alternative C2-A3 is not recommended.

Table 8. Percent changes of current velocities at the six stations (see Figure 44 for locations) under three incident wave conditions for Alternative C2-A3. The percent change was obtained by comparing with the tide-only case.

Input Wave conditions		Locations					
		1	2	3	4	5	6
Tide-only	Flood	-4%	-56%	-42%	-3%	-7%	-38%
	ebb	-3%	-25%	-56%	-47%	-23%	6%
1.5 - 196.3	Flood	12%	275%	111%	24%	18%	29%
	ebb	-30%	-33%	-8%	74%	31%	-13%
2.2 - 218	Flood	35%	252%	92%	26%	19%	30%
	ebb	-39%	-43%	2%	135%	46%	-21%
2.1 - 286	Flood	8%	-46%	-31%	-2%	-6%	-5%
	ebb	-42%	-34%	-18%	-20%	-23%	-14%

5.3.9 Alternative C2-A4

Alternative C2-A4 would remove 13,100 cubic yards of the sand (Table 4). The modeling results are in between those of C2-A3 and C2-A5 (discussed in the following) and are not repeated here. Alternative C2-A4 is recommended only under the condition that no activities should occur within 100 ft from the bridge

5.3.10 Alternative C2-A5

Alternative C2-A5 would remove 16,600 cubic yards of the sand (Table 4). The modeling results for alternative C2-A5 are shown in Figures A41, A42, and A43, in addition to Table 9. Overall, the results are quite similar to those from alternative C1-A5 and are not repeated here. Similar to the case of C2-A3, the excess sand in the vicinity of the bridge may be re-distributed to the dredged areas, and therefore would reduce the life span of the project. Leaving the sand in place would not benefit the bridge in terms of hydrodynamic and sediment processes. Alternative

C2-A5 is recommended only under the condition that no activities should occur within 100 ft from the bridge.

Table 9. Percent changes of current velocities at the six stations (see Figure 44 for locations) under three incident wave conditions for Alternative C2-A5. The percent change was obtained by comparing with the tide-only case.

Input Wave conditions		Locations					
		1	2	3	4	5	6
Tide-only	Flood	-8%	-85%	-55%	-3%	-7%	-39%
	ebb	-6%	-40%	-70%	-51%	-20%	-10%
1.5 - 196.3	Flood	23%	897%	112%	20%	16%	6%
	ebb	-27%	-32%	-21%	59%	12%	-8%
2.2 - 218	Flood	44%	1118%	191%	42%	38%	16%
	ebb	-42%	-28%	77%	206%	84%	-20%
2.1 - 286	Flood	19%	201%	-30%	-4%	-9%	-7%
	ebb	-48%	-45%	-36%	-6%	-30%	-16%

5.3.11 Alternative C3

Alternative C3 adopts a different approach from the local sand removal as discussed above. Instead of removing the excess sand in the project area, alternative C3 is designed to block the sand from reaching the marina area by artificially closing the gap between the north seawall and the north most bridge piling by installing a barrier there.

Closing the relatively narrow and presently shallow gap between the north seawall and the north most bridge piling has little influence on the overall flow field of Johns Pass except within the immediate vicinity of the closure (Figure A44). Because the tidal flow between the seawall and the north most bridge piling is blocked, the tidal flow velocity along the southside (inlet side) of the piling would increase slightly as caused by the reduction of the cross-sectional area. Closing the gap would also have minimal influence on the wave field, except at the immediate vicinity of the barrier (Figure A45). Waves are blocked directly landward (eastward) of the barrier, as illustrated by the wave-height reduction. A detailed examination of the flow conditions at the six locations reveals minimal changes, except at Stations 4 and 5 where the

flow is blocked (Figure A46 and Figure 41). Overall, closing the gap between the north seawall and the bridge piling has localized influences on current and wave conditions.

Alternative C3 is not recommended because it would not solve the existing sedimentation problem. If a considerable amount of sand is removed, e.g., with alternatives C1-A3, C1-A4, or C1-A5, there would not be a need to close the gap. Creating a sedimentation basin seaward of the bridge is more effective in preventing sand from reaching the marina facilities than a barrier directly adjacent to the facilities.

Table 10. Percent changes of current velocities at the six stations (see Figure 41 for locations) under three incident wave conditions for Alternative C3. The percent change was obtained by comparing with the tide-only case.

Input Wave conditions		Locations					
		1	2	3	4	5	6
Tide-only	Flood	-1%	-4%	-15%		-74%	13%
	ebb	-1%	-1%	-6%		-79%	-1%
1.5 - 196.3	Flood	19%	64%	28%		3%	4%
	ebb	-12%	-12%	-16%		-25%	-7%
2.2 - 218	Flood	39%	117%	61%		10%	11%
	ebb	-36%	-35%	-34%		-18%	-16%
2.1 - 286	Flood	10%	-23%	-19%		0%	-5%
	ebb	-34%	-21%	-20%		-33%	-11%

6.0 Conclusions

The sedimentation along the north bank of Johns Pass is driven by a natural process that occurs at many tidal inlets. The sand moving southward along Madeira Beach and from the shallow channel margin linear bar can be carried into the inlet by the flood tidal current. Sand accumulation occurs at locations within the channel where the ebb tidal current is not adequate to flush all the sand out of the inlet. This natural process is modified by various engineering activities at Johns Pass over the past 90 years. However, none of these engineering activities has fundamentally

changed the sand supply to the channel interior and the natural process that brings the sand into the channel.

It is proposed that local removal of the sand accumulation should be the main mitigation approach. A crucial consideration in designing and evaluating the alternatives is that local sand removal is the least likely to induce negative impacts at other parts of Johns Pass and along adjacent beaches. Three categories of mitigation measures are examined. Category 1 (C1) involves removal of excess sand from the seaward tip of the north jetty to the marina; five sand removal alternatives (C1-A1 to C1-A5) are examined. Category 2 (C2) involves removal of excess sand from the seaward tip of the north jetty to the marina, while excluding the area within 100 ft from the Johns Pass bridge; five sand removal alternatives (C2-A1 to C2-A5) are examined. Category 3 (C3) examines the option of blocking the sand from reaching the marinas by constructing a barrier between the north seawall and the north most bridge piling.

Based on the modeling results, the ten alternatives of C1 and C2 have negligible influence on the overall flow and wave fields within the Johns Pass channel. All eleven alternatives have minimal influence on the processes along the adjacent beaches. Alternative C3 is not recommended because it does not solve the existing sedimentation problem. Alternative C1-A3 which removes 14,000 cubic yards of sand is recommended as a lower limit of the mitigation measure. Alternative C1-A5 which removes 23,700 cubic yards of sand is recommended as an upper limit. Alternative C1-A4 removing 18,700 cubic yards of sand is recommended as a middle range for the mitigation. Based on the sedimentation rate estimated from existing bathymetry data, the three recommended alternatives, C1-A3, C1-A4, and C1-A5 should have a life span of 8, 11, and 14 years, respectively.

Estimating future rate of sedimentation constitutes a major limitation of this study. It is assumed that the sedimentation rate obtained during a short period of time, 2018 through 2020, can be applied to approximate future sedimentation at the project site. This assumption can be influenced by the unpredictable nature of storms and engineering activities.

7.0 References

Beck, T.M. and Wang, P., 2019. Morphodynamics of barrier-inlet systems in the context of regional sediment management, with case studies from west-central Florida, USA. *Ocean and Coastal Management*, 177, 31-51.

Beck, T.M., Wang, P., Li, H., and Wu, W., 2020. Sediment Bypassing Pathways between Tidal Inlets and Adjacent Beaches. *Journal of Coastal Research*, 36, 897-914, https://doi.org/10.2112/JCOASTRES-D-19-00141.1.

Barnard, P.L., 1998. Historical Morphodynamics of Inlet Channels: West-Central Florida. *MS thesis*, Department of Geology, University of South Florida, Tampa, Florida, 179 pp.

Bodge, K.R. and Rosati, J.D., 2002. Chapter 6: Sediment Management at Inlets. In: Coastal Engineering Manual, Part V, U.S. Army Corps of Engineers, Washington, DC.

Bruun, P., 1978. Stability of Tidal Inlet: Theory and Engineering. Elsevier Scientific Publishing Company, Amsterdam, 510 pp.

Buttolph, A.M., Reed, C.W., Kraus, N.C., Ono, N., Larson, M., Camenen, B., Hanson, H., Wamsley, T., Zundel, A.K., 2006. Two-dimensional depth-averaged circulation model CMS-M2D: Version 3.0, Report 2, sediment transport and morphology change. *ERDC/CHL TR-06-9*, U.S. Army Engineer Research and Development Center, Vicksburg, Mississippi, 149 pp.

CERC, 1984. Shore Protection Manual. U.S. Army Corps of Engineers, Coastal Engineering Research Center, U.S. Government Printing Office, Washington, D.C.

Cheng, J., Toledo Cossu, and Wang, P., 2021. Factors controlling longshore variations of beach changes induced by Tropical Storm Eta (2020) along Pinellas County beaches, west-central Florida, *Shore and Beach*, 89, http://doi.org/10.34237/1008929.

COEL, 1966. Results of current study at John's Pass, Florida. Coastal and Oceanographic Engineering Laboratory Report *UFL/COEL 66/005*, University of Florida, Gainsville, Florida, June, 1966.

COEL, 1969. An investigation to evaluate possible effects of new John's Pass bridge ion currents and inlet stability. Coastal and Oceanographic Engineering Laboratory Report *UFL/COEL 69/011*, University of Florida, Gainsville, Florida, May, 1969.

CPE (Coastal Planning and Engineering, Inc.), 1992. Blind Pass Inlet Management Plan, Pinellas County, Florida, 68 p.

CTC (Coastal Technology Corporation), 1993. John's Pass inlet management plan. CTC, Vero Beach, FL, p. 28.

Davis, R.A., 1994. Barriers of the Florida Gulf Peninsula. In: Davis, R.A. (Ed.), *Geology of Holocene Barrier Island Systems*. Springer-Verlag, pp. 167–206.

Davis, R.A., 1997. Regional coastal morphodynamics along the United States Gulf of Mexico. *Journal of Coastal Research*, 13, 595–604.

Davis, R.A. and Gibeaut, J.C., 1990. Historical morphodynamics of inlets in Florida. *Technical Paper 55*, Florida Sea Grant College Program, 81 pp.

Dean, R. G. and O'Brien, M. P., 1987. Florida's west coast inlets: Shoreline effects and recommended actions. University of Florida, Coastal and Oceanographic Engineering Department, Gainesville, FL, 100 p.

Elko, N.A., 2006. Storm-influenced sediment transport gradients on a nourished beach. Ph.D. Dissertation, University of South Florida, Tampa, FL, 177p.

Elko, N.A., Holman, R.A., Gelfenbaum, G., 2005. Quantifying the rapid evolution of a nourishment project with video imagery. Journal of Coastal Research, 21, 633–645.

Elko, N.A., Wang, P., 2007. Immediate profile and planform evolution of a beach nourishment project with hurricane influences. Coastal Engineering, 54, 54–79.

Davis, R. A. Jr. and Barnard, P., 2003. Morphodynamics of the barrier-inlet system, west-central Florida. *Marine Geology*, 200, 77-101.

Gibeaut, J.C., 1991. Morphodynamic classification, evolution, and modeling of unstructured inlets in west-central Florida. *Ph.D. dissertation*, Department of Marine Science, University of South Florida, Tampa, FL, 192 pp.

Komar, P.D., 1996. Beach Processes and Sedimentation. Prentice-Hall, New Jersey, 546 pp.

Kraus, N.C. and Rosati, J.D., 1998. Estimation of Uncertainty in Coastal Sediment Budgets at Inlets. Coastal Engineering Technical Note IV-16, pp. 12.

Loeb, W.A., 1994. Beaches of Pinellas County, Florida: A history of their comings and goings (circa 1950-present). *USGS Open File Report 94-565*.

Lin L., Demirbilek, Z., Mase, H., 2011. Recent capabilities of CMS-Wave: A coastal wave model for inlets and navigation projects. *Journal of Coastal Research*, Special Issue 59, 7-15.

Mehta, A.J. (editor), 1993. Beach/Inlet Processes and Management: A Florida Perspective. Journal of Coastal Research, Special Issue 18.

Mehta, A. J., Byrne, R. J. and DeAlteris, 1975. Hydraulic constants of tidal entrances III: Bed friction measurements at John's Pass and Blind Pass. University of Florida, Coastal and Oceanographic Engineering Laboratory, *Technical Report no. 26*, 78p.

Mehta, A.J., Adams, W.D., Jones, C.P., 1976. John's Pass and Blind Pass: Glossary of Inlets *Report Number 4*. Florida Sea Grant Program, Report Number 18, 66 pp.

Lemke L, and J.K. Miller, 2020. "Evaluation of storms through the lens of erosion potential along the New Jersey, USA coast." *Coastal Engineering*, 158, https://doi.org/10.1016/j.coastaleng.2020.103699.

Roberts, T.M. and Wang, P., 2012. Four-year performance and associated controlling factors of several beach nourishment projects along three adjacent barrier islands, West-Central Florida, USA. *Coastal Engineering*, 70, 21-39.

Rosati, J.D., 2005. Concepts in sediment budgets. Journal of Coastal Research, 21, 307-322.

Rosati, J.D. and Kraus, N.C., 1999. Formulation of sediment budgets at inlets. Coastal Engineering Technical Note IV-15, pp. 20.

Rosati, J.D. and Kraus, N.C., 1999b. Sediment Budget Analysis System (SBAS). Coastal Engineering Technical Note IV-20, pp. 14.

Rosati, J.D. and Kraus, N.C., 2003. Sediment Budget Analysis System (SBAS): Upgrade for Regional Applications. ERDC/CHL CHETN-XIV-3, pp. 13.

Sanchez, A., Wu, W., 2011. A non-equilibrium sediment transport model for coastal inlets and navigation channels. *Journal of Coastal Research*, Special Issue 59, 39-49.

Sánchez, A., Wu, W., Li, H., Brown, M., Reed, C., Rosati, J.D., and Demirbilek, Z., 2014. Coastal Modeling System: Mathematical Formulations and Numerical Methods. *ERDC/CHL TR-14-2*, pp. 104.

Wang, P. and Kraus, N.C., 1999. Longshore sediment transport rate measured by short-term impoundment. *Journal of Waterway, Port, Coastal and Ocean Engineering*, ASCE 125: 118-126.

Wang, P., 1998. Longshore sediment flux in the water column and across the surf zone. *Journal of Waterway, Port, Coastal & Ocean Engineering*, ASCE, 124: 108-117.

Wang, P., Kraus, N.C., and Davis, R.A., Jr., 1998. Total rate of longshore sediment transport in the surf zone: field measurements and empirical predictions. *Journal of Coastal Research*, 14(1): 269-283.

Wang, P. and Davis, R.A., 1999. Depth of closure and the equilibrium beach profile – A case study from Sand Key, West-Central Florida. *Shore and Beach*, 67: 33-42.

Wang, P., Tidwell, D.K., Beck, T.M., Kraus, N.C., 2007. Sedimentation patterns in a stabilized migratory inlet, Blind Pass, Florida. *Proceedings of Coastal Sediments 07*, ASCE Press, pp. 1377–1390.

Wang, P. and Beck, T.M., 2012. Morphodynamics of an anthropogenically altered dual-inlet system: John's Pass and Blind Pass, west-central Florida. *Marine Geology*, 291-294, p.162-175.

Wang, P., Horwitz, M.H., and Cheng, J., 2016. Inlet Management Study for John's Pass and Blind Pass, Pinellas County, Florida. *Technical Report*, University of South Florida, Coastal Research Lab, pp.300.

Wang, P., Beck T.M., and Roberts T.M., 2011. Modeling regional-scale sediment transport and medium-term morphology change at a dual inlet system examined with the Coastal Modeling System (CMS): A case study at Johns Pass and Blind Pass, west-central Florida. *Journal of Coastal Research*, Special Issue 59, 49-60.

Walton, T.L., JR., Dean, R.G., and Rosati, J.D., 2012. Sediment budget possibilities and improbabilities. *Coastal Engineering*, 60, 323-325.

Willmott, C. J. (1981). On the validation of models. *Physical Geography*, 2, 184–194.

Appendices

Appendix I

Table 11. Engineering History at John's Pass (JP), Sand Key (SK), Treasure Island (TI), and Boca Ciega Bay. Large scale beach nourishment projects were conducted along Sand Key since 1988. A total of 9,311,000 cubic yards of sand were placed on Sand Key along a roughly 16 km (10 miles) of beach between 1988 and 2018 (Roberts and Wang, 2012). The south end of the Sand Key beach nourishment projects is about 3 miles north of Johns Pass.

Year	Project Description	Volume (yd^3)	Comments	Start Location	End Location	Reference
1848	JP breached by a hurricane					Mehta et al, 1976
1927	JP bridge (1st) and road on TI constructed					CTC, 1993
1934	Madeira Beach groin constructed		Two 150-foot groins constructed on VA beach at Madeira Beach			CTC, 1993
1945	Hurricane (June 19-27) destroyed TI seawall and upland homes					CTC, 1993
1950	Dredge and fill in the back bay 1940s - 1950's		much of the back bay was bulk-headed			CTC, 1993
1957	Madeira Beach groins constructed		37 timber concrete groins constructed			Pinellas County comprehensive plan
1960	JP dredged	94,000	dredge material placed on the southern flank of JP ebb shoal outer bar, later formed the O'Brien's lagoon (1968)			Dean and O'Brien, 1987; Loeb, 1994
1960	56 groins constructed on TI					Pinellas County comprehensive plan

Year	Project Description	Volume (yd^3)	Comments	Start Location	End Location	Reference
1961	North jetty constructed at JP		460 ft curved jetty constructed on north side of JP filled with 30,000 cy^3 of sand from JP channel			Pinellas County comprehensive plan; CTC, 1993
1961	JP dredged	30,000	placed on beach directly north of inlet			Dean and O'Brien, 1987
1964	Federal authorization of JP		under Section 107 of the 1960 River and Harbors Act			Elko et al., 2005; CTC, 1993
1966	Revetment along south bank of JP		920 ft along south bank of JP			CTC, 1993
1966	JP dredged	78,000	placed offshore			Dean and O'Brien, 1987; CTC, 1993
1966	UF COEL conducts current study at JP					COEL, 1966, 1969
1968	JP and TI revetment construction		Sunshine Beach	R126	R131	ACE, 2014; CTC, 1993
1968	O'Brien's Lagoon formed		1960 JP dredge material migrating onshore			CTC, 1993
1968	State establishes MHW on TI					
1969	New Bridge (2^{nd}) constructed across JP					CTC, 1993
1969	First nourishment of TI	790,000	material dredged from shore parallel-offshore pit 600 m offshore Sunset Beach, and BP	R133	R141	ACE 2014; CTC, 1993; CPE, 1992

Year	Project Description	Volume (yd^3)	Comments	Start Location	End Location	Reference
1971	TI Mid-Beach renourishment	75,000	part of the seaward sediment from O'Brien's lagoon (DEP SBMP, 2008)	R131	R133	ACE 2014; CPE 1992
1981	JP dredged	53,500	placed on Sunshine Beach			ACE 2014
1981	Sunshine Beach renourishment	53,500	Dredged from JP	R127	R130	ACE 2014:FDEP-BBCS, 2008
1985	Redington shores breakwater constructed			R101		ACE compilation, 2014
1987	North jetty re-constructed at JP					Pinellas County comp plan_ch-2; ACE 2014
1988	JP dredged	380,000	from channel and ebb shoal			Barnard, 1998
1988	Renourishment of Sand Key	300,000	Redington shores/North Redington Beach	R99	R107	Pinellas County, 2006; CTC 1993; Martin, 1992: Barnard, 1998
1990	Renourishment of Sand Key	1,300,000	Indian Rocks Beach/material dredged from offshore Mullet Key and Egmont Channel	R72	R85	Loeb, 1994
1991	JP dredged	56,000	placed on Sunshine Beach			ACE 2014; CTC 1993
1991	Sunshine Beach renourishment	56,000	material dredged from JP	R127	R129	Pinellas County comprehensive plan; ACE 2014
1992	Renourishment of Sand Key	850,000	Indian Shores/North Redington Beach	R85	R107	Pinellas County, 2006; Loeb, 1994
1999	Renourishment of Sand Key (1998-99)	2,612,000	Clearwater Beach to North Redington Beach	R56	R107	Pinellas County, 2006

Year	Project Description	Volume (yd^3)	Comments	Start Location	End Location	Reference
2000	JP and BP dredged	390,000	material placed on Sunshine and Sunset beaches; NOTE DEP 2008 reports 390,000 cy			ACE 2014
2000	Terminal structure constructed on south side of JP		Last hard structure at JP			Pinellas County comprehensive plan
2000	Sunshine Beach renourishment	40,000	material dredged from JP and BP	R126	R129	Pinellas County comprehensive plan; ACE 2014
2006	Renourishment of Sand Key	1,700,000	Sand from Egmont shoals	R56	R107	Roberts and Wang, 2012
2006	Sunshine Beach renourishment - emergency	77,970	emergency renourishment - material from west Egmont Shoals	R126	R128	Pinellas County comprehensive plan; ACE 2014
2010	JP Dredging	253,000	JP channel and ebb shoal			Pinellas County, 2010
2010	Renourishment of Sunshine Beach	127,260	JP ebb shoal	R126	R128	Pinellas County, 2010; ACE 2014
2006-2011	New JP bridge (3^{rd}) construction.		Same location as the 2^{nd} bridge, larger pilings			This study
2012	Renourishment of Sand Key beaches	1,250,000	offshore	R56	R107	
2014	Sunshine Beach renourishment	67,000	material dredged from East Egmont Shoal	R126	R128	ACE 2014
2018	JP Dredging	110,000	JP channel and ebb shoal			ACE 2014
2018	Renourishment of Sand Key beaches	1,293,000	Sand from Egmont shoal	R56	R107	This study
2018	Redington Beach berm restoration	6,400	Truck haul			This study

Year	Project Description	Volume (yd^3)	Comments	Start Location	End Location	Reference
2018	Renourishment of Sunshine and Sunset beaches	273,000	Material from JP and Egmont shoal			This study

Appendix II
Aerial Images

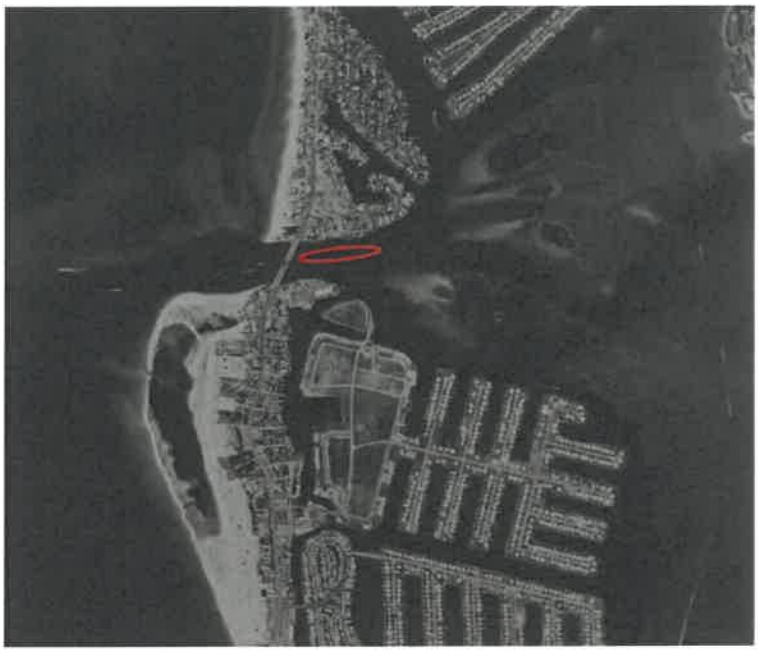

Figure A1. 1971 aerial photo of Johns Pass.

Figure A2. 1973 aerial photo of Johns Pass.

Figure A3. 1975 aerial photo of Johns Pass.

Figure A4. 1976 aerial photo of Johns Pass.

Figure A5. 1980 aerial photo of Johns Pass.

Figure A6. 1984 aerial photo of Johns Pass.

Figure A7. 1990 aerial photo of Johns Pass.

Figure A8. 1993 aerial photo of Johns Pass.

Figure A9. 2002 aerial photo of Johns Pass.

Figure A10. 2004 aerial photo of Johns Pass.

Figure A11. 2007 aerial photo of Johns Pass.

Figure A12. 2015 aerial photo of Johns Pass.

Figure A13. 2018 aerial photo of Johns Pass.


Figure A14. 2021 aerial photo of Johns Pass.

Appendix III
Modeled Wave-current Interaction

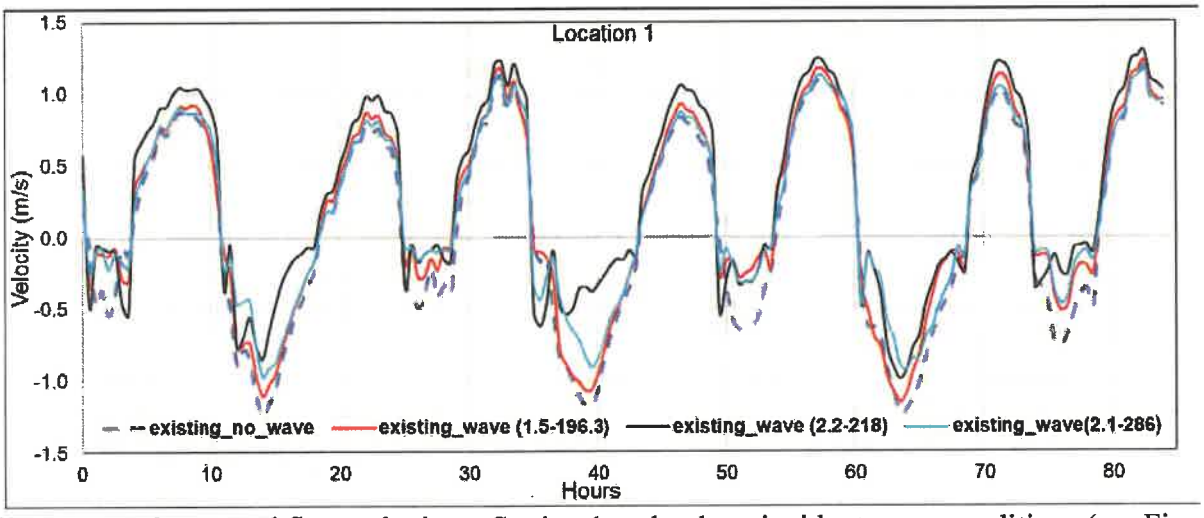

Figure A15. Computed flow velocity at Station 1 under three incident wave conditions (see Figure 41 for the location). Positive velocity represents flood current and negative represents ebb current.

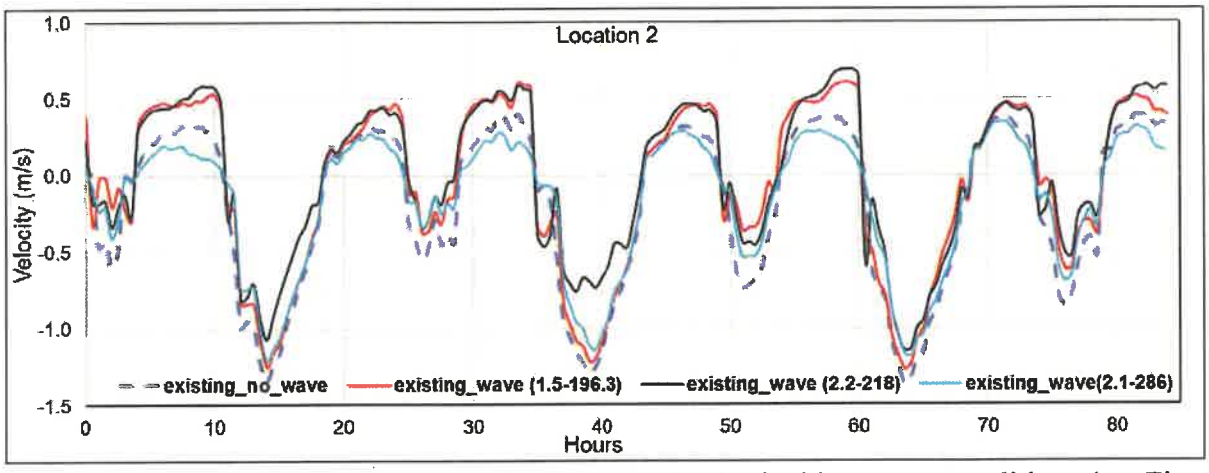

Figure A16. Computed flow velocity at Station 2 under three incident wave conditions (see Figure 41 for the location). Positive velocity represents flood current and negative represents ebb current.

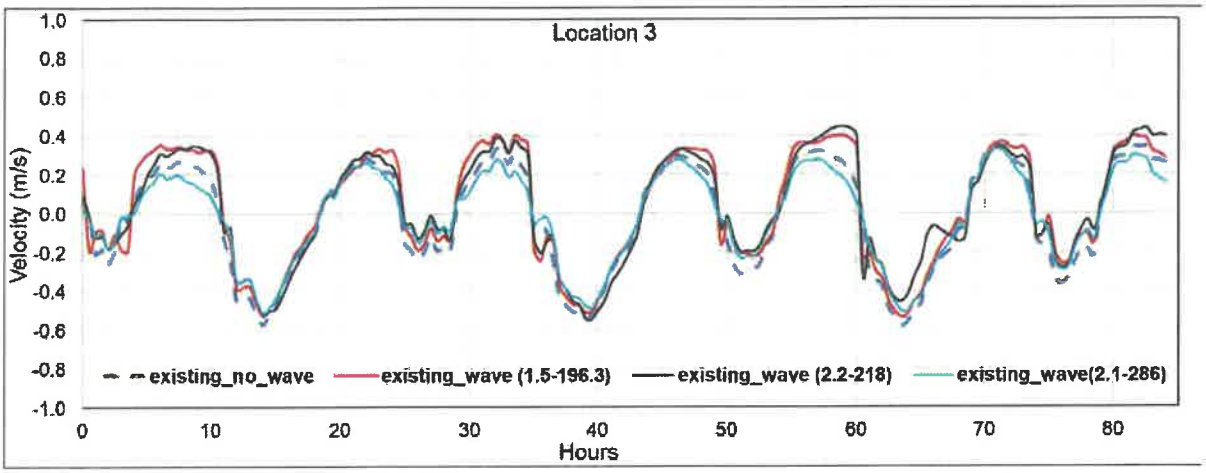

Figure A17. Computed flow velocity at Station 3 under three incident wave conditions (see Figure 41 for the location). Positive velocity represents flood current and negative represents ebb current.

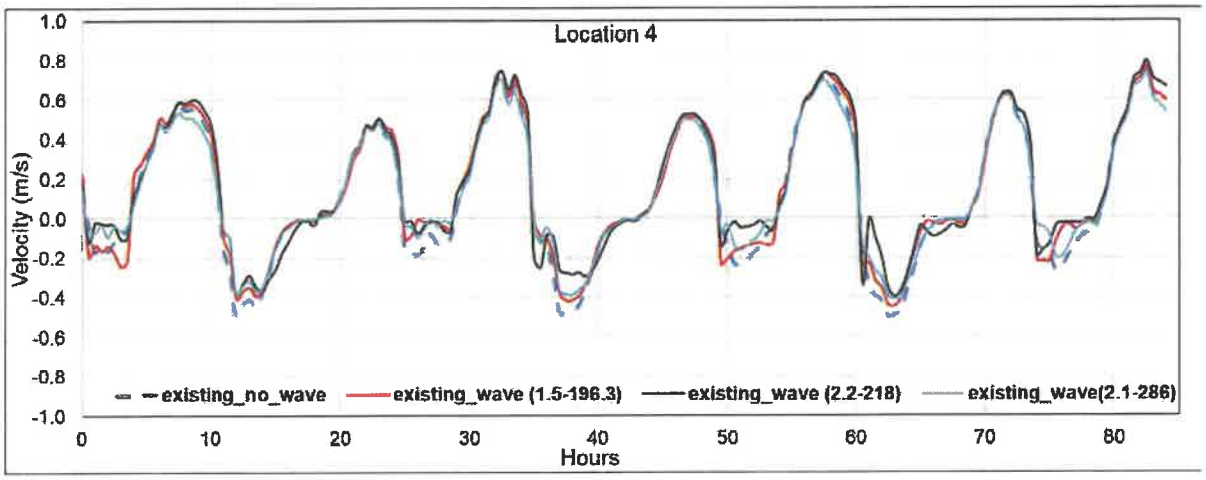

Figure A18. Computed flow velocity at Station 4 under three incident wave conditions (see Figure 41 for the location). Positive velocity represents flood current and negative represents ebb current.

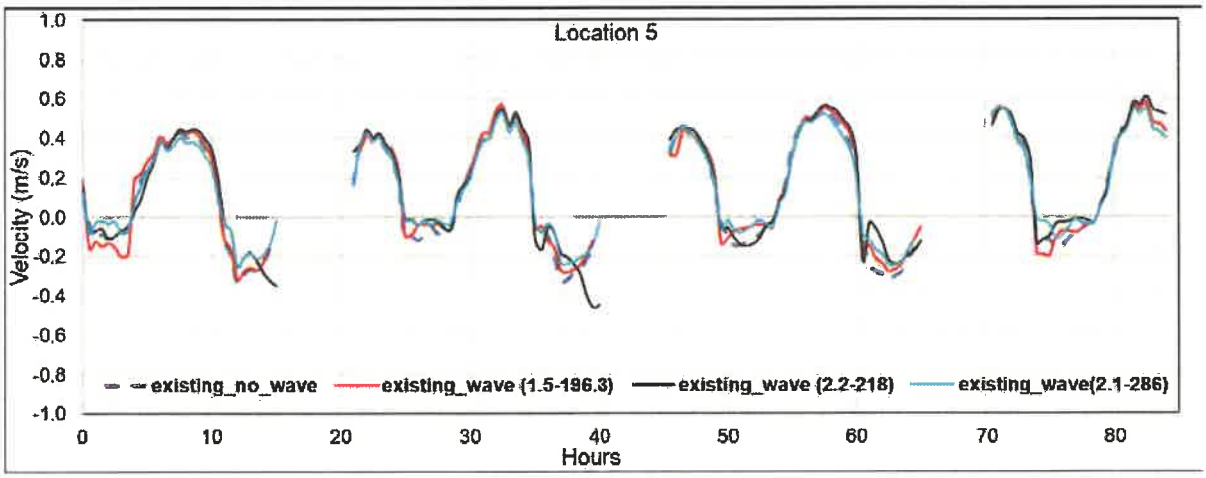

Figure A19. Computed flow velocity at Station 5 under three incident wave conditions (see Figure 41 for the location). Positive velocity represents flood current and negative represents ebb current.

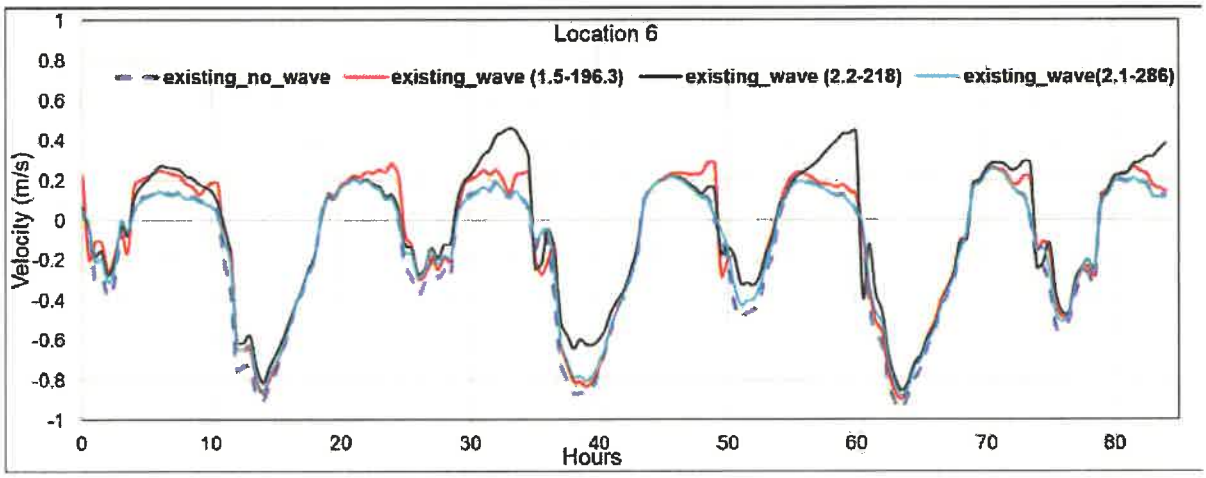

Figure A20. Computed flow velocity at Station 6 under three incident wave conditions (see Figure 41 for the location). Positive velocity represents flood current and negative represents ebb current.

Appendix IV
Johns Pass Cross Sections

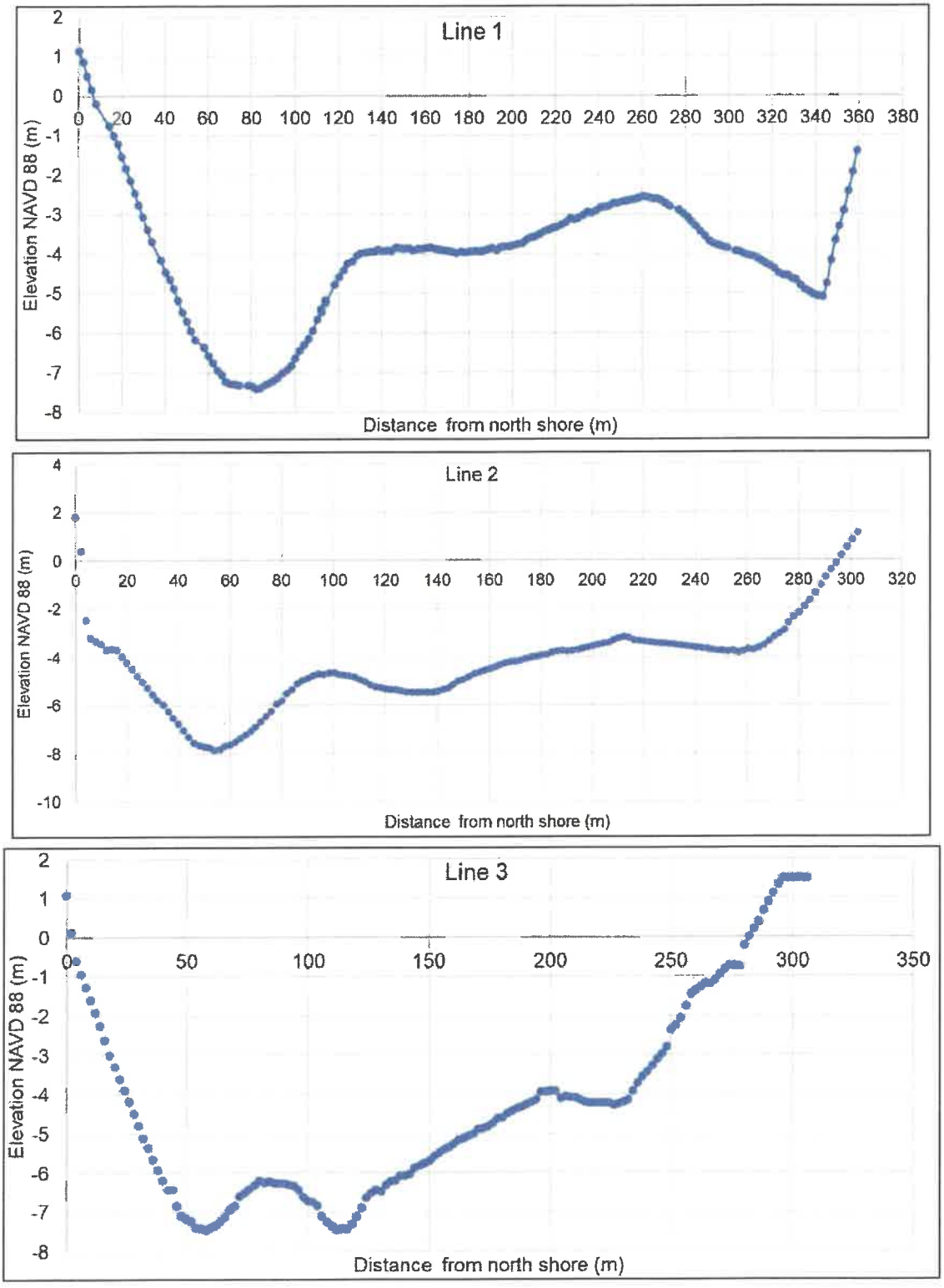

Figure A21. Cross sections 1, 2 and 3. Locations are shown in Figure 56.

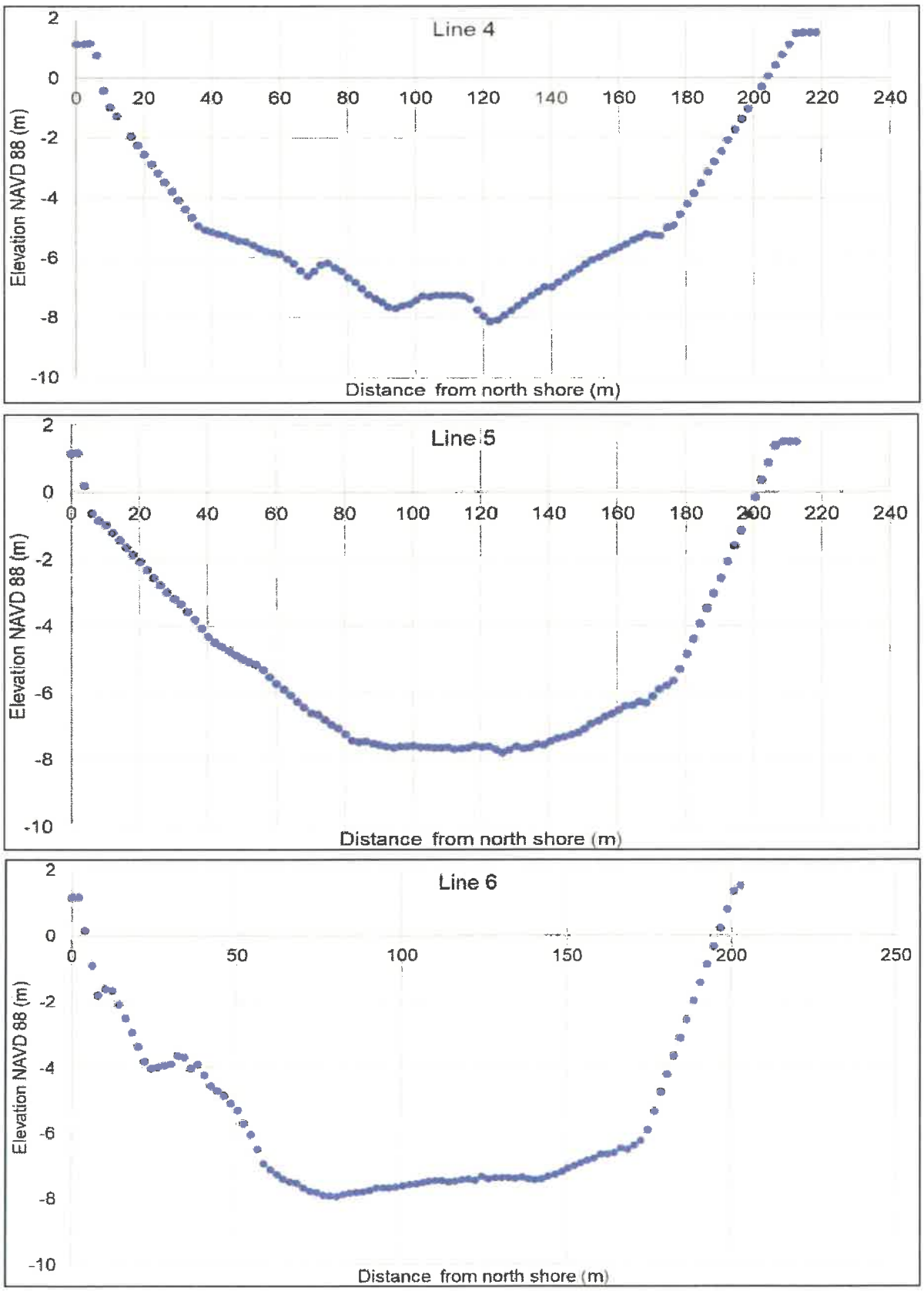

Figure 22. Cross sections 4, 5 and 6. Locations are shown in Figure 56.

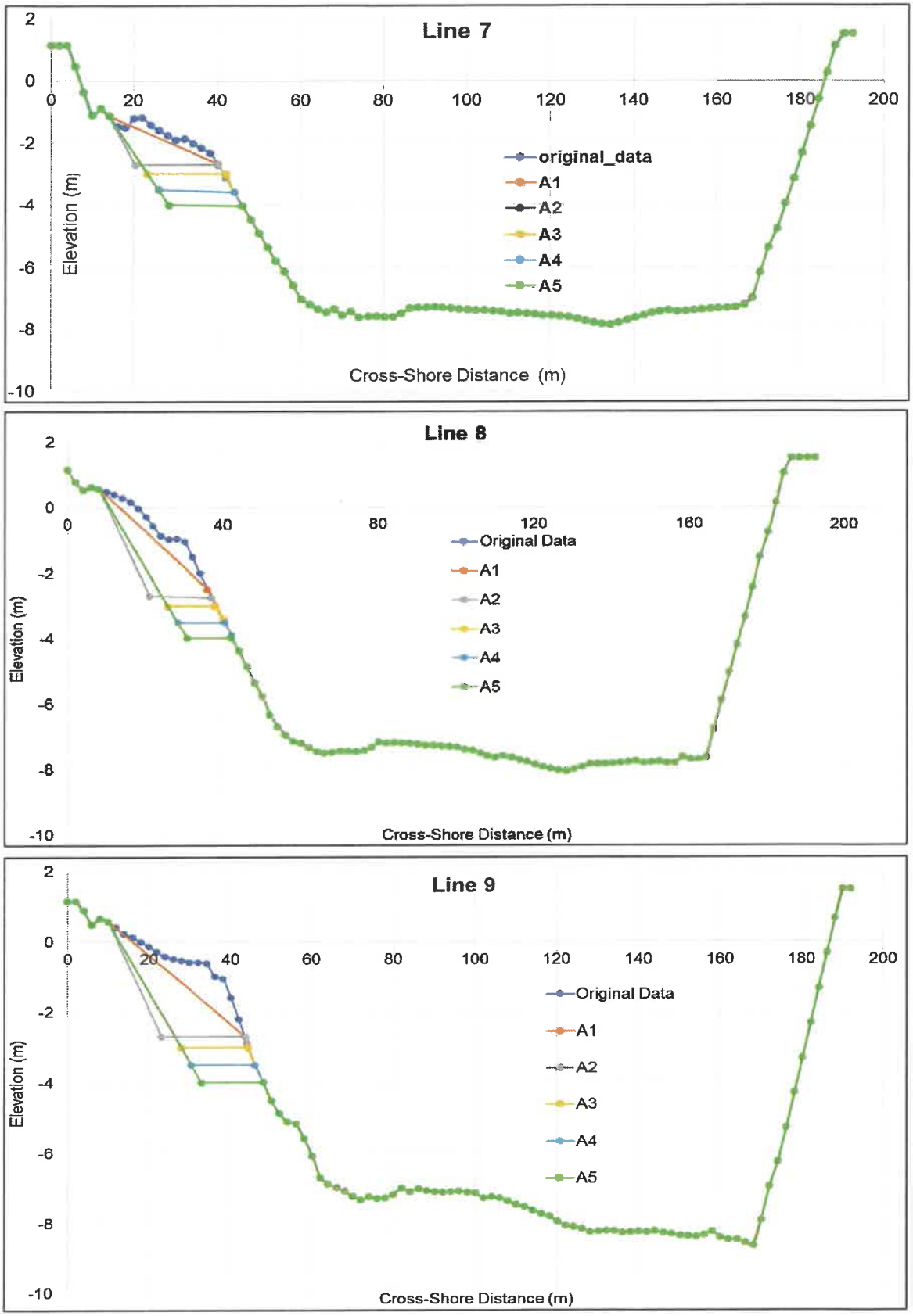

Figure 23. Cross sections 7, 8 and 9. Locations are shown in Figure 56.

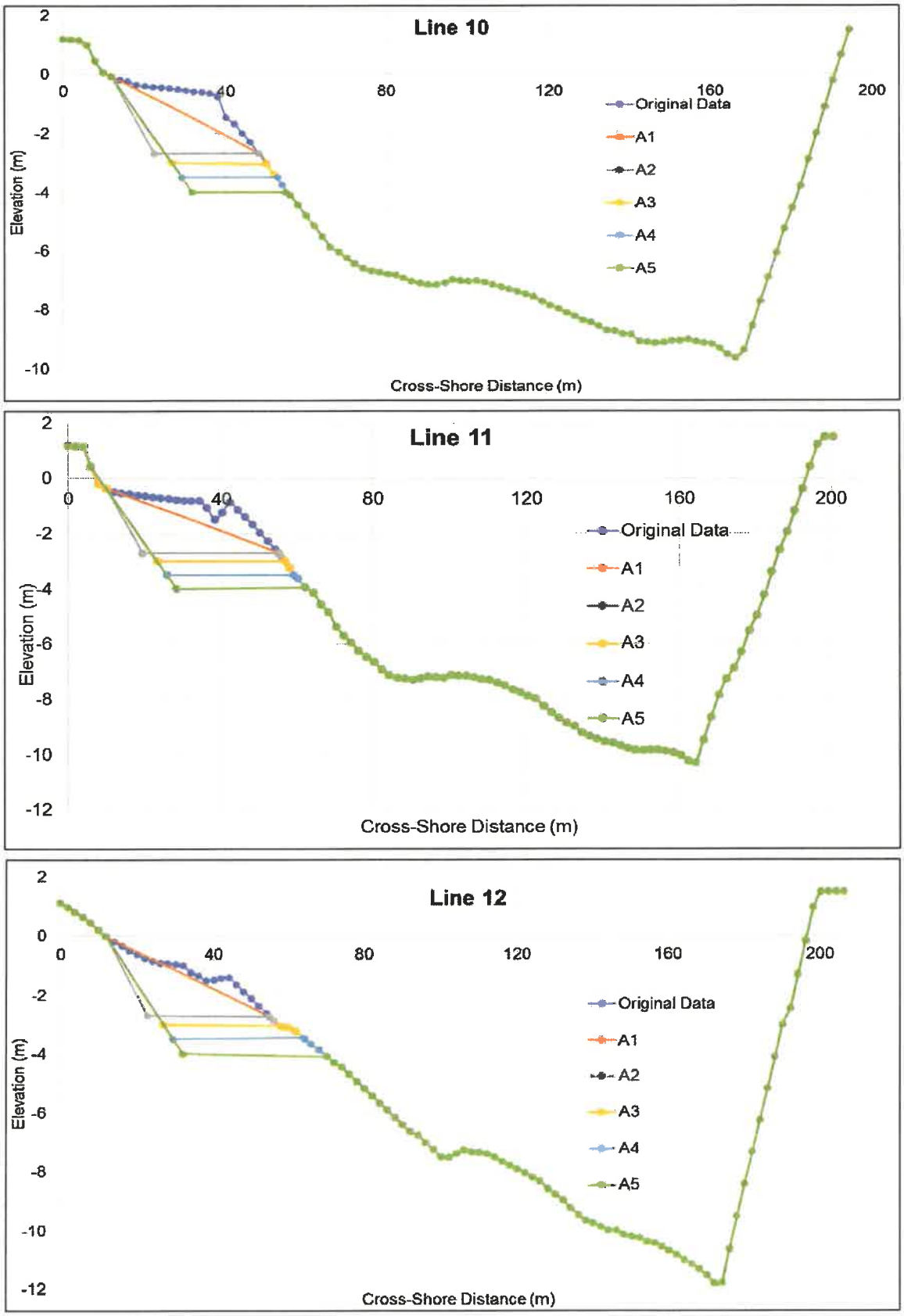

Figure A24. Cross sections 10, 11 and 12. Locations are shown in Figure 56.

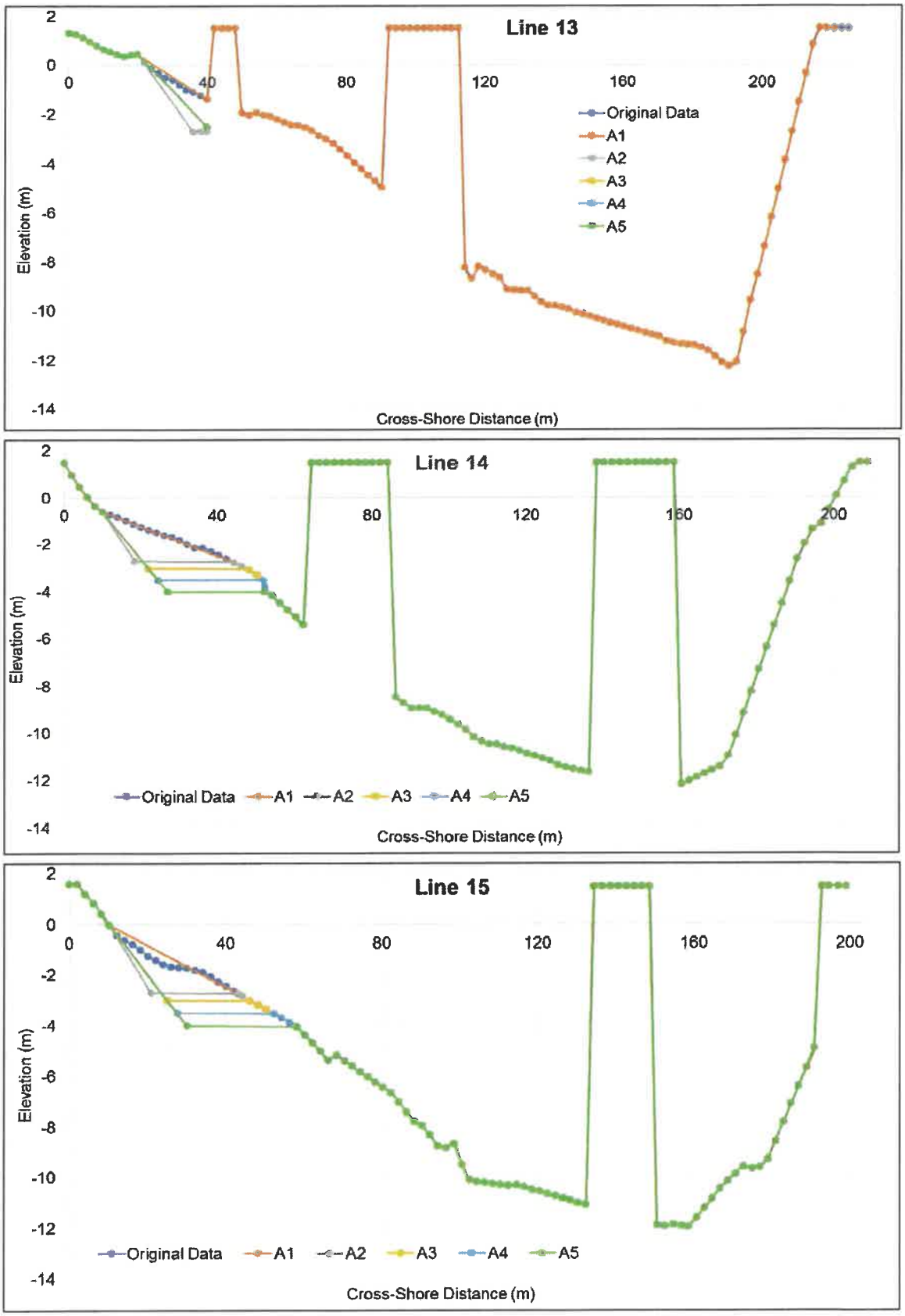

Figure A25. Cross sections 13, 14 and 15. Locations are shown in Figure 56.

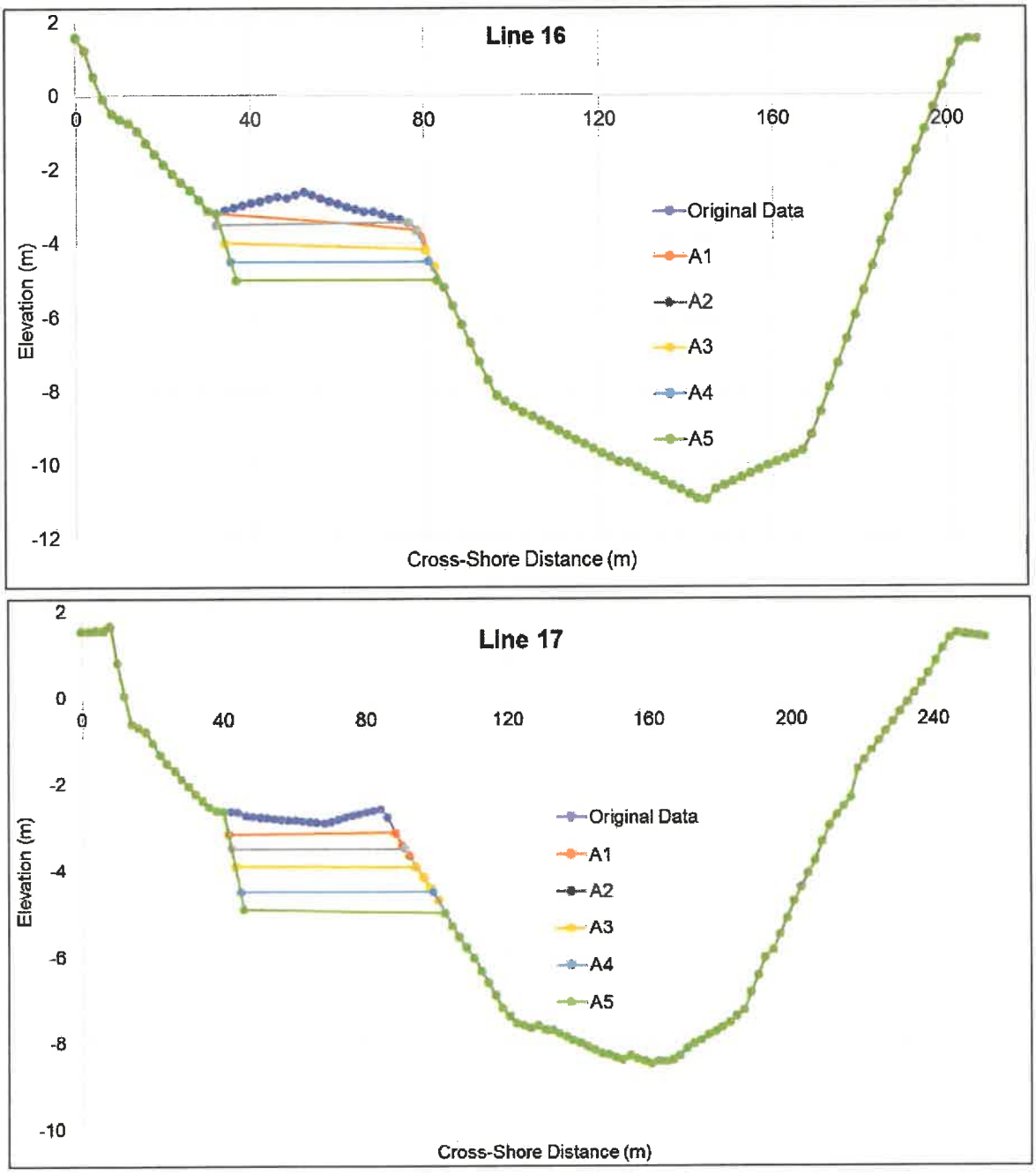

Figure A26. Cross sections 16 and 17. Locations are shown in Figure 56.

Modeling Results for C1-A1

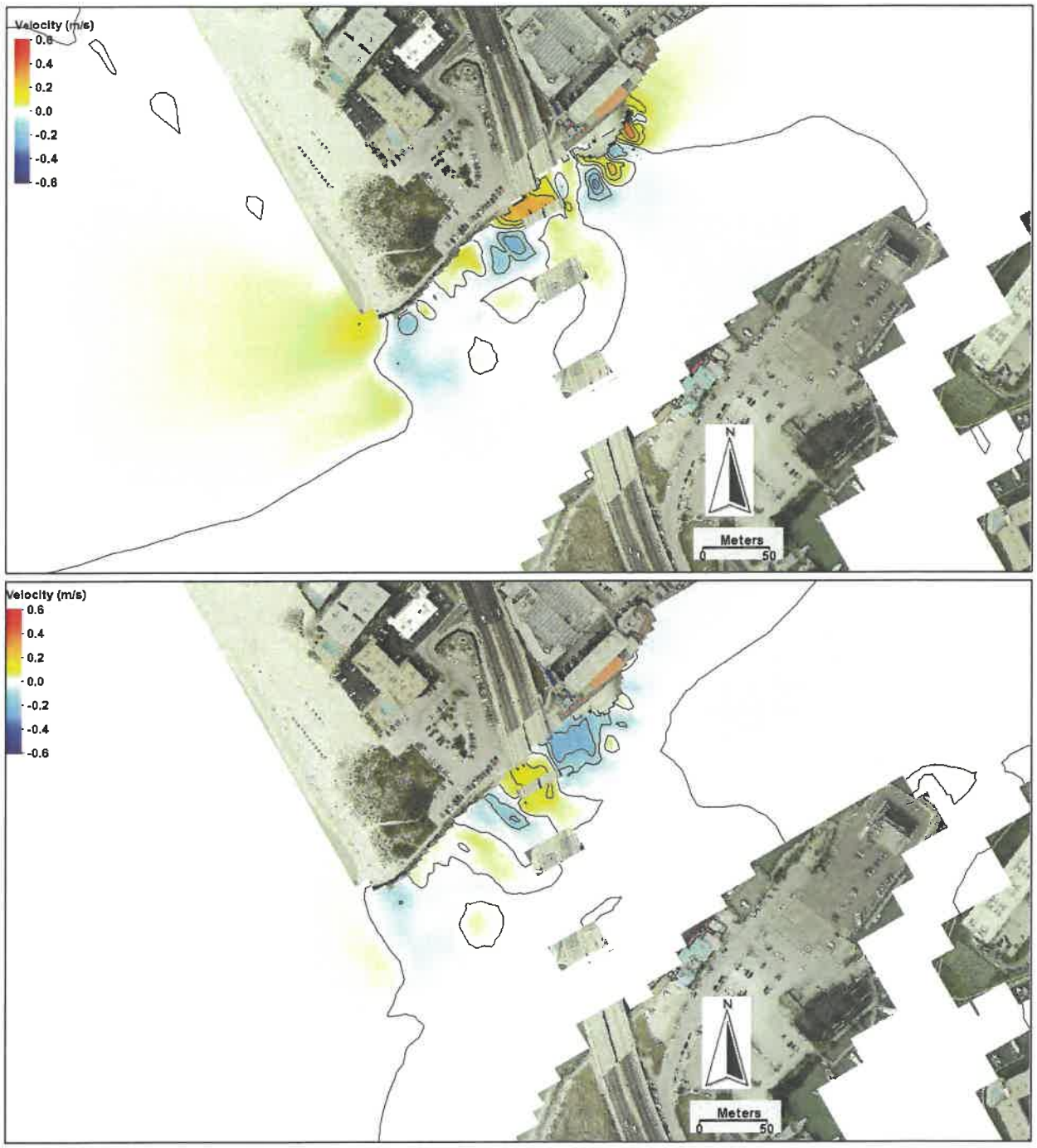

Figure A27. Difference map in velocity magnitude comparing C1-A1 with existing condition. Upper: peak ebb. Lower: peak flood. Positive: velocity increase; negative: velocity decrease.

Figure A28. Wave-height difference at high tide between C1-A1 and existing conditions. Positive values indicate higher waves for C1-A1. From top to bottom, incident wave angles are 173.25, 196.25, 218.75, and 286.25 degrees.

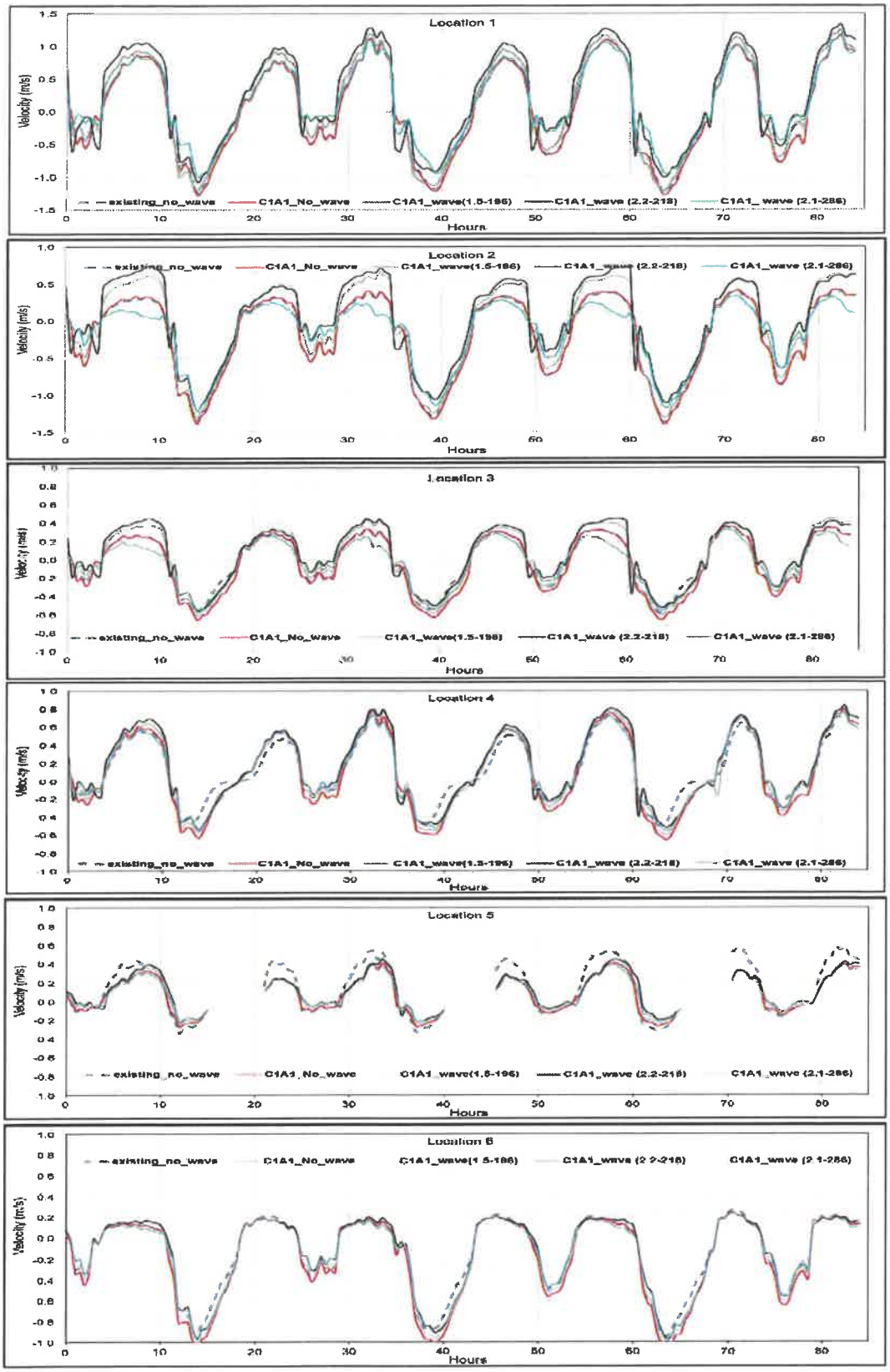

Figure A29. Wave-current interaction at the six locations for C1-A1 Alternative (see Figure 44 for the location). Positive velocity represents flood current, negative ebb current.

Modeling Results for C1-A3

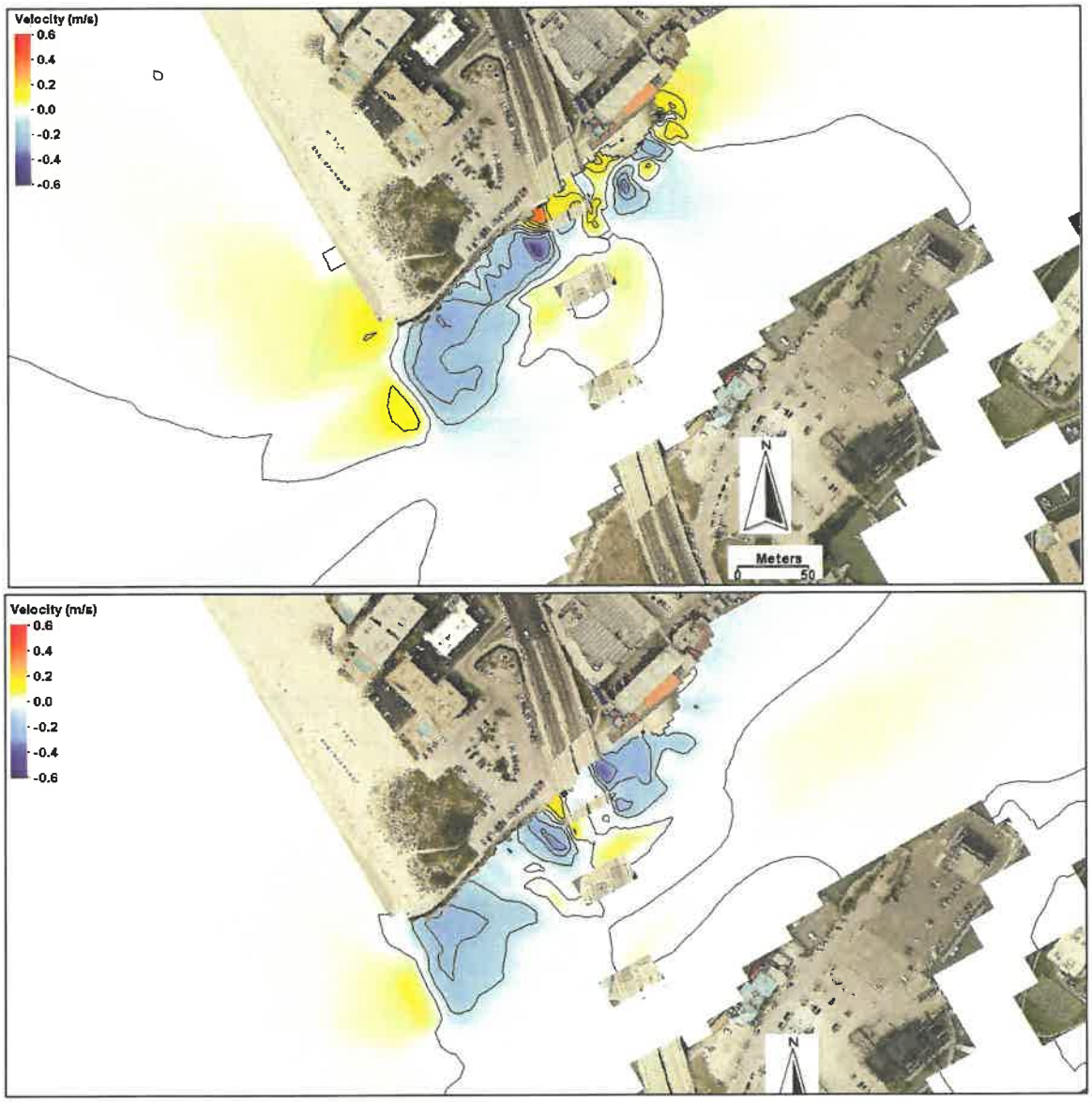

Figure A30. Difference map in velocity magnitude comparing C1-A3 with existing condition. Upper: peak ebb. Lower: peak flood. Positive: velocity increase; negative: velocity decrease.

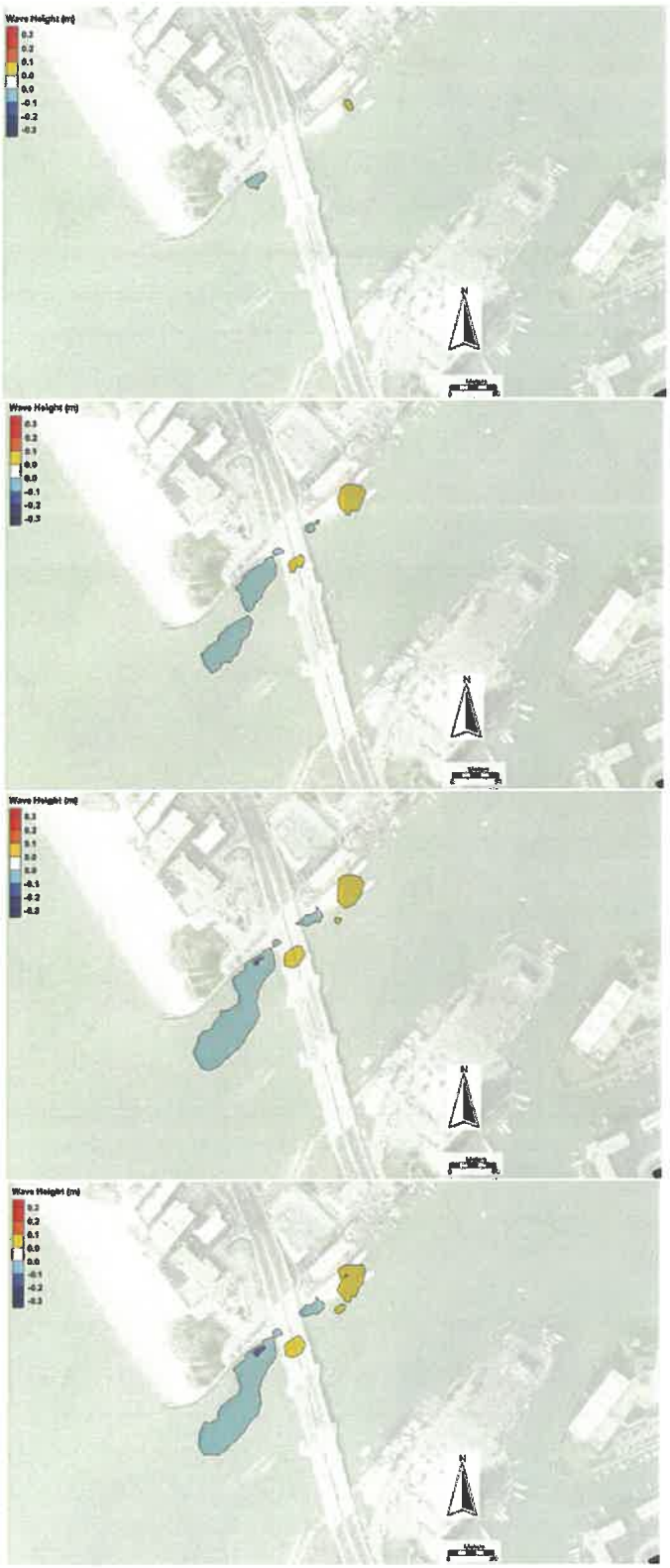

Figure A31. Wave-height difference at high tide between C1-A3 and existing conditions. Positive values indicate higher waves for C1-A3. From top to bottom, incident wave angles are 173.25, 196.25, 218.75, and 286.25 degrees.

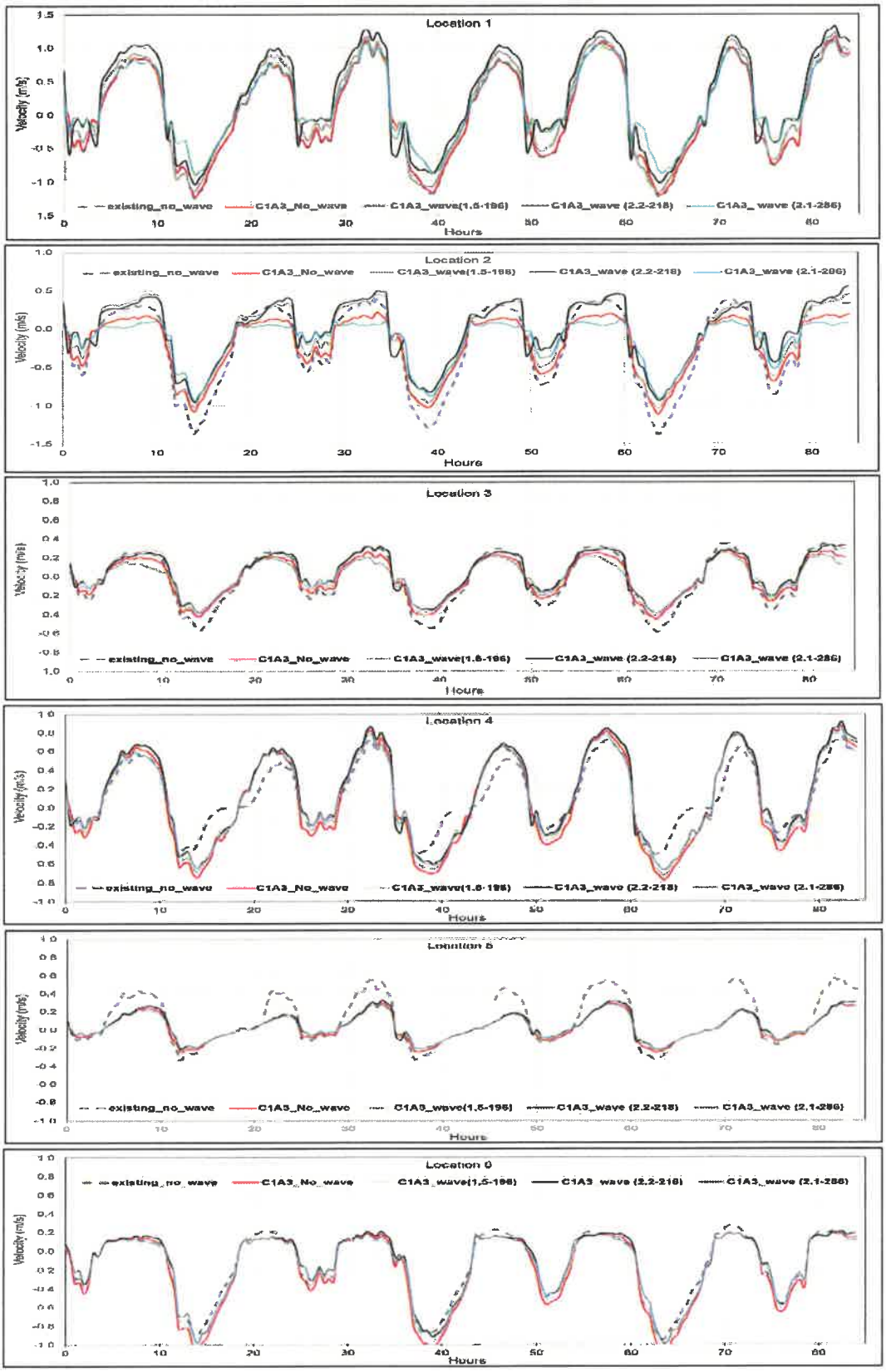

Figure A32. Wave-current interaction at the six locations for C1-A3 Alternative (see Figure 41 for the location). Positive velocity represents flood current, negative ebb current.

Modeling Results for C1-A5

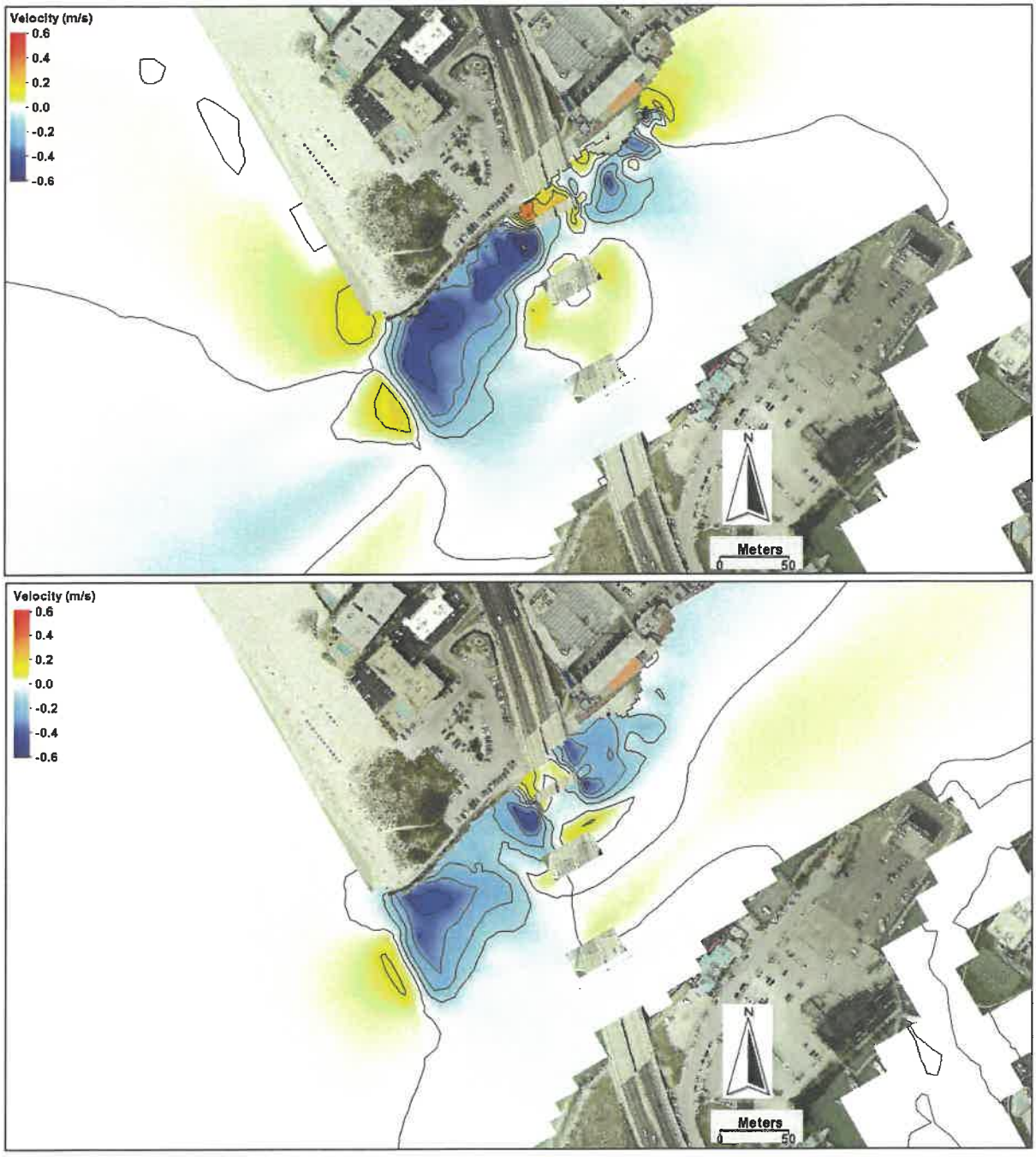

Figure A33. Difference map in velocity magnitude comparing C1-A5 with existing condition. Upper: peak ebb. Lower: peak flood. Positive: velocity increase; negative: velocity decrease.

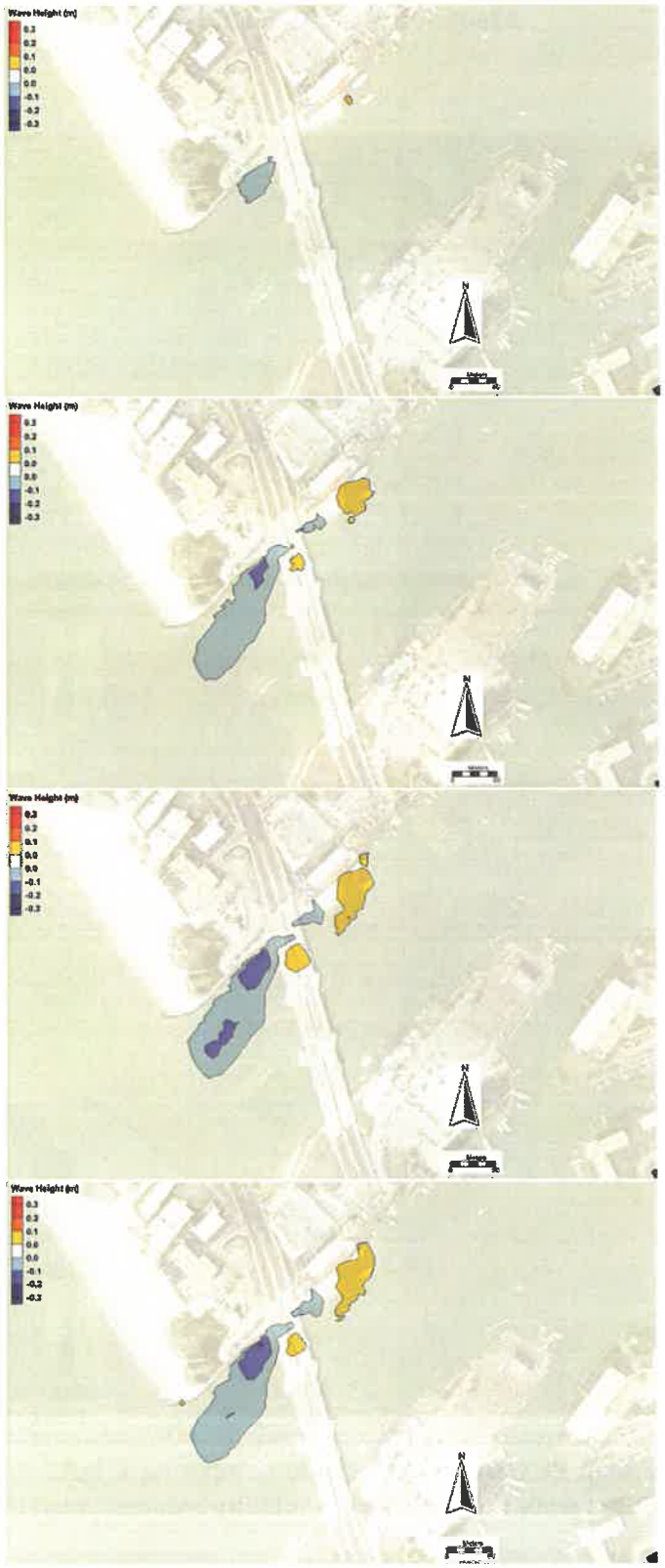

Figure A34. Wave-height difference at high tide between C1-A5 and existing conditions. Positive values indicate higher waves for C1-A5. From top to bottom, incident wave angles are 173.25, 196.25, 218.75, and 286.25 degrees.

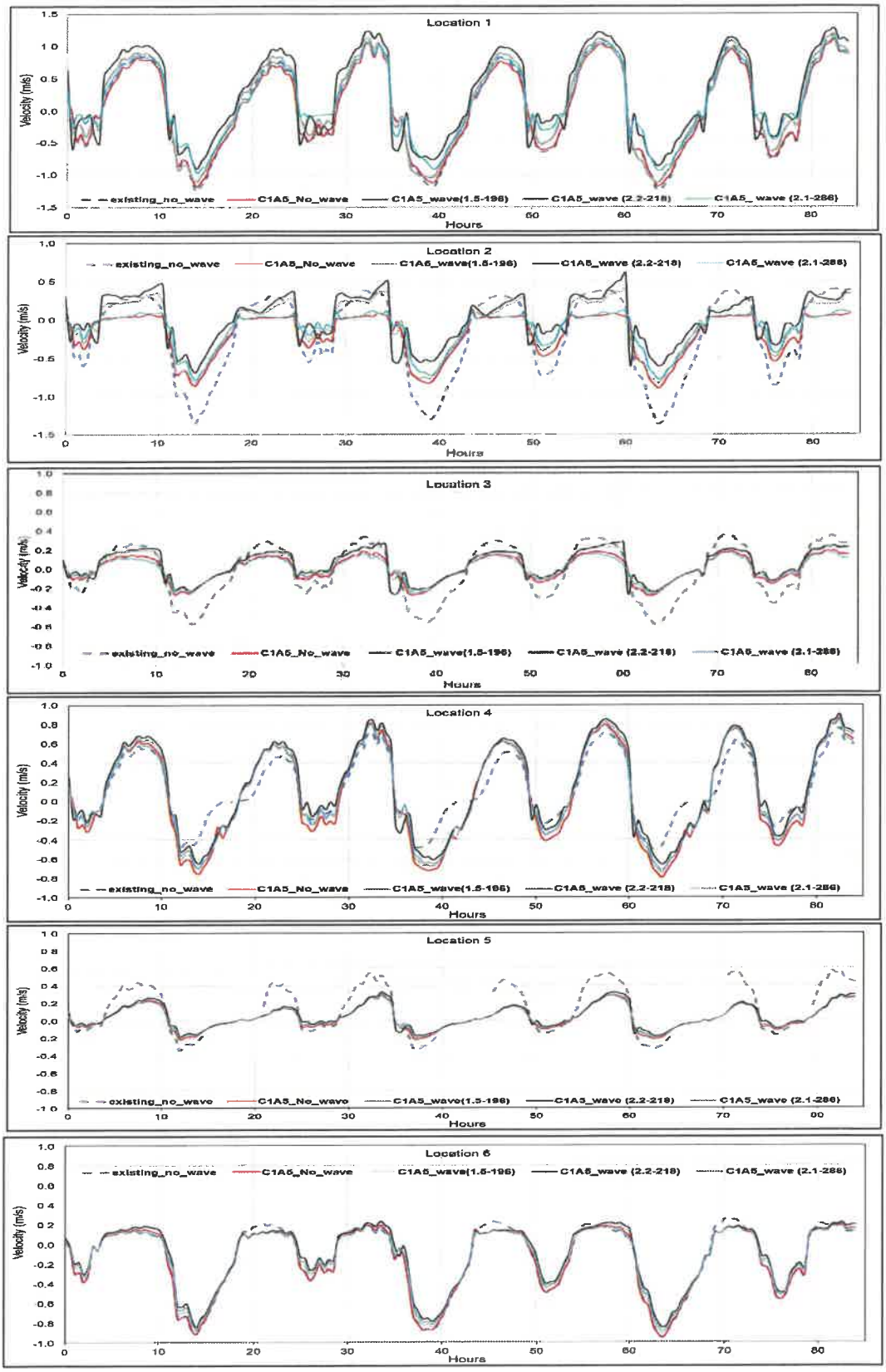

Figure A35. Wave-current interaction at the six locations for C1-A5 Alternative (see Figure 41 for the location). Positive velocity represents flood current, negative ebb current.

Modeling Results for C2-A1

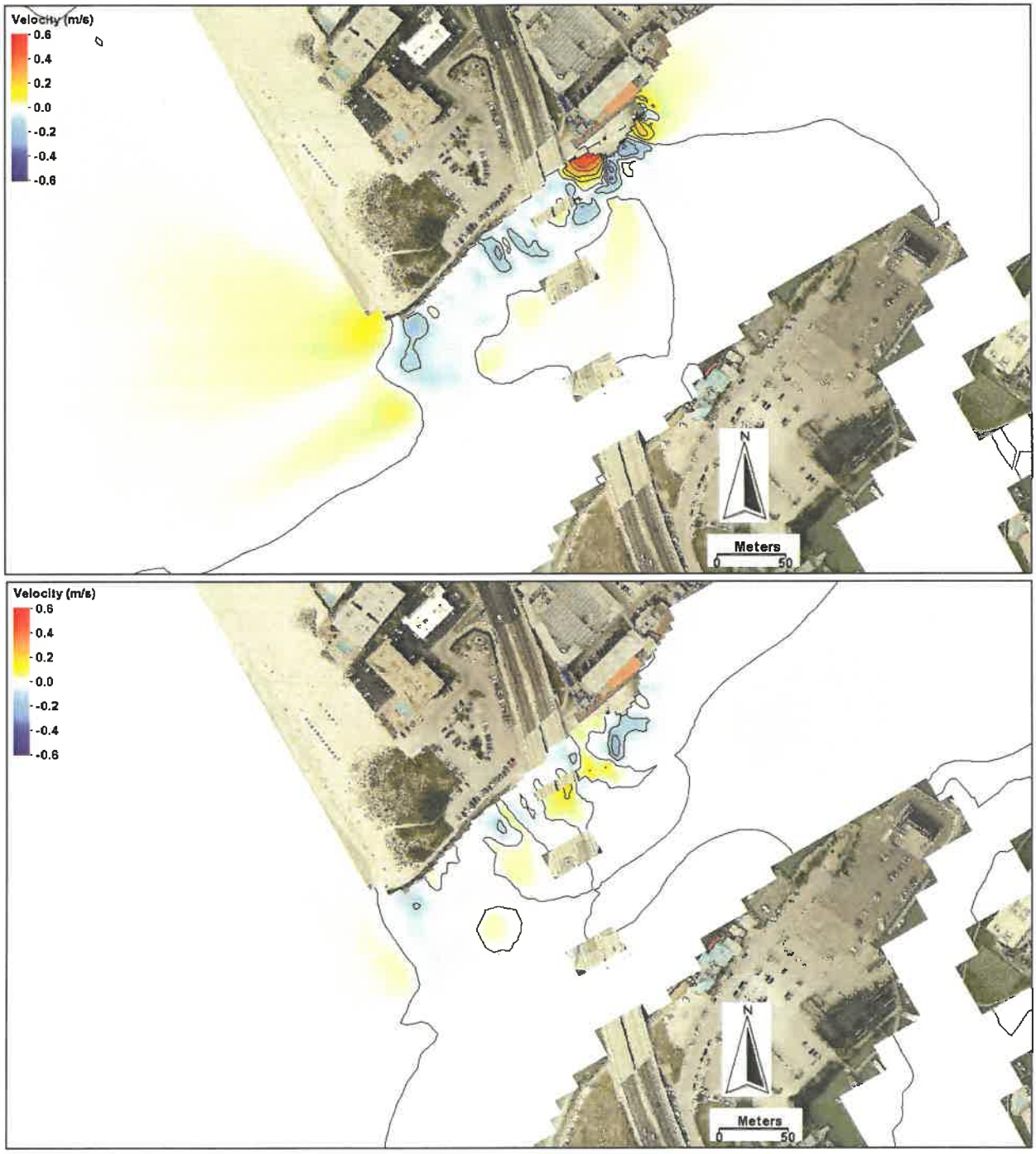

Figure A36. Difference map in velocity magnitude comparing C2-A1 with existing condition. Upper: peak ebb. Lower: peak flood. Positive: velocity increase; negative: velocity decrease.

Figure A37. Wave-height difference at high tide between C2-A1 and existing conditions. Positive values indicate higher waves for C2-A1. From top to bottom, incident wave angles are 173.25, 196.25, 218.75, and 286.25 degrees.

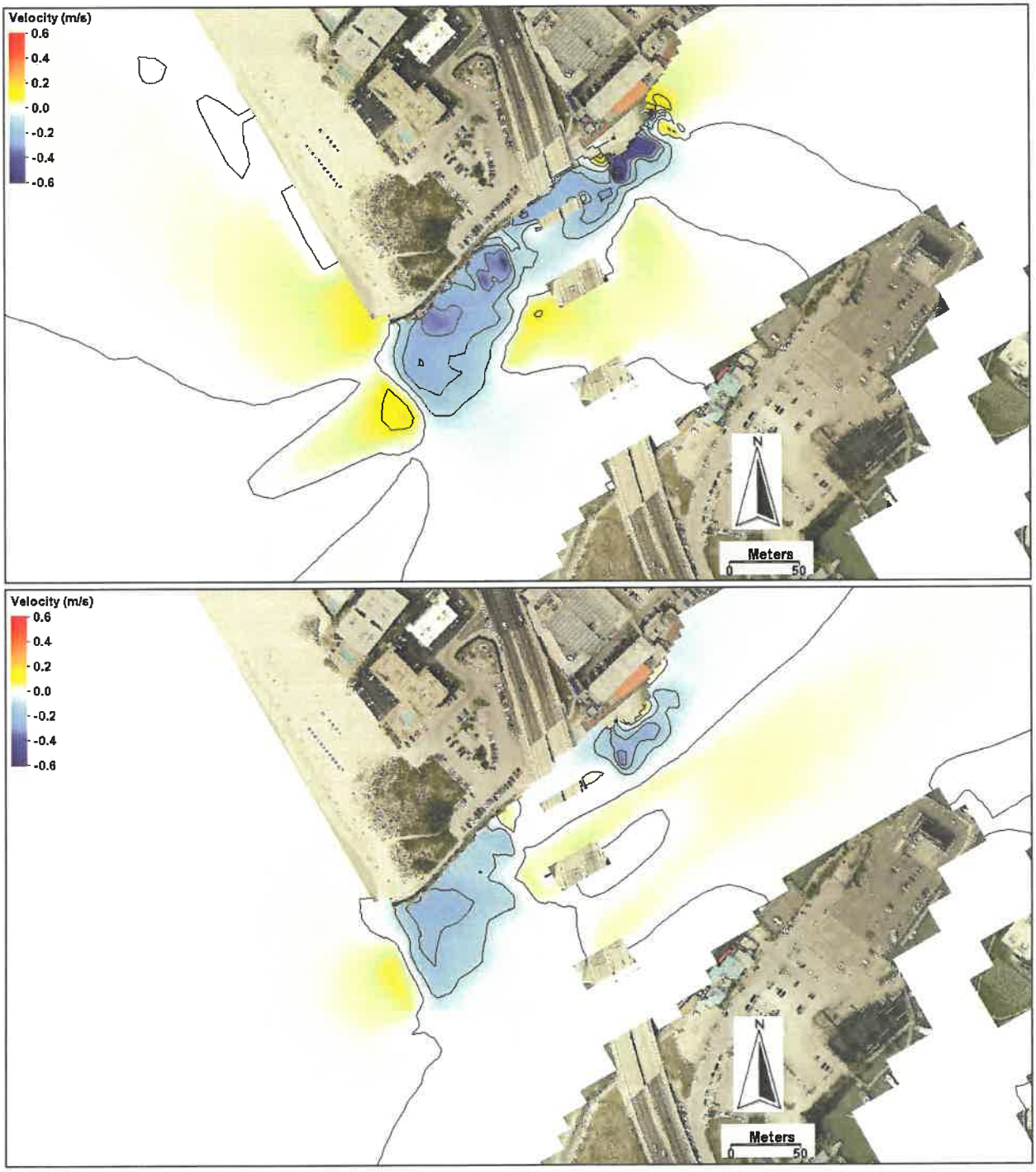

Figure A38. Difference map in velocity magnitude comparing C2-A3 with existing condition. Upper: peak ebb. Lower: peak flood. Positive: velocity increase; negative: velocity decrease.

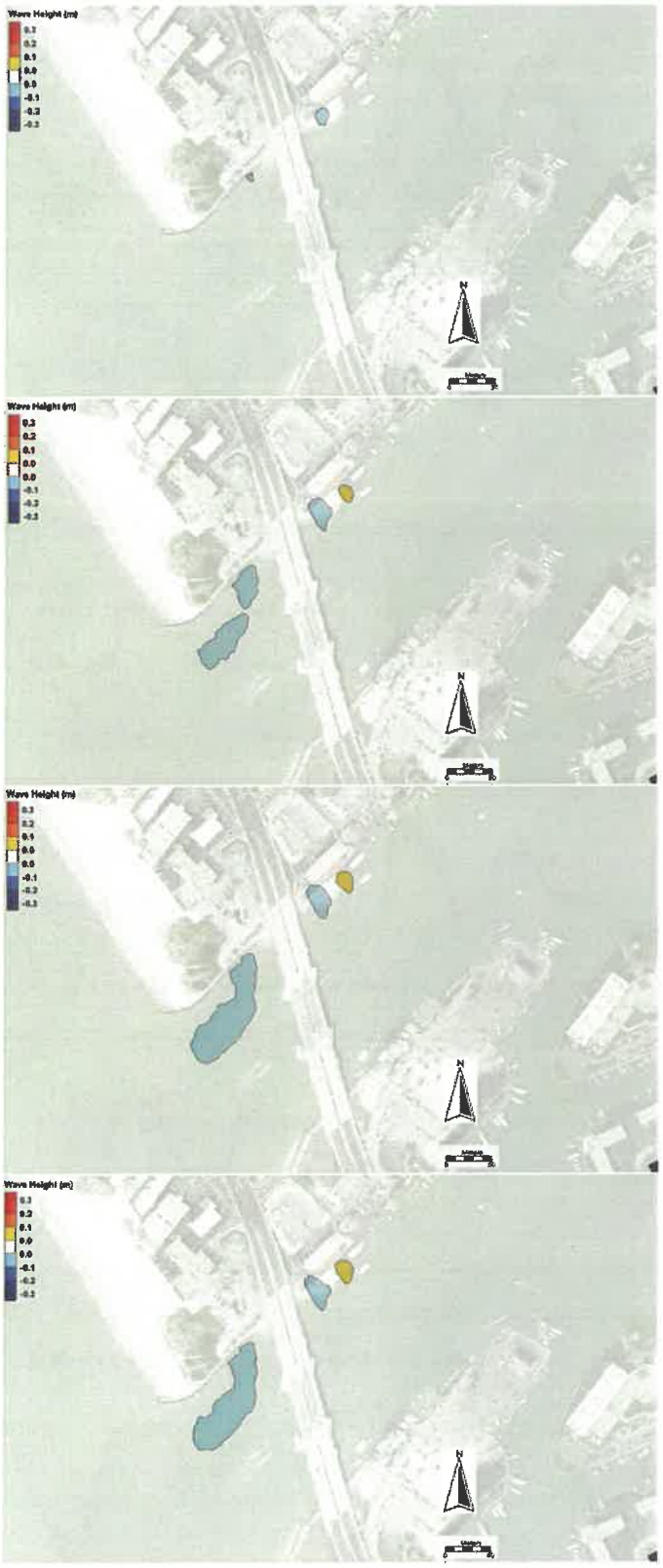

Figure A39. Wave-height difference at high tide between C2-A3 and existing conditions. Positive values indicate higher waves for C2-A3. From top to bottom, incident wave angles are 173.25, 196.25, 218.75, and 286.25 degrees.

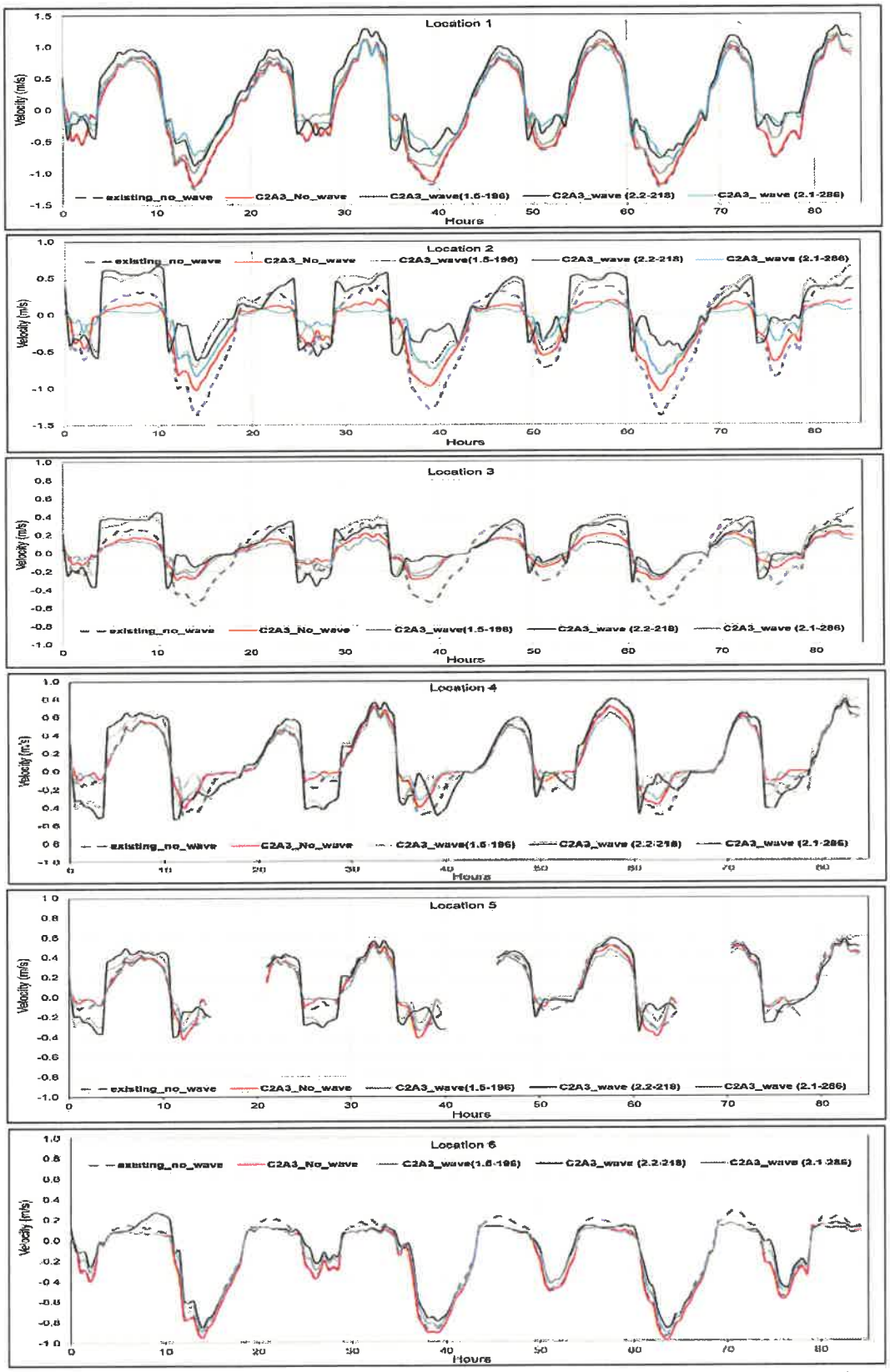

Figure A40. Wave-current interaction at the six locations for C2-A3 Alternative (see Figure 41 for the location). Positive velocity represents flood current, negative ebb current.

Modeling Results for C2-A5

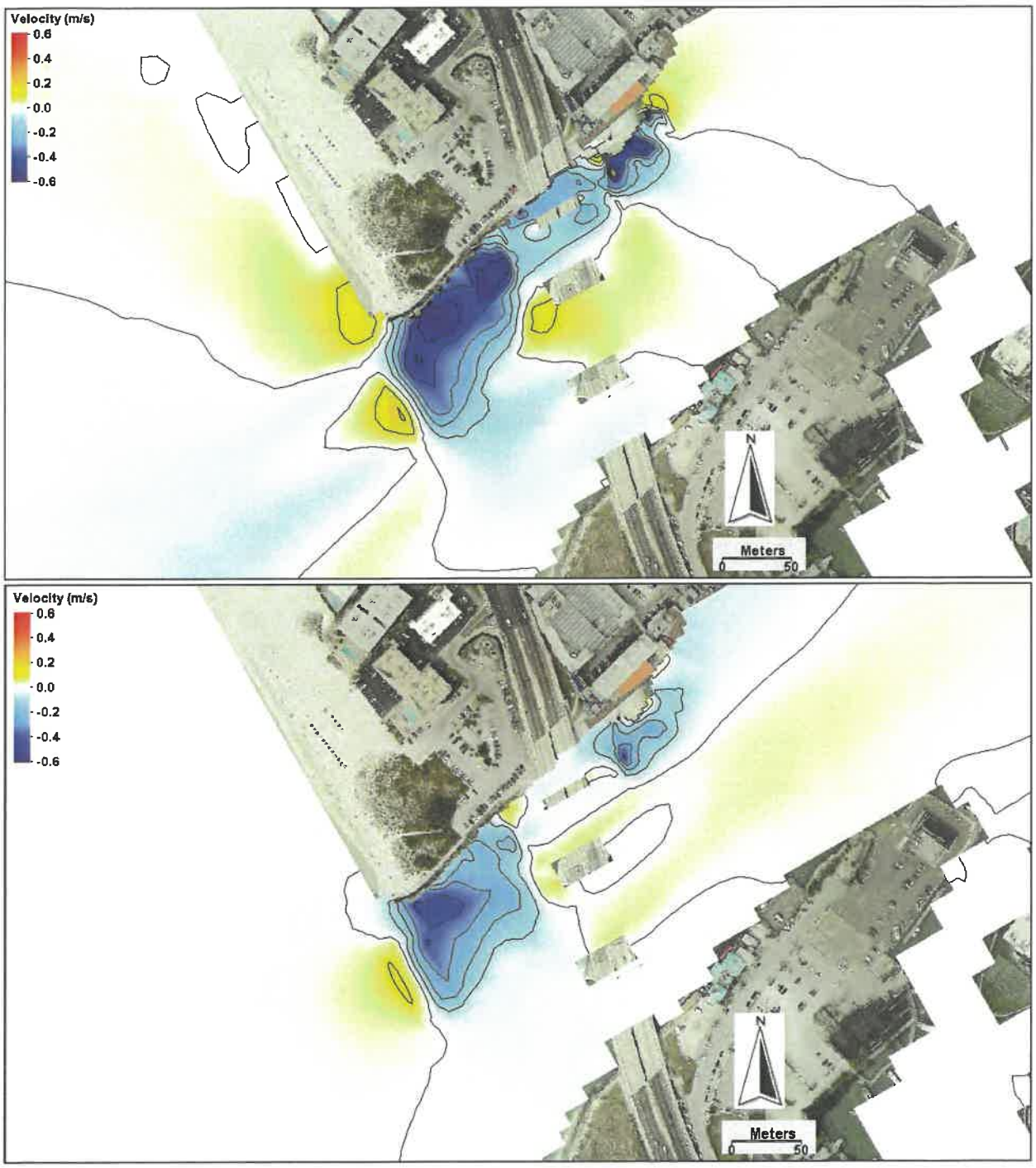

Figure A41. Difference map in velocity magnitude comparing C2-A5 with existing condition. Upper: peak ebb. Lower: peak flood. Positive: velocity increase; negative: velocity decrease.

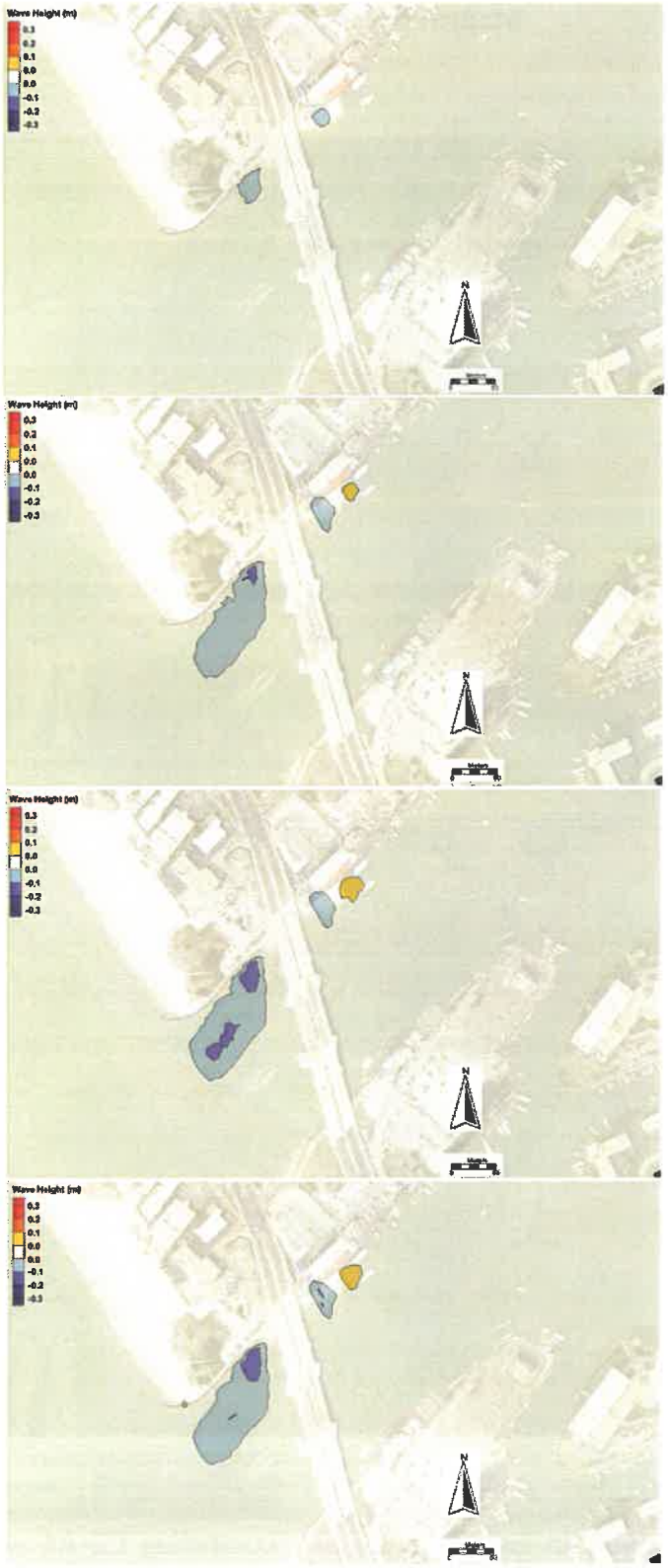

Figure A42. Wave-height difference at high tide between C2-A5 and existing conditions. Positive values indicate higher waves for C2-A5. From top to bottom, incident wave angles are 173.25, 196.25, 218.75, and 286.25 degrees.

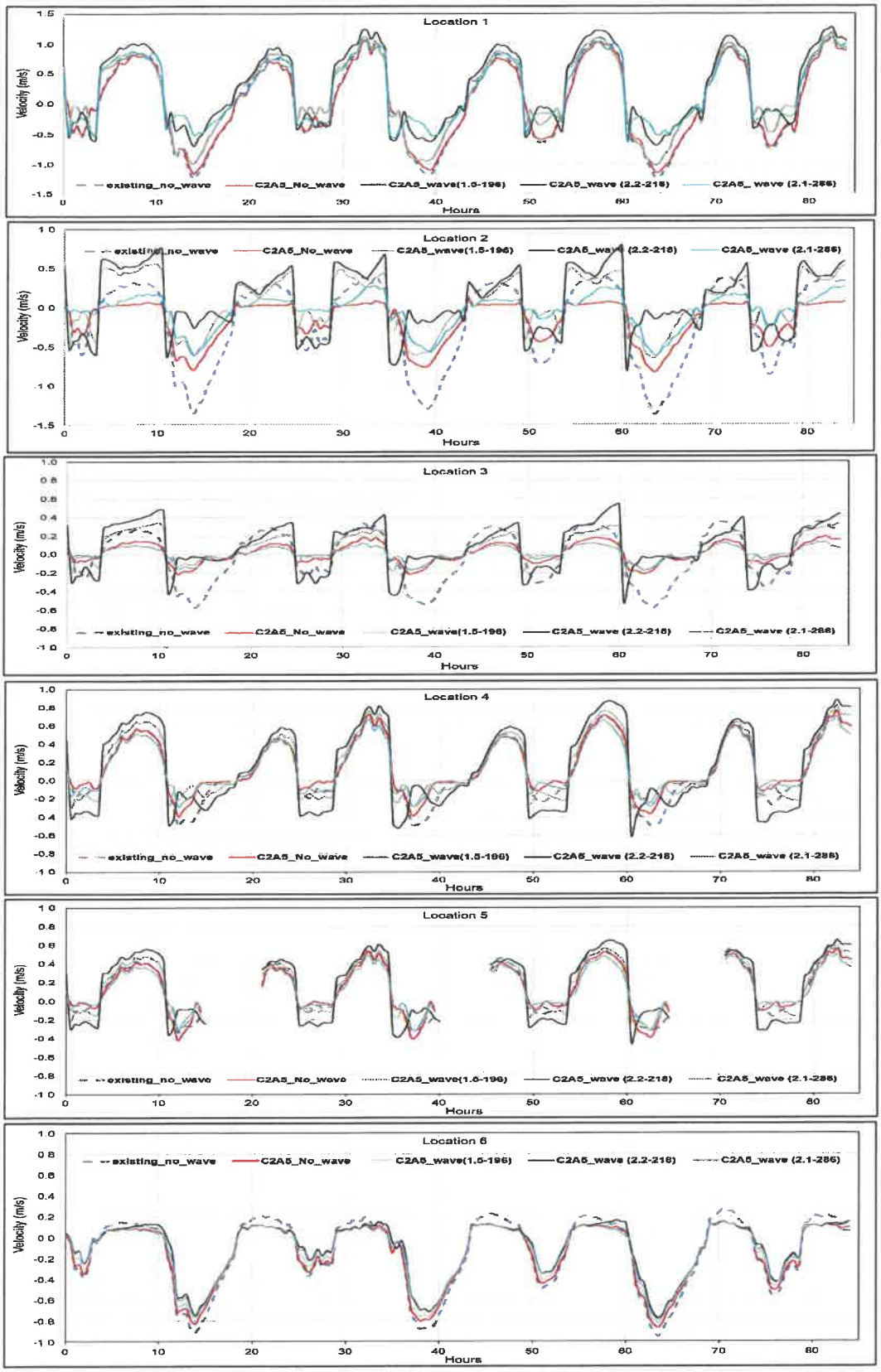

Figure A43. Wave-current interaction at the six locations for C2-A5 Alternative (see Figure 41 for the location). Positive velocity represents flood current, negative ebb current.

Modeling Results for C3

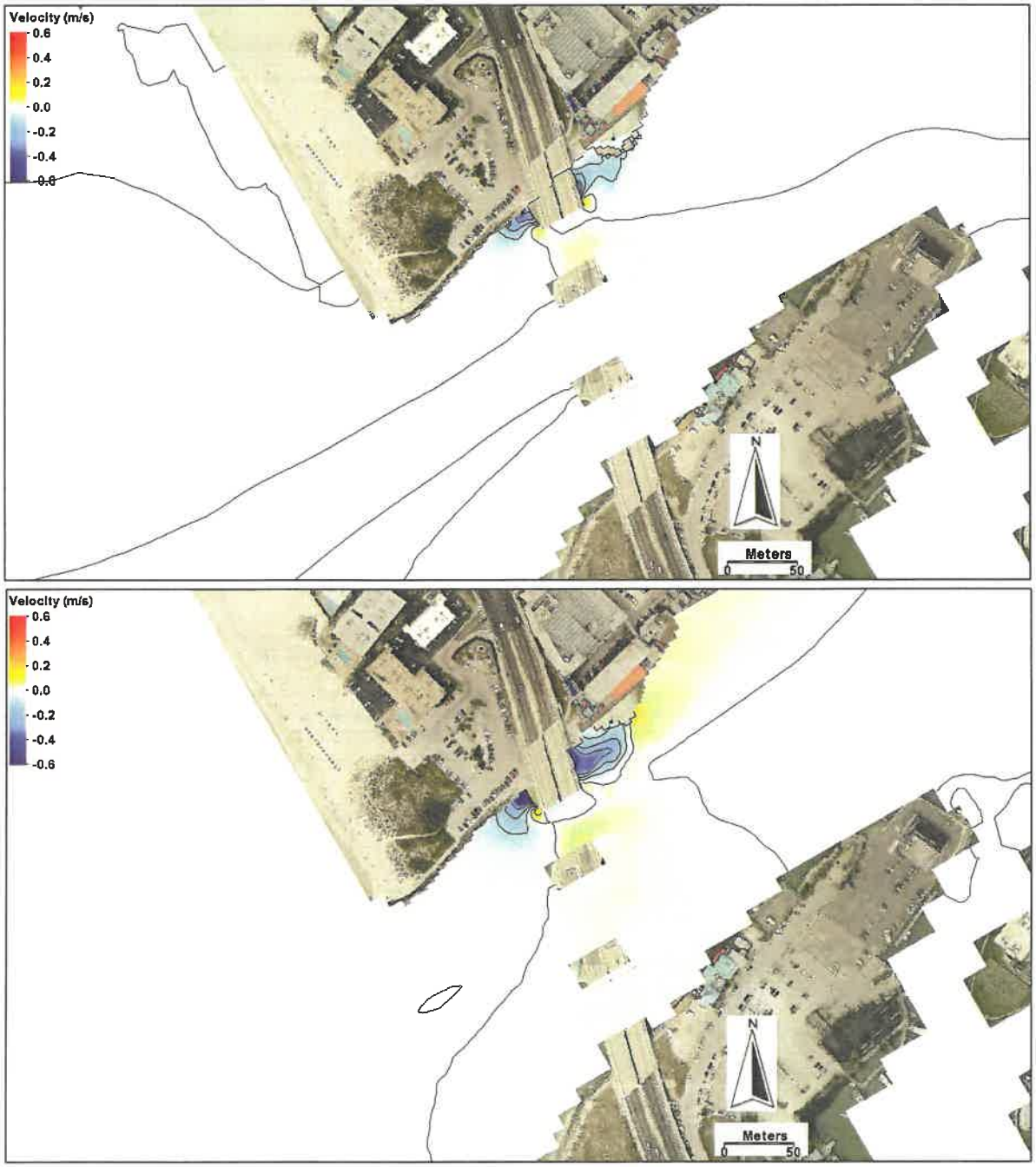

Figure A44. Difference map in velocity magnitude comparing C3 with existing condition. Upper: peak ebb. Lower: peak flood. Positive: velocity increase; negative: velocity decrease.

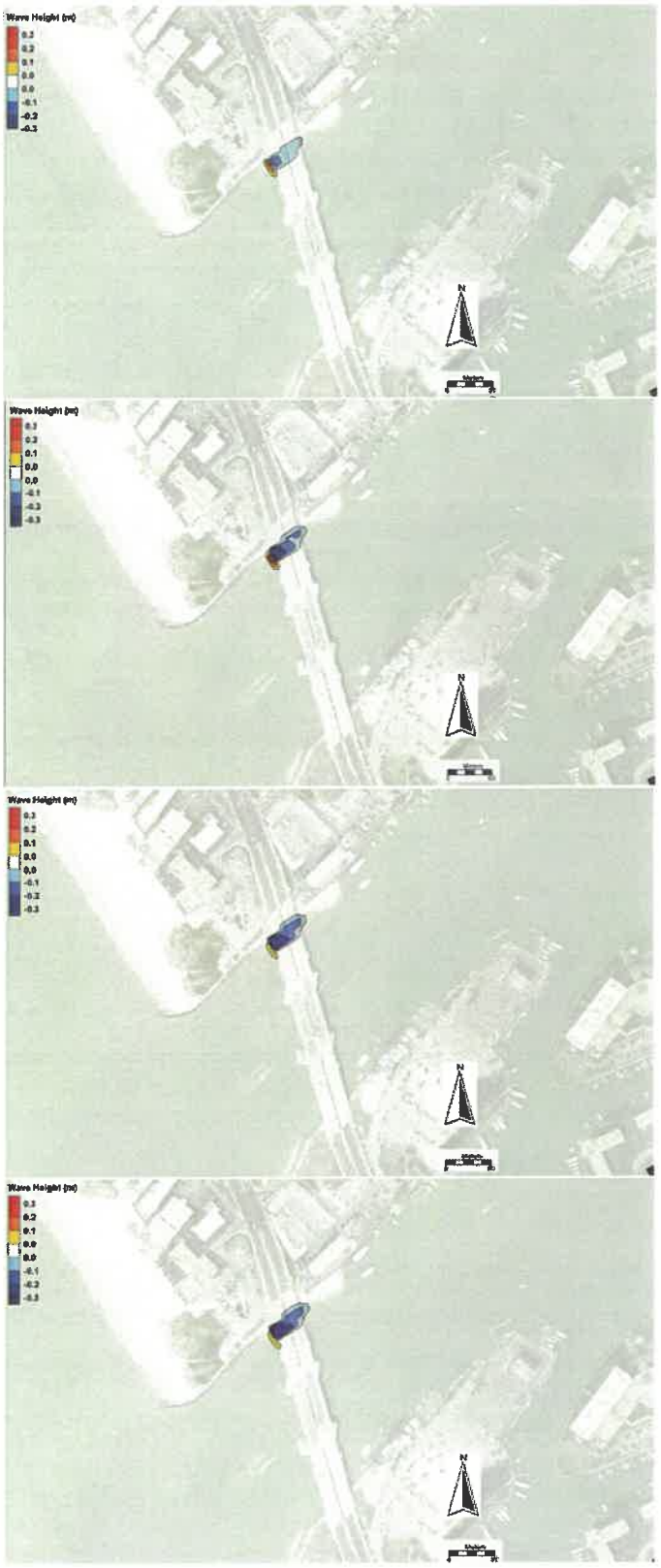

Figure A45. Wave-height difference at high tide between C3 and existing conditions. Positive values indicate higher waves for C2-A5. From top to bottom, incident wave angles are 173.25, 196.25, 218.75, and 286.25 degrees.

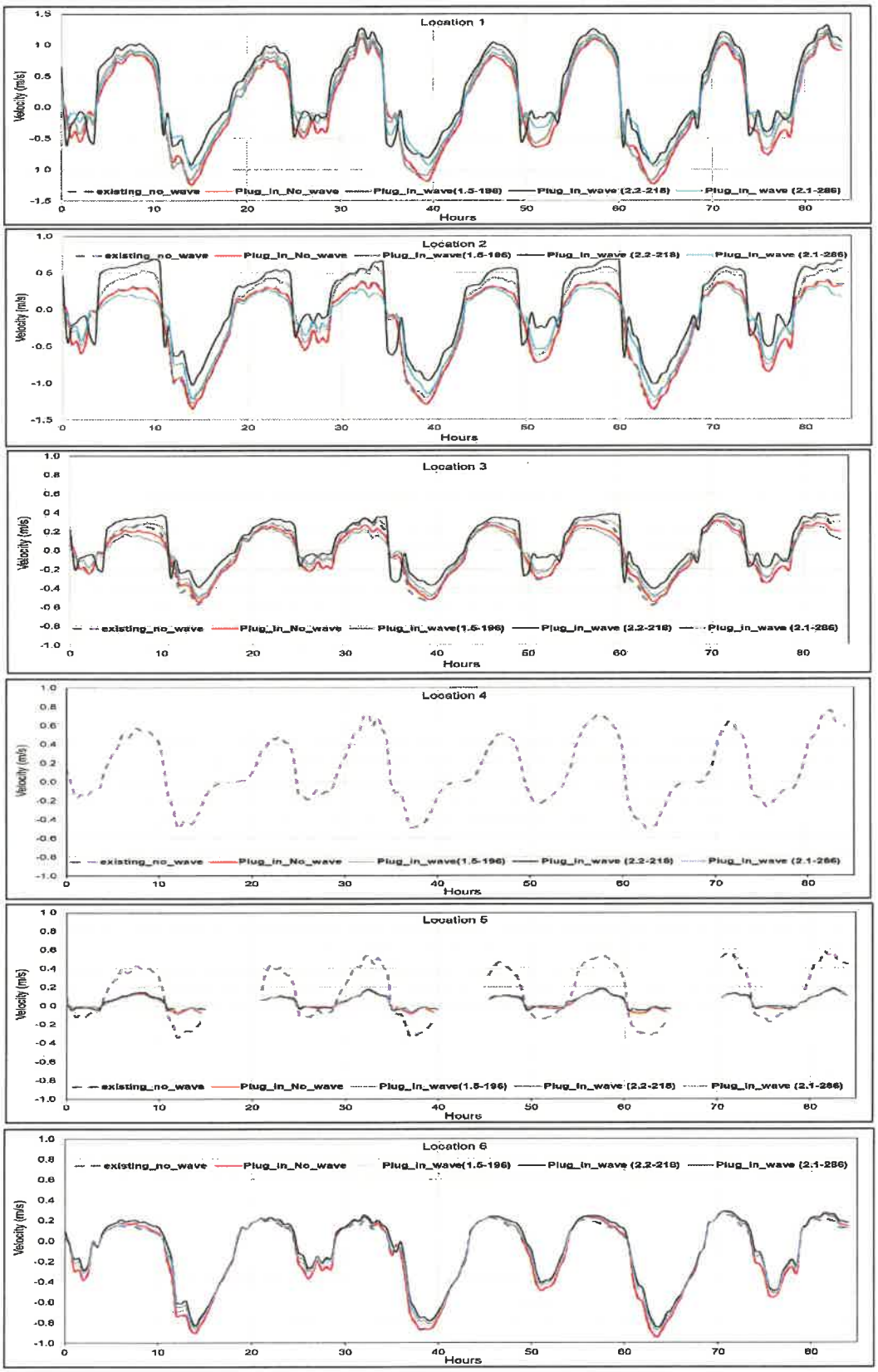

Figure A46. Wave-current interaction at the six locations for C3 Alternative (see Figure 41 for the location). Positive velocity represents flood current, negative ebb current.